ESD-TDR-65-492



1

# Radio Physics and Astronomy

1965

Prepared under Electronic Systems Division Contract AF 19(628)-5167 by

Lincoln Laboratory
MASSACHUSETTS INSTITUTE OF TECHNOLOGY
Lexington, Massachusetts

The work reported in this document was performed at Lincoln Laboratory, a center for research operated by Massachusetts Institute of Technology, with the support of the U.S. Air Force under Contract AF 19(628)-5167.



Distribution of this document is unlimited.

1

# Radio Physics and Astronomy

1965

Issued 3 March 1966

Lincoln Laboratory

MASSACHUSETTS INSTITUTE OF TECHNOLOGY

Lexington, Massachusetts

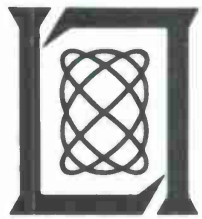

ABSTRACT

Much of the Laboratory's general research work in the fields of radio physics and astronomy is done with the facilities* and by the staff of the Laboratory's Millstone Hill Field Station. This first issue of the Radio Physics and Astronomy report is intended not only to report our most recent research findings and experiment preparations in these fields, but also to provide sufficient background in our past work to give the reader an overall acquaintanceship with the extent and history of such work at Lincoln Laboratory.

Radar measurements on the moon and nearer planets with the Millstone radar are described as are preparations for similar more accurate measurements at Haystack Hill. Applications of techniques that were developed for radar astronomy to the improved detection and tracking of artificial satellites are also described.

Considerable interest is evident in radio astronomy, both for its own sake and for the techniques of instrument evaluation which result from the research. These techniques will be useful in evaluating other new large radar and radio antenna systems.

Studies of the electron and ion behavior in the ionosphere continue and the results are being coordinated with work elsewhere.

Haystack Hill, the newest facility, is still in its early operating phase, with much of the effort of the station complement going into its increasingly complex instrumentation.

Accepted for the Air Force
Franklin C. Hudson
Chief, Lincoln Laboratory Office

*Millstone L-band steerable radar; UHF ionospheric radar; Haystack Research Facility.

# CONTENTS

# FOREWORD

This report, the first in a new series on research in the field of radio physics and astronomy being carried out at Lincoln Laboratory, was planned and largely written under the supervision of Dr. James W. Meyer, until recently Head of the Radio Physics Division. Primarily, it encompasses activities during the past six months but contains enough background material to establish continuity for programs having run for a longer period. Our objectives are to report serially to our sponsors, colleagues, and other interested persons on our activities in the field, and to provide a medium of disclosure of scientific results, technical and engineering developments, studies, and reviews of background material carried out in the process of program planning, that for one reason or another cannot be published in one of the regular scientific or engineering journals. This medium is in no way intended to supplant regular publication in the journals but rather to supplement journal publications with operational, engineering, and data detail that cannot be allowed in today's cover-bursting journals. In part, this publication will serve as a kind of observatory report for the Millstone Hill Field Station. It will include disclosure of work done by others using Lincoln Laboratory facilities. Material will be chosen for inclusion in this report on the basis of its relevance to the field of radio physics and astronomy and not on the basis of the source of support. We hope, in the future, to draw rather widely on the several Laboratory programs involving related research, to give a more comprehensive picture of Lincoln Laboratory's work in radio physics and astronomy.

# I. SUMMARY

## A. SPACE SURVEILLANCE TECHNIQUES

The present L-band Millstone steerable radar has a tracking range of about 5000 nautical miles (nm) on a one-square-meter target. Thus it continues to render assistance on occasion to the Air Force, to NASA, and to the Space Communications Program of the Laboratory, particularly for observation of small or distant targets observed poorly, if at all, by other sensors. Such activities will, of course, be continued to the extent that they are of value.

The real-time, on-site data processing capability at Millstone will be increased by nearly an order of magnitude once the newly accepted high-speed commercial computer has been completely integrated with the radar system, replacing the CG 24. Utilizing this capability, it is planned to develop improved computer-assisted tracking techniques and an ability to compute satellite orbits on-site from radar data. A programming study has been completed as the first step in applying the integration techniques used in radar astronomy to the observation and tracking of satellites, with the hope of at least doubling the tracking range of the radar. The study shows that the new computer is able to handle such a problem in real time.

The so-called digital monopulse (DIGIMON) system has been given extensive tests and found to be limited by the operating speed of presently available A/D converters. The availability of the higher-speed real-time computer now makes other means of accomplishing nearly the same result more attractive for the immediate future. DIGIMON has thus been shelved for the present, even though it has some advantages over the other means now being implemented.

## B. RADIO ASTRONOMY

During this year, a powerful array of radiometric observing equipment was successfully completed and used on the Haystack antenna. The equipment includes broad-band radiometers at 5, 8 and 15.5 GHz and spectral line receiving equipment. To date, this equipment has been used at H- and OH-line frequencies but, provided with proper front ends, it will make spectral line searches possible at many different promising frequencies.

Major radio sources were carefully measured at 8 and 15.5 GHz by means of the radiometric equipment and the results used to determine Haystack antenna aperture efficiencies at these two frequencies. Pointing accuracies for the system were also derived from the data.

From the results of these observations, it appears that an overall antenna efficiency, including radome losses, of about 46 percent has been achieved at 8 GHz and about 23 percent at 15.5 GHz. These results imply an rms surface deviation from a true paraboloid on the order of 50 to 60 thousandths of an inch. Pointing precisions of a few thousandths of a degree also seem to have been achieved. The results indicate further that no measurable "squint" of the RF beam results from the space-frame radome. Observations of known polarized radio sources also seem to show that no appreciable polarization effects result from the radome or from any peculiarities of the antenna system itself.

Using operating capacity in excess of that required for the antenna pointing task, the Haystack U490 computer has been programmed to perform the major signal processing functions for radio

astronomical observation. In addition to performing the integration process used in measuring weak radio sources, the computer is able to scan the antenna across discrete sources, and to determine their angular center of gravity as well as the antenna temperature measured at that point. It also performs the transformations from the time to the frequency domain of the data output from the digital correlator during spectral line work.

## C. RADAR ASTRONOMY

The Millstone radar continued a long history of engagement in radar astronomy with a seven-month series of observations on Venus in 1964. A significant achievement was the measurement of range (time of flight) to an accuracy of ±1.5 km during two months of this period. Echoes from Mercury were also obtained. Mars was the only planet favorably located for detection during the first six months of 1965. Data appeared to indicate that Mars has a cross section of about 14 percent of the projected area.

In studies of the moon, the most significant achievement was the development of a polarimetric method of investigation of the surface. Interpretation of the strength of echoes as a function of the angle of the radar wave polarization relative to the plane of incidence on the lunar surface has led to a theory that radar waves actually penetrate a tenuous surface layer and are reflected after encountering a much denser layer at least one wavelength below the surface. With this model, it is also possible to explain for the first time the past divergence in values of the dielectric constant for the surface as derived from radar and from radiometric data.

Mercury was observed at X-band for the first time in April 1965 by using the Haystack radar. This measurement, which appeared to show a cross section on the order of 5 percent of projected area, was the first in a planned series which is intended to culminate in a precise measurement of time of flight between Earth and Mercury, when the latter is near superior conjunction. This measurement should be possible with sufficient precision to permit observing relativistic effects due to the solar gravitational field, as proposed by Shapiro.* An extensive instrumentation and construction program designed to provide greatly increased radar performance with Haystack is under way to support this experimental program.

## D. ATMOSPHERIC RESEARCH

A large ionospheric radar with a 220-foot-diameter antenna pointed at the zenith and 440-MHz radar equipment having an average transmitted power of 150 kw has been used since early 1963 to determine electron density profiles and electron and ion temperature profiles by incoherent backscatter techniques. Incoherent integration over long periods provides data for the density profiles, while spectrum measurements yield ion temperatures and the electron-to-ion temperature ratios. Both this radar and the Millstone L-band steerable radar are used on a regular schedule to gather data.

Much effort is currently going into analysis of the data. The three years' observations now available should provide an accurate description of the F-region behavior at midlatitudes

*I. I. Shapiro, "Effects of General Relativity on Interplanetary Time-Delay Measurements," Technical Report 368, Lincoln Laboratory, M.I.T. (18 December 1964), DDC 614232.

near sunspot minimum. Observations will be continued with somewhat increased emphasis as solar activity increases over the next few years.

System rearrangements have been designed and partially implemented to facilitate both the gathering and reduction of data in order to reduce personnel demands.

An auroral observation and study program was initiated early this year to determine the extent to which auroras can be expected to interfere with high-performance L-band radar operation. A body of spatial and spectral distribution data has been collected and the program will be continued at a modest level.

# II. SPACE SURVEILLANCE TECHNIQUES

## A. INTRODUCTION

The present Millstone radar tracker operates at a frequency of 1295 MHz. It began operation in the summer of 1963, replacing the original UHF missile and satellite tracker, the capability of which had been matched by a number of other installations.

The present Millstone radar system has a wide range of objectives, including research programs in radio physics, radar astronomy, and in the development of improved space surveillance techniques. The changes brought about through rebuilding Millstone resulted in an immediate improvement of about 17 db in performance against "hard" targets in a conventional closed-loop tracking operation. This improved performance is in itself a considerable achievement and gives Millstone a capability on distant small targets which is unique at the present time. Since the advent of a new generation of earth satellites with great apogee heights, Millstone has been requested on a number of occasions to obtain radar data on objects which are either very difficult or impossible for other radars to observe.

The space surveillance techniques effort consists primarily of two parts:

(1) Maintenance and improvement of the present capability. This will permit support of the Laboratory's own related programs and will provide assistance when necessary to military and other governmental organizations in difficult or otherwise special situations.

(2) A program of research in space surveillance techniques. Primarily, this program involves development of advanced data handling techniques. It will require full and efficient use of a modern high-speed digital computer such as the SDS 9300 now in use at Millstone and soon to be interfaced with the radar.

Millstone is also engaged with MITRE Corporation in the experimental use of phase-coherent radar interferometric techniques to obtain accurate position and velocity data for calculation of satellite orbital elements. The original experiments which demonstrated the feasibility of a long-baseline (≈15 miles), phase-coherent radar interferometer were performed by Lincoln Laboratory in 1959 and 1960.[1] In the present experiment, the dominant role is with MITRE. Millstone, because of its high transmitter power and large antenna, illuminates the target and, through a slaving system, points two smaller MITRE antennas which form the other two terminals of a three-station system. The three stations form a triangle approximately 15 miles on a side and are connected for data transmission and control functions by microwave links.

The interferometer has been installed and the initial test phase completed. It is now being operated on a regular basis (one night a week) for making satellite measurements. These measurements have been principally of the electrical phases of the signals at the several stations, although, in some cases, amplitude measurements have been made of the satellites' echoes at the three stations. These results are processed centrally at the MITRE installation at Bedford to derive information about the satellite.

A polarization control system has been installed recently in the Millstone L-band radar system to provide complete flexibility in the selection of the transmitted and received polarization.

Polarization can be set with any degree of ellipticity from circular of either sense to linear at any angle within a range of 90° with respect to the vertical. Moreover, polarization adjustments can be made while transmitting. Polarization control is accomplished by adjusting the relative phase and amplitude of the power fed to the two electrically orthogonal inputs to the antenna feed-horn assembly. The received signal is separated into two orthogonally polarized components by the microwave plumbing in the feed-horn assembly. The principle of operation of the polarization system is shown in Fig. II-1.

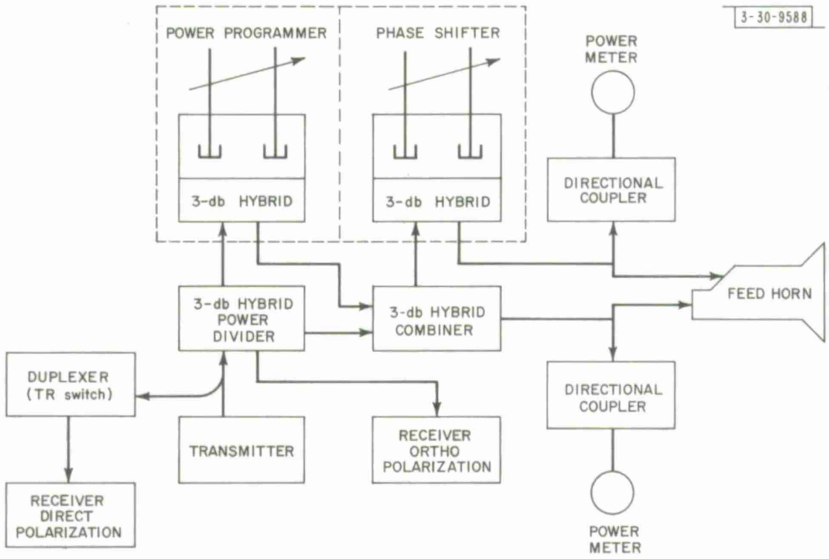


Fig. II-1. Millstone L-band polarization control system.

The polarizer is calibrated using a monitor antenna mounted on a boresite tower about 1500 feet from the 84-foot dish. The monitor antenna was designed by Dr. J. Ruze of Lincoln Laboratory and consists of a six-foot paraboloid with a rotating dipole feed. Great care was taken to assure that rotational perturbations in emission and pattern of the dipole would be negligible. Controls for both the polarizer and the monitor antenna dipole are located in the equipment shelter (doghouse) on the azimuth turret of the 84-foot dish.

The total polarization flexibility provided by this system is believed to be a unique capability in a radar of this kind. The provision of such a system was proposed by Dr. T. Hagfors in connection with a requirement in the lunar surface studies program. It also has interesting possibilities in connection with studies of artificial satellites.

## B. MILLSTONE TRACKER PERFORMANCE

The Millstone radar is a monopulse system with an 84-foot parabolic antenna and Cassegrainian microwave optics. Nominal values for other parameters of the radar applicable to conventional satellite tracking operations are:

| | | |
|---|---|---|
| Frequency: | | 1295 MHz |
| Antenna: | Half-power beamwidth | 0.7° |
| | Gain | 47.0 db |
| | Polarization | completely flexible |
| Transmitter: | Coherent amplification | |
| | Peak power | 5 Mw |
| | Average power | 150 kw |
| | Pulse width (typical) | 2 msec (CW) |
| | Prf (typical) | 15 pps |
| Receivers: | Parametric amplifiers in sum and error channels | |
| | Effective system temperature referred to the antenna | 100° to 250°K |
| Range capability: | 5000 nm on a one-square-meter target for a single pulse with 10-db signal-to-noise ratio | |
| Data processing: | Real-time digital computer providing smoothed and/or unsmoothed values of range, range rate, elevation, azimuth, time, and (optionally) pulse-by-pulse radar cross section | |

Over the past six months, data on about 140 tracks representing 53 different objects of special interest were passed to Space Track. These are objects placed on a priority list by SPADATS/Space Track which, because of their size, range, or outdated orbital elements, are difficult to observe. Data from a number of other satellite tracks were also passed to Space Track.

Some of the recent more significant skin-tracking observations were as follows:

During September and October 1964, Cosmos 41 (Object 869), in a highly elliptical orbit, was tracked a number of times to the longest ranges yet recorded at Millstone. The most distant track made was to a range in excess of 10,000 nautical miles (nm). On one occasion incoherent integration was used to detect the object near apogee at a range of 20,000 nm. Figure II-2 shows a computer display of tracking data for one of these observations.

The Imp I Satellite (Object 693) was tracked on several occasions at the request of NASA to assist in updating the orbital parameters during a period when its transmitter was silent. It, too, is in a highly elliptical orbit with an apogee of about 100,000 miles and a perigee of 2000 miles. This object is of the order of one square meter in size. The most distant detection took place at about 6500 nm with most of the automatic tracking done in a 2000- to 4000-mile range interval.

The Laboratory-sponsored LES-2 Satellite (Object 1360) provided an opportunity for Millstone to test its full capability on an operation that would take place at the threshold of its sensitivity. Its small size (0.1 to 0.2 square meter) and the extended range to the target (4300 miles at closest approach) made it a marginal undertaking at best. The pulse width was increased to 3.5 msec and added system sensitivity was achieved by reducing the receiver noise

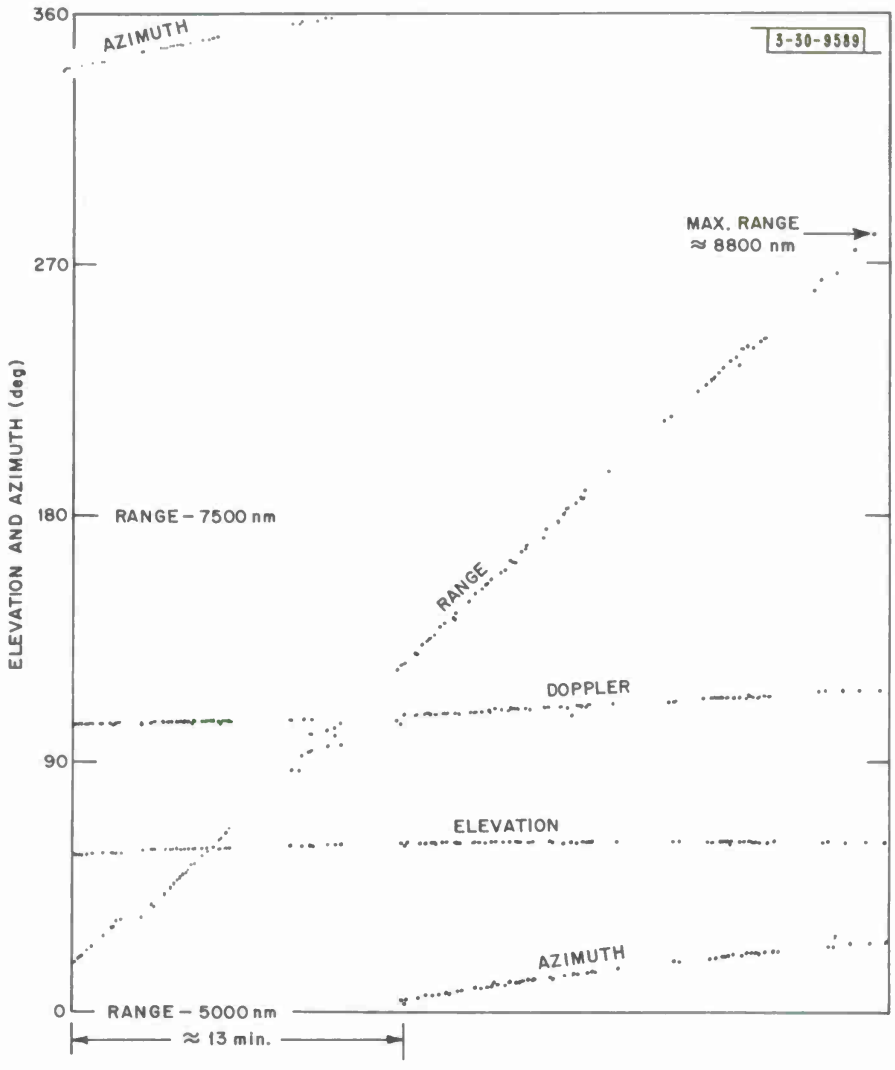


Fig. II-2. Millstone track data, Cosmos 41, 8 September 1964.

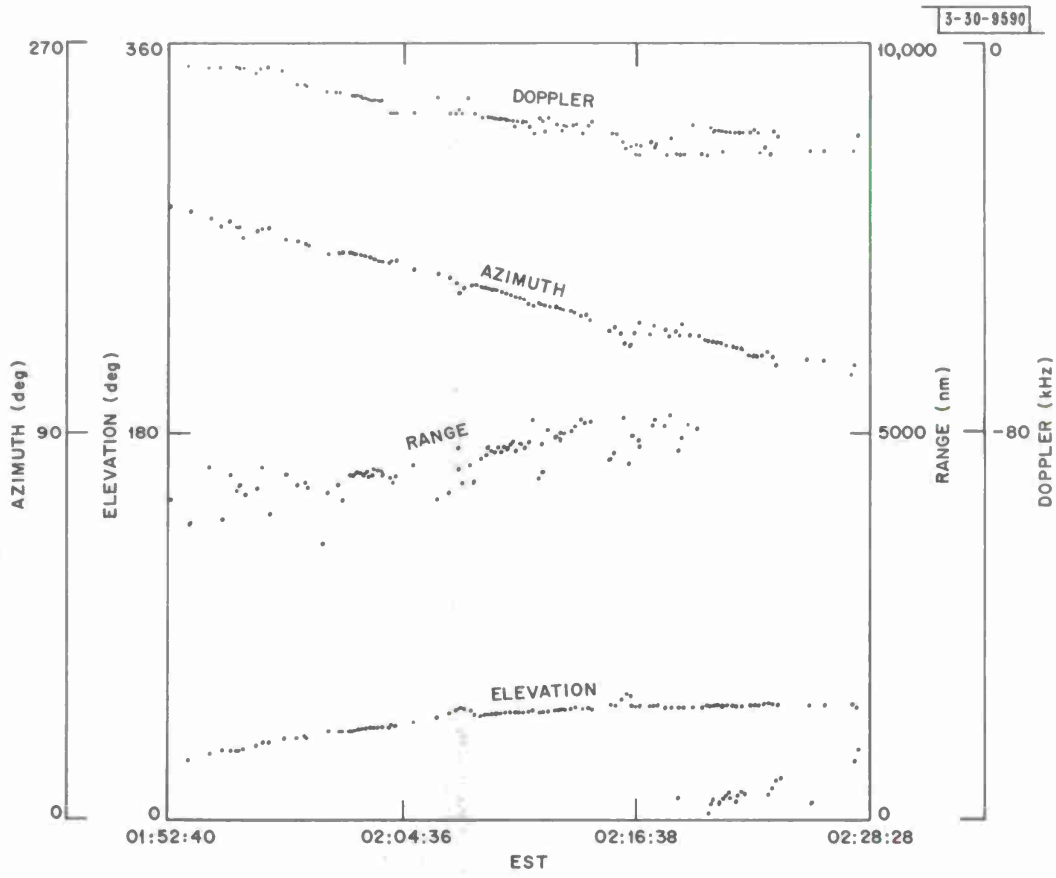


Fig. II-3. Millstone track data, LES-2, 13 May 1965.

temperature to 100°K and eliminating unnecessary portions of the Doppler filter bank. Target signal fluctuations of about 9 db above the average cross section allowed tracking to 5500 nm. Tracking data are shown in Fig. II-3.

Millstone continued to support the Laboratory's Wallops Island re-entry experiments until the program was terminated on 1 July 1965. In these operations, the Millstone tracker followed the flight of the multistage rocket to re-entry. Identification of the several targets that could appear in the beam as the various stages separated was accomplished by Doppler discrimination techniques. A Doppler Analyzer Display (DAD) system developed several years ago for this purpose permits the tracker to lock onto a Doppler-selected target. During the past six months, there were three such operations. The vehicles were tracked through all stage separations to re-entry on two of these occasions. On the third occasion, a wrong stage was acquired during a separation and the re-entry body was missed. Figure II-4 shows a DAD presentation during a Trailblazer run. This display is typical of nearly all the Trailblazer operations undertaken. Figure II-5 shows a plot of the DAD Doppler frequency vs time near re-entry. The payload separation is observable followed by the fourth stage and payload track to re-entry.

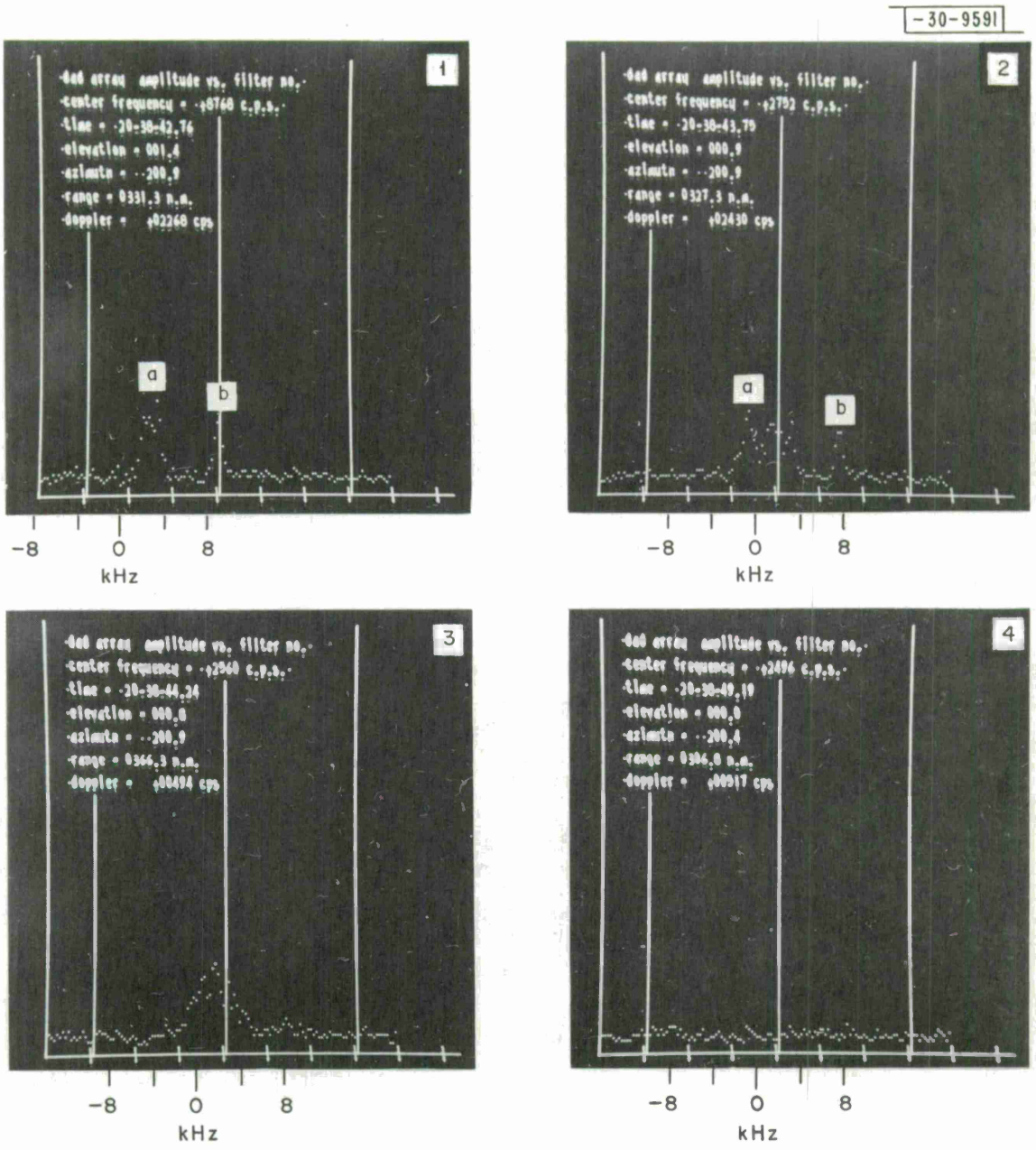


Fig. II-4. Calliscope displays of Trailblazer spectra obtained during re-entry phase. Frames 1 and 2 show (a) Doppler-spread echo and (b) higher velocity, hard-target type echo. In Frame 3 only the Doppler-spread echo remains. No echoes can be seen in Frame 4.

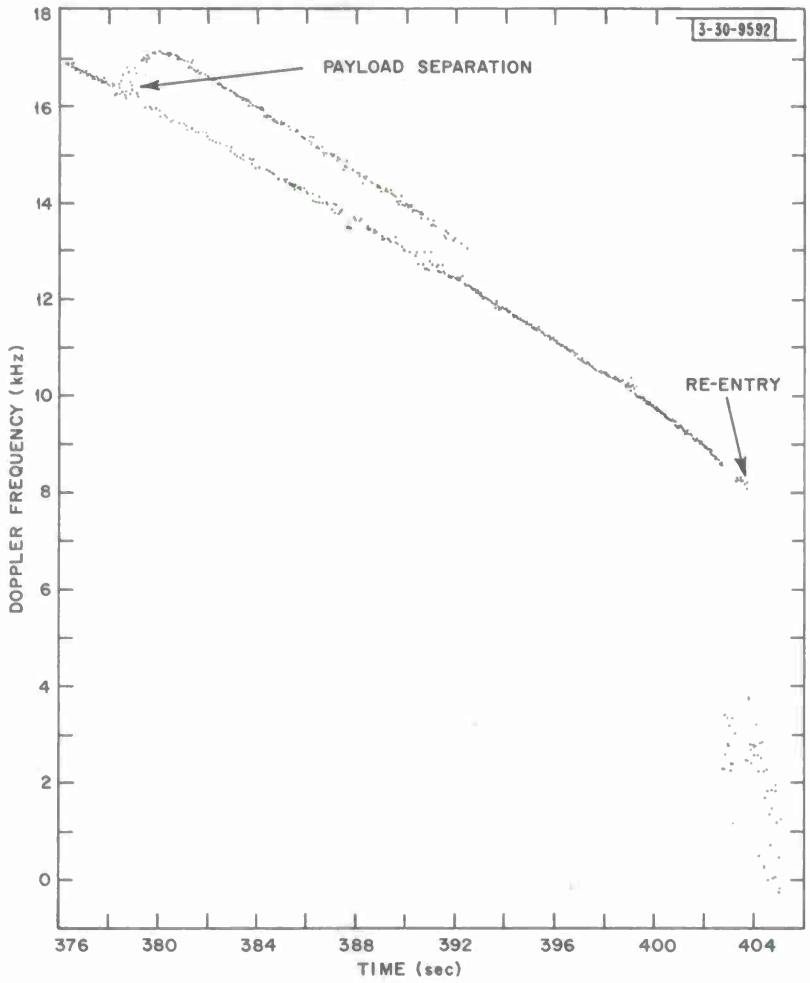


Fig. II-5. Trailblazer Millstone calliscope DAD time vs Doppler frequency, 376.0 to 405.1 seconds.

## C. SENSOR IMPROVEMENT PROGRAM

This program, called SIP for convenience, will be conducted in two overlapping steps. The objective of the first step is to improve the accuracy of measurements on targets that can be tracked with the present system. The objective of the second step is to extend substantially the range capability of the radar by using signal integration techniques.

One requirement basic to SIP is the development of an adequate computer capability for directing the radar semiautomatically, based upon nominal orbital elements as corrected in near-real time from such data as the radar obtains. This "bootstrapping" technique should increase the probability of weak target acquisition and improve substantially the reliability of tracking. TRW Systems (formerly TRW Space Technology Laboratories) has been given a contract to prepare programs to our specifications for the Millstone SDS 9300 computer to provide these capabilities. The orbital portion of these programs will be based upon the ESPOD* programs developed for the Air Force.

The present analog system of deriving the monopulse error signals is to be replaced with a digital system which will provide digitized data for real-time processing in the computer as well as radar steering directions. The digital system will provide more accurate measurements of range, Doppler, and angle errors in connection with step-one goals. According to present plans, the hardware and computer program acquired for step one will be compatible with the ultimate objectives of step two. Indeed, the greater burden in step two will be in the development of computer programs that will extend the capabilities of the existing hardware and software systems.

The use of both coherent and incoherent integration to permit observation of radar targets that cannot be observed on a single pulse is now a well-known technique employed by a number of investigators during recent years in radar studies of the planets. This technique has been used at Millstone to detect satellites at distances in excess of 35,000 km, and to detect extremely small objects (cross sections less than 10 $cm^2$ at 1000 km) in the West Ford belt. However, all these operations have depended upon a precise knowledge of the planetary ephemerides or satellite orbital elements in order to hold the radar beam on target for the required time. In all cases, except for West Ford searches, the data were processed in nonreal time. The goal of the range-extension part of SIP is to adapt these integration techniques to real-time radar tracking. Success of the program depends entirely on the development of adequate signal processing techniques, including both hardware and some very efficient computer programs.

The range-extension part of SIP will be attacked in two phases. The first phase deals with an artificial satellite in an elliptical orbit which brings it close enough to the sensor that radar echoes, when obtained, will be strong enough to actuate automatic tracking equipment (i.e., angle, Doppler, range), but eventually the satellite recedes to a distance so great that further detection is possible only with signal integration techniques. It is assumed that the orbit is

* Electronic Systems Precision Orbit Determination.

well enough known that the volume of uncertainty that must be searched for initial acquisition in range, angle, and Doppler is a reasonable one, although a computer-directed search pattern may be required to optimize the chance of success. The orbit upgrading capability provided by ESPOD can be used during the late phases of a pass on a satellite such as described above to provide steering information from data obtained earlier on the same pass.

Phase two is similar, but deals with satellites which, because of either extreme distance or small size, return echoes that are too weak to be detected except by integration techniques, and whose orbital elements are only approximately known. It will be necessary to define and search a volume of uncertainty and specify the maximum permissible integration period. If a priori knowledge of the target's coherence interval is lacking, the integration period would be determined by the geometric and dynamic properties of the situation. It is evident that a computer will be required to perform these functions, either as an aid to a human operator or in a fully automated program. It will also be necessary for the machine to determine when echoes have been obtained and compute the range, Doppler, and off-boresite angle errors. Then, assuming echoes have been obtained, there must be a capability, as in phase one, to upgrade the orbit and reduce the volume of uncertainty for future searches along the same pass.

One of the more difficult signal processing problems in SIP results from the large dynamic range in echo strength that is characteristic of the great majority of satellites. The lobe patterns and motions of typical nonspherical satellites cause deep fluctuations which, together with changes due to distance, often result in variations in echo strength in excess of 70 db during a single pass. While it is not very difficult to make the RF portion of the system sufficiently linear to accommodate a dynamic range even greater than 70 db, it seems to be quite difficult to reach even a 70-db range in the A/D conversion process with presently available equipment. If one needs to process only one signal channel, the problem can be avoided by predetection logarithmic compression. This does not appear to be a very good solution, however, for a radar tracker in which signals in several channels must be compared in phase and amplitude.

There are presently two systems under consideration for providing the precomputer digital signal processing operations required for SIP. Both systems exist in part at Millstone but neither one has yet been used in satellite tracking operations. One of the systems is called the Digital Monopulse System (DIGIMON for short). The other is called the Multiplexed Analog Converter System (MACS).

Historically, DIGIMON was conceived in 1962 during studies in connection with changing the Millstone radar from a conical-scan to a monopulse tracking system. It extends digital techniques over the receiver portion of the tracking loop as far as practical. However, because DIGIMON seemed a rather complex machine and required very fast circuitry, it was decided to implement a simpler analog system for near-term use. A slower effort was started on DIGIMON in Group 22 at Lincoln Laboratory with the idea that it would eventually replace the analog system. All components of the system have been received and installed at Millstone during the past year. During the past six months, the system has been undergoing intensive testing and debugging.

A theoretical discussion of DIGIMON by Dr. E. Gehrels is presented in Appendix A. A description of its operation and its present status follows.

DIGIMON is primarily a set of four digital filters with a monopulse error signal normalizing computer. It has the advantage of being a set of invariant filters matched to rectangular pulses with wide dynamic range. It should produce accurate off-boresite antenna pointing information. The antenna tracking loop is closed by converting the digital pointing errors to analog voltages that drive the antenna servo electronics.

The system frequency-multiplexes four radar receiver signals at 1-MHz spacing, each having approximately one megahertz of noise bandwidth. This allows as far as possible common receiver electronics (Fig. II-6). These multiplexed signals are as follows: (a) orthogonally polarized sum, (b) direct polarized sum, (c) azimuth difference, (d) elevation difference. Multiplexing is accomplished by converting the four received signals to +32, 30, +31, and 29 MHz and linearly adding them. This multiplexed signal is then mixed in both sine and cosine phase detectors with a 30-MHz-plus-Doppler local oscillator derived from the sequential Doppler processor. The two quadrature phase detector outputs having center frequency components at +2, 0, +1 and −1 MHz are then quantized by two 7-bit A/D converters operating at a 4-MHz sampling rate.

To demultiplex the signals and remove the three carrier frequencies after quantizing, it is necessary to do only a simple digital complementing and selection of the appropriate phase components because of the frequency spacing and sampling rate chosen.[2] Matched filtering is accomplished by adding these selected phase components into four sine and four cosine accumulators over a pulse length which is variable in 1-msec increments to a maximum of 8 msec. Six of these vector components are then used in a special-purpose computer that calculates the ratios of the real part of the azimuth and elevation off-boresight signals to the orthogonal sum signal. These ratios represent the amount and direction that a target echo is off boresight. They are coupled to the station computer to correct for antenna pointing errors and connected to the antenna servo to close the tracking loop.

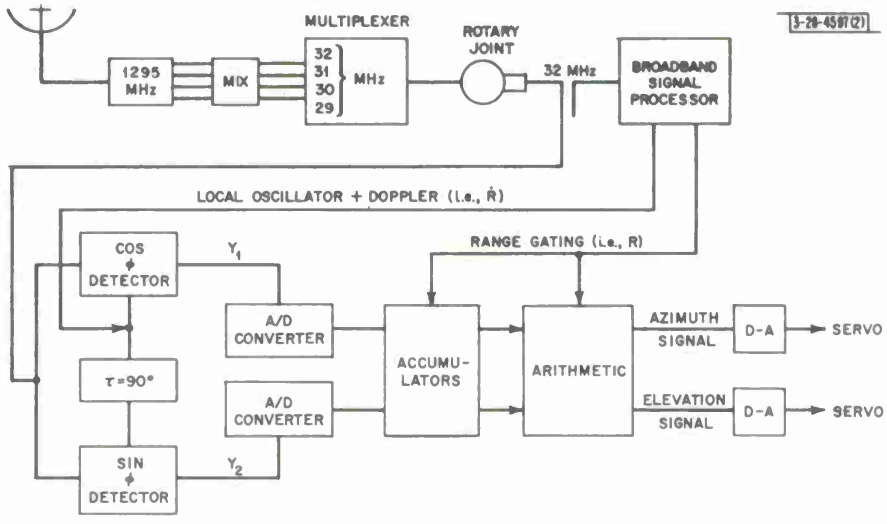


Fig. II-6. Digital monopulse tracking system.

Although the broadband multiplexed signal is quantized to only seven bits, the system should have sixty-nine decibels* of dynamic range when used at a 2-msec pulse length. The coherent digital filtering narrows the bandwidth from 4 MHz to 500 Hz, producing the wide dynamic range. Note that frequency multiplexing not only reduces the analog components and A/D converters required, but also accounts for 6 db of dynamic range due to the prefiltering noise bandwidth.

The complete DIGIMON has been built and checked out. The analog portion was constructed by W. W. Smith of Group 31. T. C. Bartee and M. I. Schneider of Group 22 provided the digital equipment, which embodies new developments in high-speed digital equipment. Both portions fully meet design specifications. The A/D converters, however, supposedly off-the-shelf items, do not perform properly at the required 4-MHz rate. Successful use of DIGIMON in the tracking radar system awaits solution of this problem.

Since failure of the original A/D units to perform according to expectations has temporarily halted work on integrating DIGIMON into the system, alternative means for accomplishing the precomputer digital data processing are under consideration. The most attractive alternative at present is the previously mentioned MACS. It is attractive because it can be put together with presently available equipment. A relatively simple version of MACS is now in use for lunar observations where the dynamic range and data rate requirements are both less than they would be in satellite tracking. Its disadvantages relative to DIGIMON are less dynamic range and dependence on an external analog system to derive error signals. Nevertheless, since the MACS principle is already in use for lunar and planetary radar studies and may yet be the best intermediate means of getting on with SIP, it is appropriate to include a description of it in this report.

MACS grew out of the Pettengill-Henry moon-mapping instrumentation[3] in which the outputs of sine and cosine phase detectors were encoded by means of sample-and-hold circuits and A/D converters. The digitized data were processed later for pulse-to-pulse coherence. This scheme has now been further developed to allow the simultaneous sampling of as many as eight analog signals which are then quantized sequentially by one A/D converter. MACS is presently used with the coherent planetary instrument known locally as the Cra-Fleck apparatus, named for the designers Craig and Fleck. The Cra-Fleck machine provides the extremely accurate range and Doppler corrections required for coherent planetary and lunar radar observations. A block diagram of the present MACS as used in planetary and lunar radar work is shown in Fig. II-7.

## D. APPLICATIONS OF SIGNAL INTEGRATION TO RADAR DETECTION OF ARTIFICIAL SATELLITES

The first use of signal integration techniques for the radar detection of man-made objects was made at Millstone in connection with the Lincoln Laboratory West Ford dipole belt communications experiment. The first attempt at forming a belt of orbiting dipoles was made in October 1961. The launch was successful but the dipoles failed to dispense. In an attempt to

* Arrived at as follows:

| | |
|---|---|
| By bandwidth reduction | +39 db |
| By 7-bit quantization | +42 db |
| Quantizing noise | −12 db |
| | 69 db |

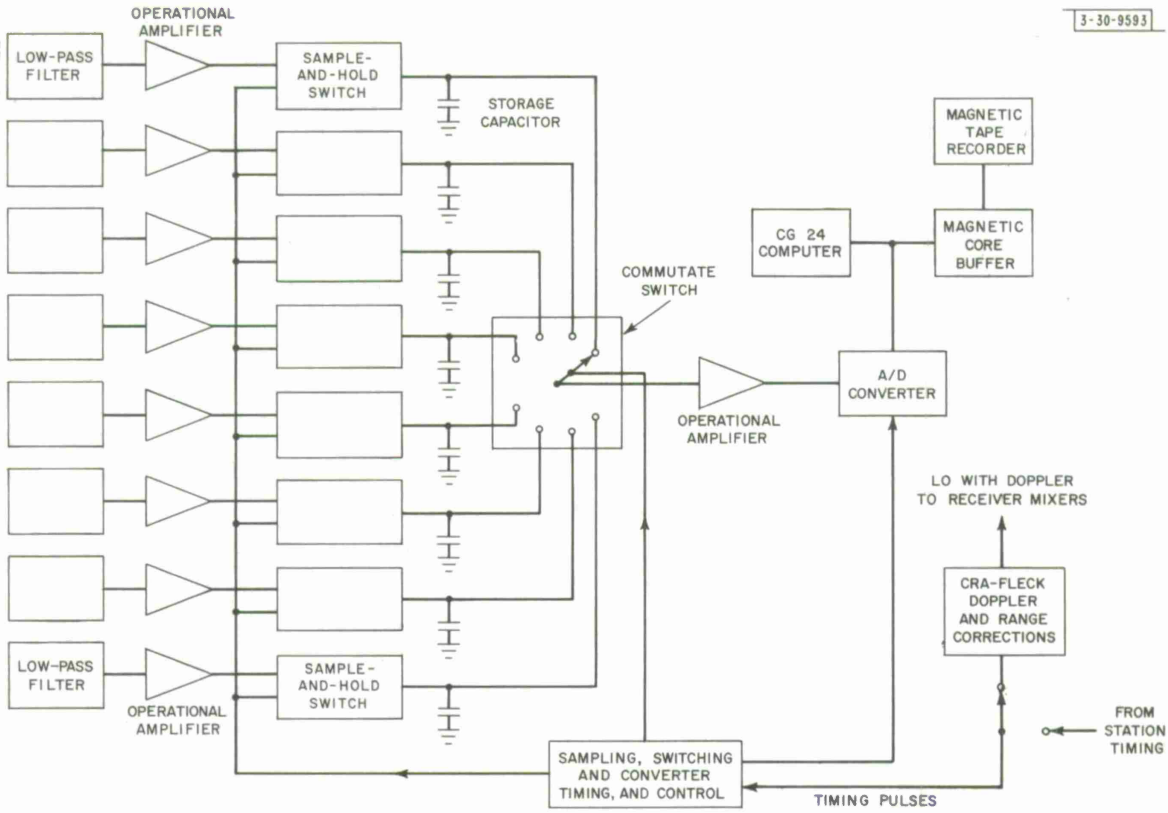


Fig. II-7. MACS.

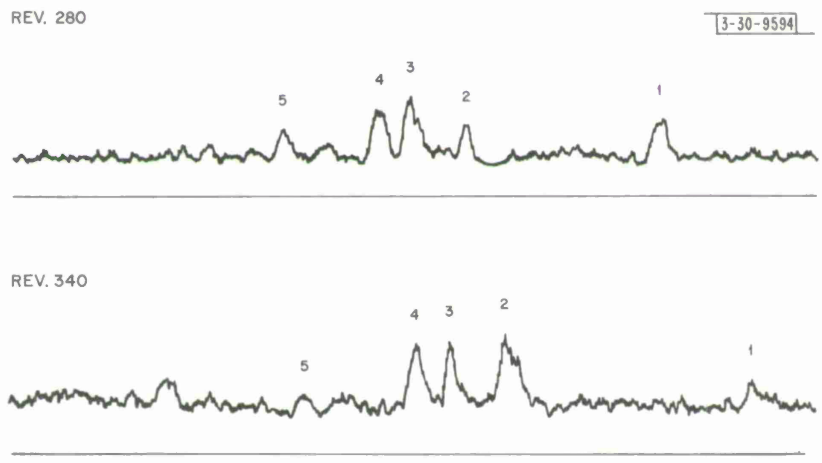


Fig. II-8. Weak targets in the orbit of the first West Ford launch detected in February 1962 with the Millstone UHF radar, using incoherent integration. (Integration period: 5 seconds.)

find out what happened, Millstone made a search of the orbit of the parent vehicle. The scheme employed was to hold the antenna beam on one point of the orbit for an extended time by constantly correcting the pointing and approximate Doppler for effect of Earth's rotation. In order to optimize the chances of detecting very small targets in the orbit, incoherent integration for periods approximating the flight time through the beam was employed. In this way, some ten targets were detected that were slowly separating from the parent vehicle and from each other along the orbit. The measured separation velocities provided the clues, later verified in Laboratory simulation tests, that the dispenser had not spun properly for dispensing the dipoles. Figure II-8 shows returns from five of these objects obtained on two passes, 60 orbits (about one week) apart. Each trace shows the receiver output after 5 seconds' integration in the CG 24 computer at a particular range. Elapsed time progresses in the direction indicated by the target numbers. Objects 1 and 5 have changed position along the orbit, both with respect to each other and with respect to the other three objects.

In another West Ford launch, six very light UHF tin dipoles were placed in orbit on 9 April 1962 to study charge drag effects. Millstone made the initial radar observations on these objects, using incoherent integration techniques to confirm that orbit had been achieved. In the meantime, RCA engineers at the FPS/49 tracker in Moorestown, New Jersey had been assisted in implementing this technique for their radar so that they could support the experiment after Millstone closed for the changeover to L-band. The results of the experiment were published in a paper by Shapiro, et al.[4]

The successful West Ford X-band dipole belt launched 10 May 1963 has been observed a number of times with the Millstone L-band radar during the past two years. A considerable number of very small targets have been detected which are slowly separating in angle, range, and Doppler from the region that produces X-band echoes. At present, it is conjectured that these L-band targets detected with signal integration techniques are parts of incompletely dispensed dipole packages, a result attributed to launch perturbations that altered the solar heating effects. Although these measurements have helped to clarify some events in connection with West Ford launches that might have otherwise remained unknown,[5] the purpose of discussing them here is to demonstrate the effectiveness of incoherent integration to extend the detection range for small targets. Some objects detected in this manner have apparent cross sections of less than one-tenth square meter. One of the latest of these L-band observations of the orbital plane of the West Ford X-band belt is shown in Fig. II-9. The range intervals are about 40 nm while the pulse width is 2000 μsec, equivalent to a range of 162 nm; hence, the same targets appear in several consecutive range intervals. In this case, the antenna was pointed in a westerly direction at an elevation angle of about 60° and data were recorded as the earth moved the radar beam through the plane of the orbit. The horizontal lines show average power received from different range intervals (or heights). Some 60 apparently discrete objects were observed flying through the beam, which they traversed in 5 to 10 seconds. The height of the observations varied from about 1000 nm (altitude of the X-band dipole cloud at this part of the orbit) to about 2000 nm (altitude of the launch vehicle). The Doppler settings, which also change with time, were automatically set by the radar tracking electronics in accordance with precomputed instructions. No echoes were observed from the X-band dipole cloud region itself.

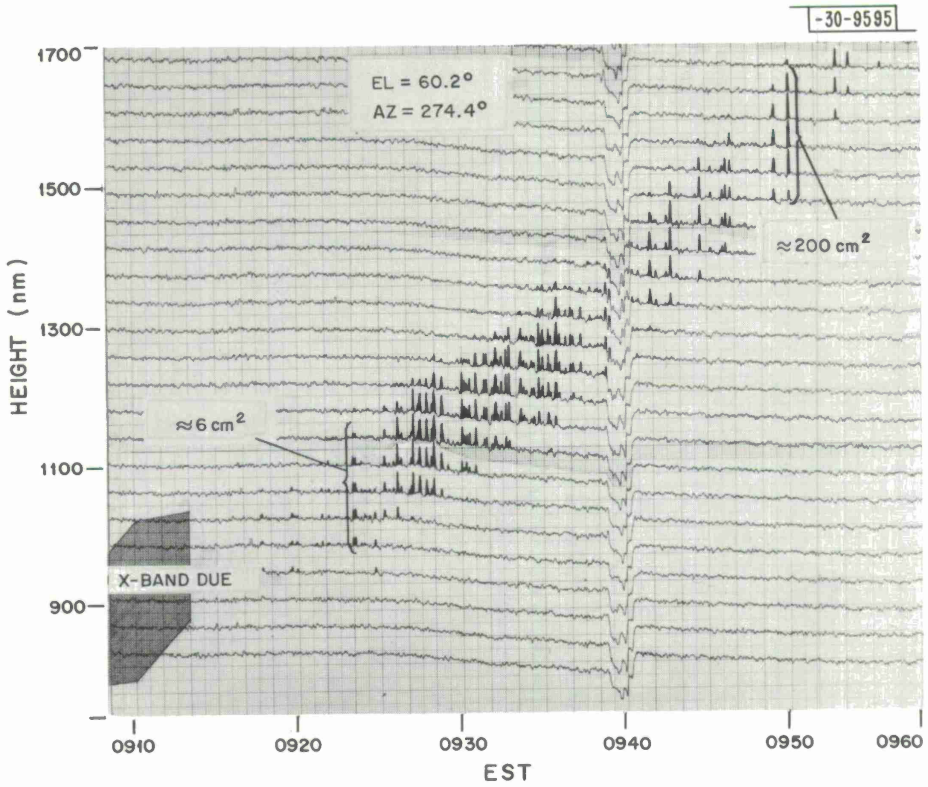


Fig. II-9. Millstone L-band observation of West Ford orbit, 3 November 1964.

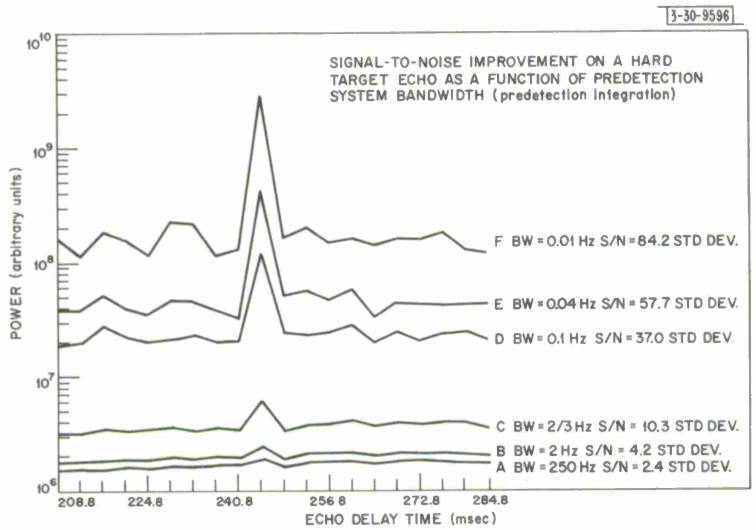


Fig. II-10. Coherent processing results. Syncom II echoes, Millstone L-band radar.

Detection by coherent integration of a distant artificial satellite was demonstrated with the Millstone L-band radar on Syncom II at a range of about 20,000 nm. The orbital elements of this satellite are so precisely known that very accurate pointing, Doppler, and acceleration corrections can be maintained for a long time. The satellite is also well stabilized so that it causes negligible phase dispersion of the echo. Thus the coherence interval extends over many pulses. Results of a coherent integration operation on Syncom II are shown in Fig. II-10. The digitized data were first recorded on magnetic tape and processed later in an IBM 7094 computer. The signal was cycled through computer-synthesized digital filters of progressively narrowing bandwidths until the point was reached at which further reduction produced little improvement of the signal-to-noise ratio. This optimum bandwidth is of the order of 0.05 Hz, corresponding to a coherence interval of the order of 20 seconds. Running the radar at its normal PRF of 15 pps would allow the coherent addition of 300 pulses to produce an improvement in S/N of about 25 db, enough to quadruple the maximum detection range of the radar. This experiment further demonstrated short term frequency stability of the Millstone system on the order of a few parts in $10^{11}$.

## E. RADAR RANGE EXTENSION TECHNIQUES

Methods of statistical signal processing have long been used at Millstone and other stations to receive weak signal returns buried in noise. These techniques have received little or no use in the tracking of artificial earth satellites, not because of any inherent difference in the methods used, but because of the different orders of magnitudes of the quantities involved.

The optimum method of pulling a weak radar signal out of the noise is to compare it by means of cross-correlation techniques against a replica of what one would expect it to be, taking advantage of all a priori information such as target range, range rate, acceleration, etc. For planetary observations, these quantities have been available from a backlog of optical observations made over centuries. Using these data, compiled by the U. S. Naval Observatory and others, an ephemeris is made up for the particular days, hours, and minutes to tell where to point the antenna and which values of range and range rates to search as a function of time. Even with the best available ephemerides, it has still been necessary to test the received signals at a reasonable number of different ranges and range rates.

The problems in searching for artificial earth satellites are the same, except that orbits may not be quite so well known, and angle and Doppler changes are faster. First an ephemeris* is needed. This is normally based on previous optical or radar observation or even on nominal launch parameters of the satellite. Space Track provides orbital elements of all the satellites in its catalog and regularly upgrades the orbital elements of all those of interest as new observations are obtained.

In order to generate our own ephemerides at Millstone and to update orbital parameters as soon as observations are made, the Laboratory has, as mentioned earlier, contracted with TRW Systems to adapt to the needs of real-time operation a program called ESPOD. This is a computer program that fits a set of current observations and past data to achieve a maximum likelihood orbital fit. It is one of several programs used at Space Track and is the most accurate available for high altitude satellites.

* We define this to be a table of predicted positions and velocities, in radar coordinates, as a function of time.

The method most used in obtaining data on weak planetary targets is coherent integration, which takes advantage of the large improvement in the signal-to-noise ratio obtainable from summing in phase the signal from successive received radar pulses. The improvement in signal-to-noise power is theoretically equal numerically to the number of pulses that can be added coherently, which is, in turn, dependent on the observation time available and the coherence interval of the target return. Thus, in applying this technique to artificial satellite observations, if one could coherently integrate 100 pulses* returned from a stable, nonscintillating target, a signal-to-noise improvement of 20 db over that from a single pulse should result.

Unfortunately, many artificial satellites exhibit scintillating radar returns owing to their shapes and motions, and the signal bandwidth resulting from this effect limits the coherence interval of such targets. Incoherent integration is still of value in these cases, but here, since the S/N improvement is related only to the square root of the number of pulses, a 100-pulse integration would yield only a 10-db improvement.

An analysis was made of the problem of acquiring the Lincoln Experimental Satellite.† For this satellite at 12,000-nm range with assumed errors in injection velocities of 10 percent, one might get uncertainties of 4 kHz in Doppler, 500 nm in range, and 6 $Hz^2$ in acceleration. Coherent integration over 8 seconds in time requires

| | | |
|---|---|---|
| | 16 coarse frequencies at | 250 Hz spacing |
| × | 64 fine frequencies | 1/8 Hz |
| × | 16 accelerations | 0.4 $Hz^2$ |
| × | 4 ranges | 150 nm |
| = | 64,000 hypotheses | |

This corresponds to a data processing rate over two orders of magnitude higher than the current rate used in planetary processing. A study was conducted this summer to determine the practicability of achieving these computation rates, using the higher-speed computer now available at the site and certain techniques for Fourier analysis under development here and by others.[6] Portions of the actual program were prepared and run to assist in predicting running times, with the result that it now appears possible to solve the problem outlined above, essentially in real time.

When interfacing of the SDS 9300 with the radar and the Millstone orbital programs are complete, implementation of a real-time coherent integration range extension method will begin in earnest. The goal will be a radar having a 10,000-mile tracking capability on a one-square-meter target.

* At typical Millstone PRF this would represent nearly 7 seconds of data.

† The acquisition problem is the difficult part. Once the satellite is actually acquired and the correct range and Doppler are ascertained, a relatively simple locked-oscillator system may be used for maintaining track.

## REFERENCES


1. E. Gehrels and A. Parsons, IRE Trans. Mil. Electron. MIL-5, No. 2, 139 (April 1961).
2. M. Schneider and N. T. Gaarder, Group Report No. 1964-11, Lincoln Laboratory, Lexington, Massachusetts (1964) DDC 430297, H-561.
3. G. H. Pettengill and J. C. Henry, in The Moon, Ed. by Z. Kopal and Z. K. Mikhailov (Academic Press, London, 1962), p. 519.
4. I. I. Shapiro, I. Maron, and L. G. Kraft, J. Geophys. Res. 68, No. 7 1845 (April 1963).
5. D. MacLellan, et al., Proc. IRE 62, No. 5, 564 (May 1964).
6. J. W. Cooley and J. W. Tukey, Math. Comp. 19, 297 (April 1965).

# III. RADIO ASTRONOMY

## A. INTRODUCTION

Radiometric observations with the Haystack* antenna began in December 1964. The first objective of these observations was the evaluation and calibration of this new system. This included radiometer calibration, measurement of the background antenna temperature, determination of the antenna efficiency, measurement of antenna patterns, calibration of the antenna pointing, and evaluation of effects of the radome. By the end of March 1965, these initial measurements were far enough along to begin some astronomical observations. Measurements to improve the pointing and gain calibrations have continued, but the observing time devoted to them has decreased, while that devoted to astronomical observations has increased.

Concurrent with the observing program at 8 and 15.5 GHz, equipment for spectral-line observations of H and OH and an additional radiometer at 5 GHz have been constructed.

During this time, three computer programs were being written: a program for automatic measurements on discrete radio sources, a program for drawing contour maps of extended radio sources, and a program for obtaining spectra from the digital autocorrelator, which is an essential part of the spectral-line radiometer.

Massachusetts Institute of Technology and Harvard College Observatory have provided very valuable assistance in programming, in the pointing calibration, and in construction of radiometric equipment for the Haystack system. This assistance comes as a result of arrangements under which portions of our radio astronomy program are planned and carried out jointly with scientists from these locations.

In the following sections, the Haystack radiometric equipment will be described, followed by a summary of the antenna evaluation and a description of two of the computer programs.

## B. HAYSTACK RADIOMETRIC EQUIPMENT

The Haystack radiometric system contains equipment for receiving the noiselike signals emitted by the atmosphere, the moon, the sun, the planets, and many galactic and extragalactic sources of radiation. A block diagram of the system is shown in Fig. III-1. The RF portion of this equipment is housed in an 8 × 8 × 12-foot equipment box which can be installed on or removed from the antenna in approximately one hour. The equipment box can also be used with a standard-gain cornucopia horn antenna for testing and calibration purposes; this configuration is pictured in Fig. III-2. A portion of the radiometric system which is housed in the Haystack control room is shown in Fig. III-3.

The radiometric system has incorporated several concepts and devices which are new to radio astronomy. The following is a list of areas where novel approaches have been taken:

*The Haystack Research Facility is described in Appendix B.

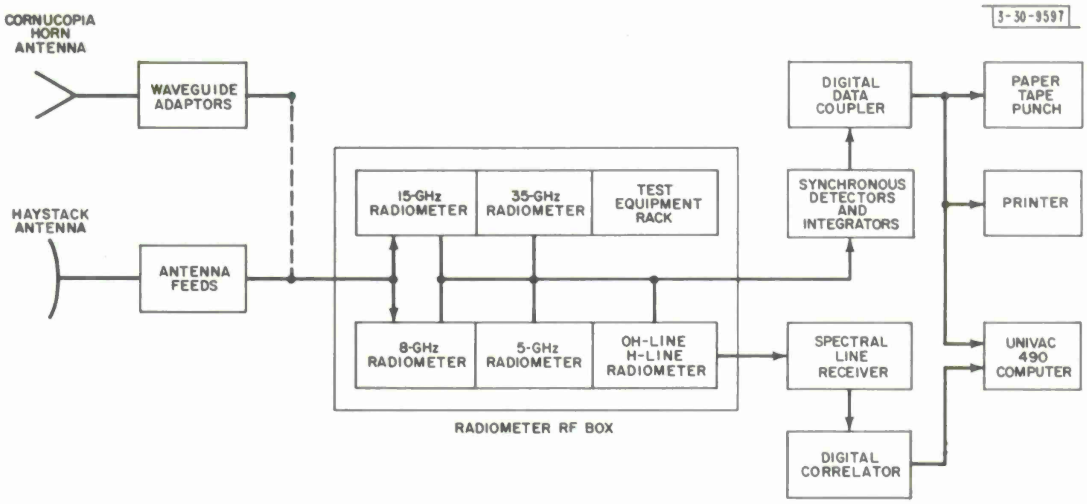


Fig. III-1. Haystack radiometric system.

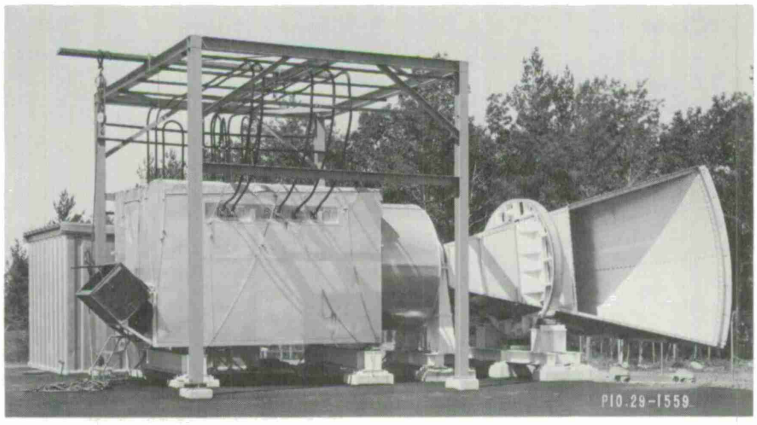


Fig. III-2. Radiometer box installed on cornucopia standard-gain antenna.

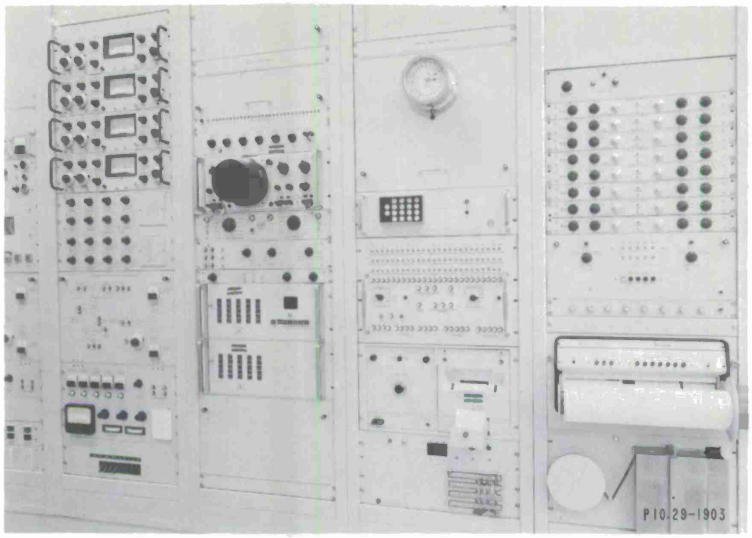


Fig. III-3. Radiometric equipment racks, Haystack control room.

(1) Wide-band tunnel-diode amplifiers have been used for the input amplifiers in the 5-, 8-, and 15.5-GHz radiometers. Since radiometer sensitivity is proportional to the system noise temperature divided by the square root of the RF bandwidth, a tunnel-diode receiver with 1000° system temperature and 1000-MHz bandwidth is equivalent for radiometric use to a maser or paramp receiver with 100° system temperature and 10-MHz bandwidth (provided interference does not limit the usable bandwidth). The reliability, stability, and absence of cryogenic equipment makes the tunnel-diode approach very attractive.

(2) The large plug-in antenna box concept at Haystack makes it possible easily to maintain and change over front-end equipment. The flexibility of the system with regard to change of operating frequency is unmatched at H-line and above.

(3) A precision square-law detector, synchronous detector, and integrator system have been designed for use with high accuracy digital processing. The synchronous detector and integrators are solid state and have a drift which is 0.01 percent of maximum output. These devices are especially designed for radio astronomy operation and should find use at other installations.

(4) A very flexible data coupling system has been incorporated. Any combination of seven 30-bit digital data sources and sixteen analog data sources may be fed into the computer, a paper-tape punch, or a printer at a fast buffered rate. In addition, a batch of fifty pieces of analog data representing monitor points in the system can be fed into any of the above devices at a low unbuffered rate.

(5) The U490 computer which is regularly used for Haystack antenna pointing is used simultaneously for real-time processing of radiometric data. The computer programs now in use are discussed in the following section.

(6) The spectral-line receivers utilize the accurate and versatile 1-bit digital autocorrelation method of spectral analysis. A 100-channel, 10-MHz clock rate correlator has been incorporated in the system. A 40-channel system of this sort was in use at Millstone when the OH-line was discovered in 1963.

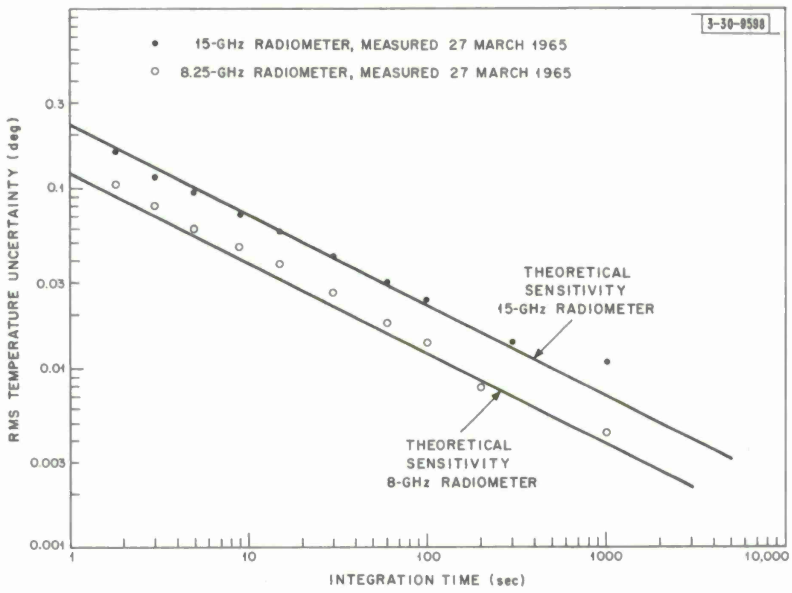


Fig. III-4. Theoretical and experimental radiometer sensitivity.

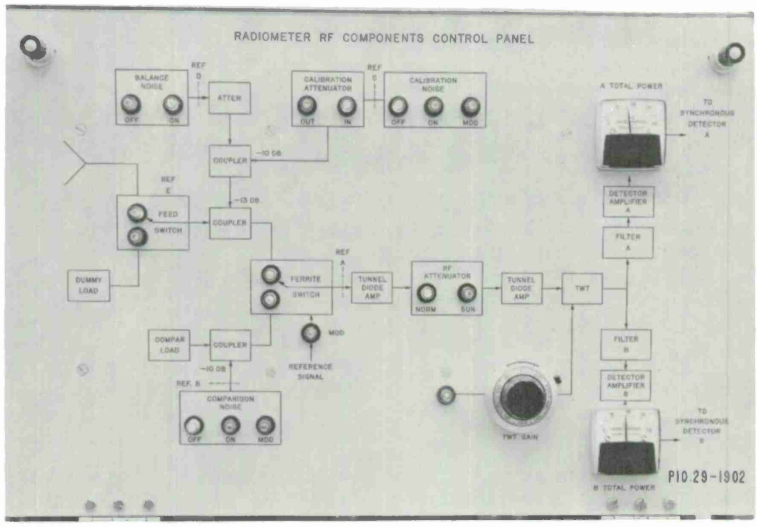


Fig. III-5. Radiometer RF components control panel.

The 8- and 15-GHz radiometers have been operational for about one year and have performed quite satisfactorily. Curves indicating the measured and theoretical sensitivities of the radiometers are given in Fig. III-4. (The measurements for this figure were taken by R. J. Allen of M. I. T. Research Laboratory of Electronics.) The 5-GHz radiometer has been completed but has not yet been used with the antenna.

The 5-, 8-, and 15-GHz radiometers have essentially the same block diagram, which is shown in Fig. III-5. This diagram is engraved on the control panel shown in the photograph. The round buttons in each block are combination push buttons and indicators which are used for control and monitoring of the element represented by the block.

In normal operation, the feed switch is in the "antenna" position, the comparison noise source and calibration noise source are "off," the balance noise source is "on," the ferrite switch is modulated at a 40-Hz rate, and the RF attenuator is in the "normal" (no attenuation) position. The ferrite switch is then switching the receiver input between the comparison load (a thermally insulated termination at 300°K) and the antenna with balance noise (~300°K) added. A 40-Hz signal whose amplitude is proportional to antenna temperature is thus produced at the detector output, where it is amplified, synchronously detected, and integrated over periods between 0.3 and 30 seconds.

The basic receiver is of the tuned radio-frequency (TRF) type, including a 4-stage tunnel-diode amplifier followed by a single traveling-wave-tube amplifier. The TWT state is needed because the maximum linear output of present tunnel diode amplifiers is not quite enough to drive properly the diode detectors. The characteristics of the amplifier chain are: 60-db gain, 1000-MHz bandwidth, and system noise temperatures of 1000°K at 5 and 8 GHz, and 2500°K at 15 GHz. The output of the amplifier chain is divided into two 500-MHz bandwidth bands (for interference detection purposes) before detection. The detectors are operated at approximately −25-dbm input power. At this power level, the detector noise is negligible and good square-law operation is obtained; furthermore, the detector load resistor is chosen for best square-law operation. The detector DC output of 6 mv is amplified to one volt before it is sent to synchronous detectors and integrators in the control room.

The link between the radiometers and the data recording system is the synchronous detector-integrator shown in Fig. III-6. This unit was designed for operation on radiometer signals which are to be digitally processed. Most commercial synchronous detectors are designed for analog recording or display purposes and have drift and noise which is of the order of 0.5 percent of maximum output. The design goal of the Lincoln Laboratory unit is drift and noise levels which are 0.01 percent of maximum output. This is a worthwhile goal because the post-integration signal-to-noise ratio on strong sources observed with Haystack will approach 10,000 to 1 and the A/D conversion equipment has an accuracy of 0.01 percent. In addition, such a wide dynamic range synchronous detector makes scale changes unnecessary and simplifies observations.

The synchronous detector contains both an RC integrator for analog pen recorder display and a true finite-time integrator for digital recording equipment. The true integrator is sampled by a high-speed A/D converter at the conclusion of the integration period, which can be varied between 0.3 and 30 seconds. The high-speed A/D converter can be used to sample many true integrators. This is a more flexible and economical approach than the method commonly used in radio astronomy of using an integrating A/D converter for each radiometer channel. The


Fig. III-6. Radiometer system, synchronous detector panel.

synchronous detector contains a post-detection gain modulator which is an innovation to radiometry. Like the more common pre-detection gain modulator, this feature greatly reduces the effect on the radiometer data of gain drift in the radiometer amplifiers. Circuitry, however, is more tractable. The synchronous detector is all solid state, utilizing approximately 75 transistors.

A block diagram of the radiometer data-handling system is shown in Fig. III-7; the data control panel is shown in Fig. III-8. Data are collected in two types of scans: the data scan, which is for the main radiometer data, and the auxiliary scan, which is for monitor data. In the data scan, 16 sources of analog data are multiplexed into an A/D converter and the analog voltages are converted into 17-bit digital numbers. In addition, seven sources of digital information are scanned. The 23 words of data are collected in 23 msec and stored in a circulating delay-line memory. Any combination of these 23 data words can then be fed into either a printer, a paper-tape punch, or the Univac 490 computer as selected by the toggle switch banks on the panel shown in Fig. III-8. A new data scan is initiated periodically at intervals between 0.1 and 100 seconds as selected with a switch. In normal operation, the analog information collected in a data scan would consist of synchronous detector outputs and the digital information would consist of such quantities as system status, sidereal time, and feed polarization.

The auxiliary scan consists of a stepping-switch scan of up to 50 sources of analog monitor data. This information is converted in the same 17-bit A/D converter as the analog data scan data (for clarity, two A/D converter blocks are shown on the block diagram). The batch of data can be fed into either the printer, paper-tape punch, or computer. The auxiliary scan is slow (a few seconds) and is not buffered. Each piece of data must be accepted by all the selected output devices before the stepping switch can proceed to the next position. The auxiliary scan can be initiated by manual push button or after every 1, 10, 100, or 1000 data scans.

A similar block diagram control panel for the spectral-line radiometer is shown in Fig. III-9. This system has been completed and tested, and is in initial use for investigations of the galactic OH- and H-lines. It will also be used in attempts to detect other spectral lines. A 1-bit autocorrelation-function method of spectral analysis is used.* With this technique, bandwidths of 4 and 1.2 MHz and 400, 120, and 40 kHz can be analyzed with a resolution that is one-fortieth of the total bandwidth.

* S. Weinreb. "A Spectro Analysis Technique and Its Application to Radio Astronomy," Technical Report 412, Research Laboratory of Electronics, M.I.T. (30 August 1963).

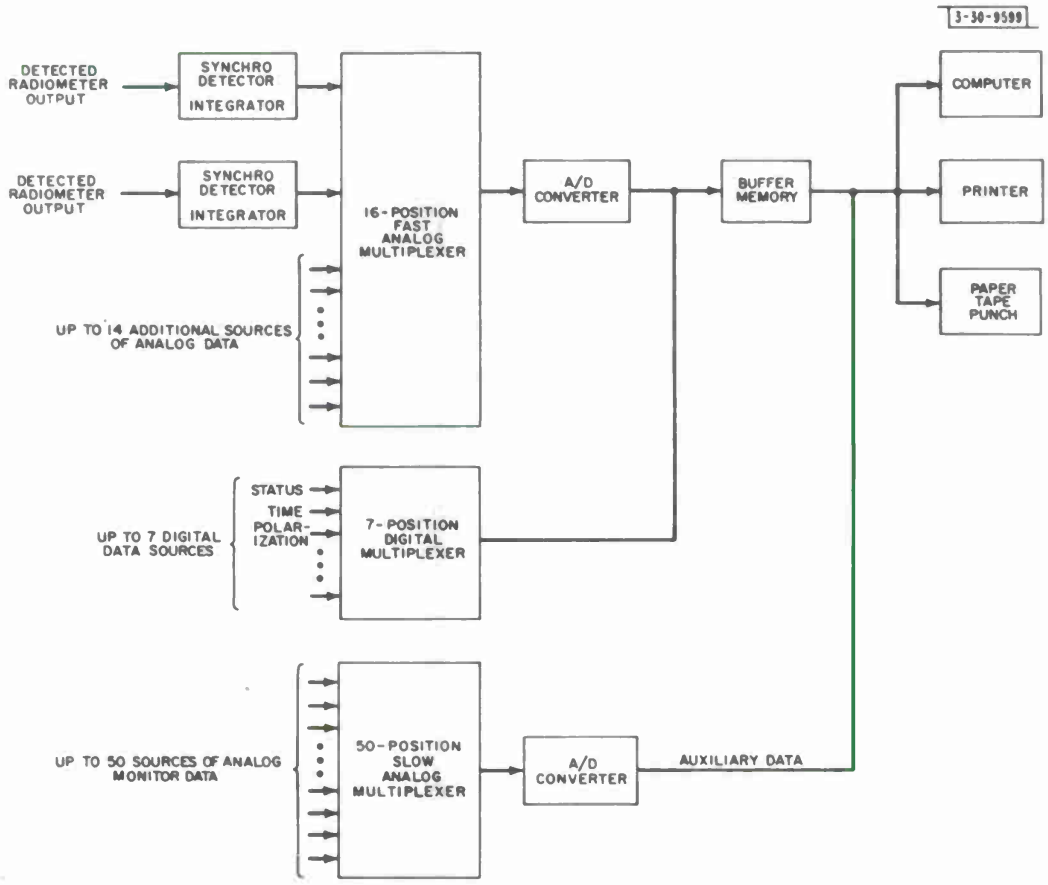


Fig. III-7. Radiometer system, data handling block diagram.

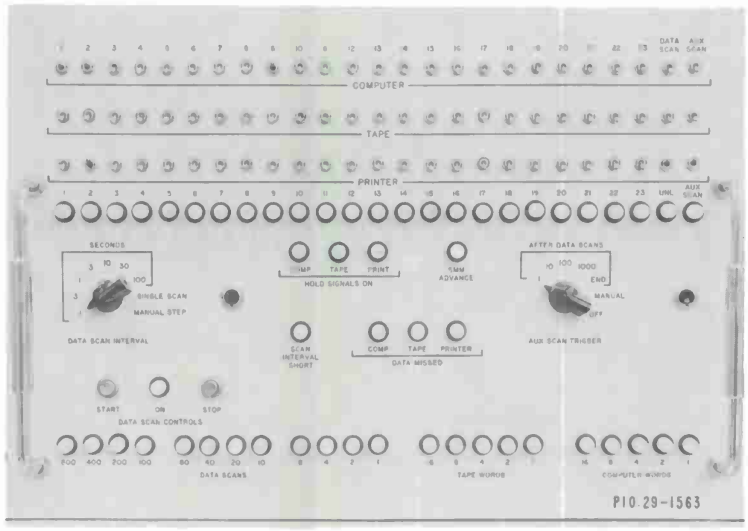


Fig. III-8. Radiometer system, data control panel.

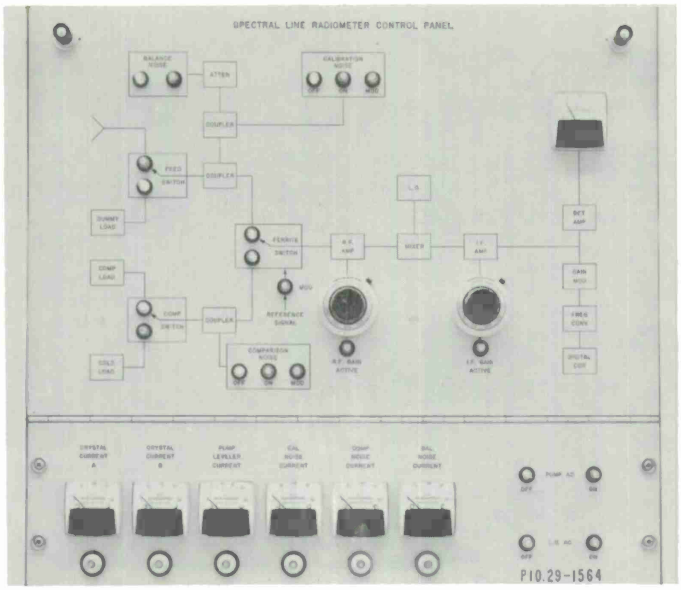


Fig. III-9. Spectral line radiometer control panel.

The OH-line (1667 MHz) front end for the spectral-line receiver utilizes an uncooled parametric amplifier which was constructed by Airborne Instruments Laboratory. The amplifier has a noise temperature of 80°K which is achieved by using a high pump frequency (26.3 GHz). A feedback loop has been designed to stabilize the gain of the amplifier. The quantity which is stabilized by the loop can be switch-selected to be one of the following: (1) a sample of the pump power going into the parametric amplifier; (2) the varactor bias current (which is a function of bias current); or (3) a gated total power output from the radiometer. We will determine experimentally which stabilization method is best for actual operation.

## C. HAYSTACK ANTENNA EVALUATION

### 1. Radiometer Calibration

Before the calibration and evaluation of the Haystack antenna began, the radiometers were calibrated very carefully. The equivalent temperatures of the calibration noise sources at 8 and 15.5 GHz were determined by comparison with: (a) standard noise sources (Bendix) with calibration traceable to the National Bureau of Standards, and (b) terminations immersed in liquid nitrogen. The agreement between these two methods was within 4 percent or less on all channels, and the mean values were adopted for the calibration-signal temperature.

All temperature measurements are referred to a waveguide reference plane about 6 feet from the feed output flange. Losses between the reference plane and the feed output flange have been measured, and our results are corrected for this loss. The antenna temperatures and efficiencies are referred to signals measured at the feed output flange.

### 2. Background Antenna Temperatures

The background noise temperature of the antenna results from thermal radiation picked up through antenna sidelobes, reflection of ground radiation by the radome, and resistive losses in the radome and feed. The amount of thermal radiation picked up is a function of elevation

angle. Determination of background noise vs elevation is of considerable importance in evaluating the antenna performance, and this was measured for both the Haystack and the cornucopia antennas. At 15 GHz, two types of antenna feeds have been used to illuminate the Cassegrainian secondary of the Haystack antenna: a small disk of the Clavin type, and a simple horn. These two feeds give quite different antenna background temperatures. At 8 GHz, only the Clavin feed has been used for this type of measurement.

Figure III-10 shows the results of these antenna background temperature measurements. Temperature contributions due to waveguide losses, rotary-joint losses in the Clavin feeds, and feed mismatch have been removed from the data represented in this figure. However, the contribution due to the atmosphere is included. These measurements were made on an average clear winter day. As long as the sky remained clear, the antenna temperature varied little from day to day. For example, the 8.25-GHz zenith antenna temperature for the Haystack antenna varied within ±2°K on all the clear days during the calibration. During rain or snow, however, the zenith antenna temperature increased appreciably.

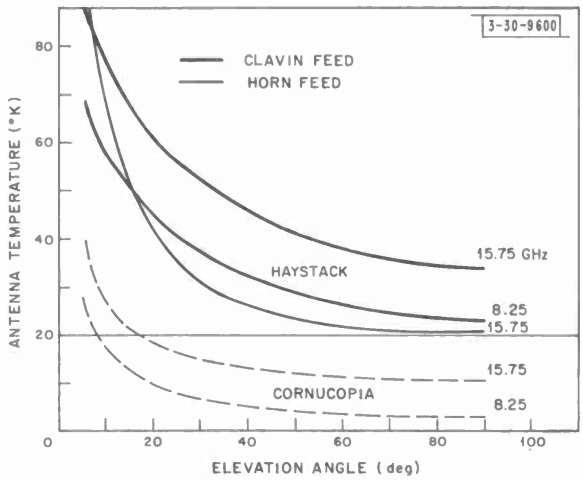


Fig. III-10. Antenna temperatures for Haystack and cornucopia antennas.

### 3. Antenna Efficiency

Initial measurements of the antenna efficiency were based on measurements of Jupiter and the radio sources Taurus A, Cygnus A, and Cassiopeia A at 8.25 and 15.75 GHz with the Clavin feeds. These measurements are uncertain because the mean brightness temperature averaged over the disk of Jupiter is not precisely known. Further, since the other sources are not small compared with the antenna beamwidths, the measured antenna temperatures must be corrected for source size. Two simple models are available for these corrections. These models assume a Gaussian beam shape with either a Gaussian source-brightness distribution or a uniform disk brightness distribution. If the source width $\varphi_s$ is comparable with the antenna beamwidth $\varphi_a$, the measured antenna temperature will be reduced by a factor $\alpha$ from that which would be measured with a point source of the same flux. The reduction factor is given by

$$\alpha = \varphi_a^2 / \varphi_n^2 \quad , \tag{1}$$

TABLE III-1

MEASURED EFFICIENCY OF HAYSTACK CLAVIN FEEDS
(Listed in Order of Decreasing Certainty)

| Measured Efficiency $\eta$ (percent) | Source | Measured Temperature $T_a$ (deg) | Measured Width $\Phi_m$ (minutes of arc) | Source Width $\Phi_s$ (minutes of arc) | Width Factor $\alpha$ | Assumed Flux S | Remarks |
|---|---|---|---|---|---|---|---|
| | | | 8.25 GHz | | | | |
| 35.8 | Jupiter | 1.1 | 4.2 | 0.59 | 1.0 | (disk) 170°K | Assumed brightness temperature |
| 33.0 | Taurus A | 41.6 | | 3.5 | 0.58 | 580 | Flux in units of $10^{-26}$ watt $m^{-2}$ $(Hz)^{-1}$ |
| 27.0 | Cygnus A | 19.5 | | $1.6 \times < 0.3$ | 0.93 | 207 | |
| 34.5 | Cas A | 42.8 | | $3.8 \times 4.2$ | 0.55 | 600 | $\alpha$ based on published $\Phi_s$ |
| 27.0 | Cas A | 42.8 | 5.0 | | 0.70 | 600 | $\alpha$ based on measured $\Phi_m$ |
| | | | 15.75 GHz | | | | |
| 13.2 | Jupiter | 2.1 | 2.1 | 0.73 | 0.96 | (disk) 160°K | Assumed brightness temperature |
| 14.9 | Taurus A | 9.1 | 3.6 | | 0.34 | 485 | Flux in units of $10^{-26}$ watt $m^{-2}$ $(Hz)^{-1}$ |
| 11.3 | Cygnus A | 3.2 | | $1.6 \times < 0.3$ | 0.79 | 96 | |
| 20.0 | Cas A | 5.5 | 4.4 | | 0.23 | 320 | $\alpha$ value doubtful |

where $\varphi_n$ is the apparent width of the source when measured with a beamwidth $\varphi_a$. The published values for the flux of the bright radio sources are probably accurate to ±10 percent. The temperature measurements are probably accurate to ±3 percent or 0.1°K, whichever is greater. The correction factor $\alpha$ was calculated through Eq. (1) with measured values of $\varphi_a$ and either measured values of $\varphi_n$ or published values of $\varphi_s$.

Our results are summarized in Table III-1. The efficiency values are listed in order of decreasing uncertainty, and the efficiency is referred to the output of the feed.

The most certain efficiency measurements were obtained with the planet Jupiter. The correction factor $\alpha$ is very nearly unity. The temperature of the planet has been measured at microwave frequencies and at infrared frequencies, and there is strong evidence that the value is between 140° and 180°K from 8 GHz through the infrared.

In summary, these measurements indicate that the overall Haystack antenna efficiency (including the radome) with the Clavin feeds at 8.25 GHz is 32 ± 6 percent and at 15.75 GHz is 15 ± 5 percent.

Antenna temperature measurements on Cassiopeia A were subsequently made with a multimode horn feed on the radar/communications box. These measurements give by comparison an efficiency of 46 percent at 7.75 GHz. A simple horn feed was then constructed for the radiometer box, and comparative measurements with the horn and Clavin feeds at 15.75 GHz were made on the radio source 3C273. These measurements showed a 2-db increase in the measured antenna temperature of this source with the horn feed, thus indicating an efficiency of 23 percent at 15.75 GHz.

It is possible to determine the efficiency more accurately by obtaining better flux values with the radiometer box on the cornucopia antenna and combining these data with integrals of the antenna temperature obtained from radiometric maps of the sources. These measurements are currently under way.

### 4. Antenna Patterns

In order to measure the antenna patterns, test transmitters were located on Pack Monadnock mountain, 25.9 miles from Haystack at azimuth 308.566. At this distance, the transmitter is not quite in the far field of the antenna, but the subreflector can be moved remotely to permit defocusing from infinity to the range of the transmitter.

The 7.75-GHz pattern transmitter operated on an antenna with 2° beamwidth and circular polarization. The 15.75-GHz antenna had a 13° beamwidth and vertical polarization. Both receiving feeds had vertical polarization.

Before measuring the antenna patterns, the focusing was checked by comparing the relative on-axis gain of the antenna for various subreflector positions. The azimuth antenna patterns for Haystack at 7.75 and 15.75 GHz are shown in Figs. III-11(a-b). Both patterns appear approximately as expected with regard to beamwidth and sidelobe level.

### 5. Pointing and Tracking Errors

The requirements for pointing accuracy with the Haystack antenna are set by the width of the antenna beam. At 8 GHz, the beamwidth between half-power points is 4.2 minutes of arc

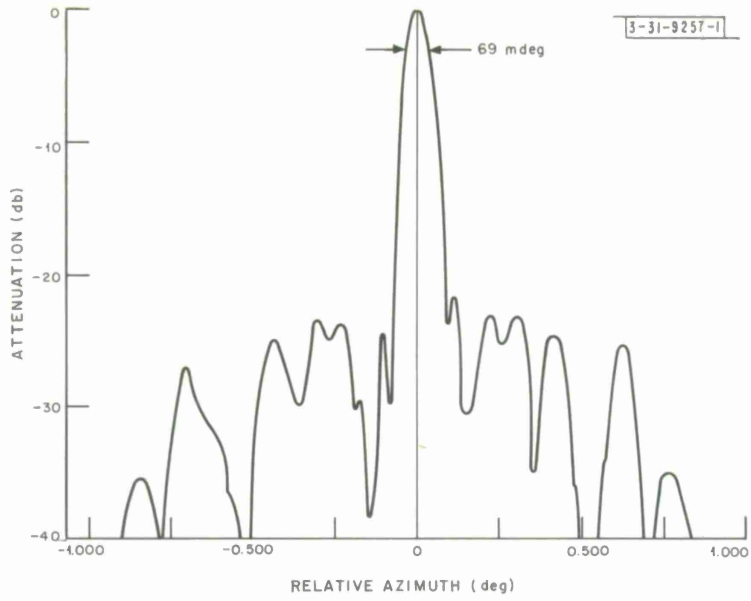


(a) 7.750 GHz.

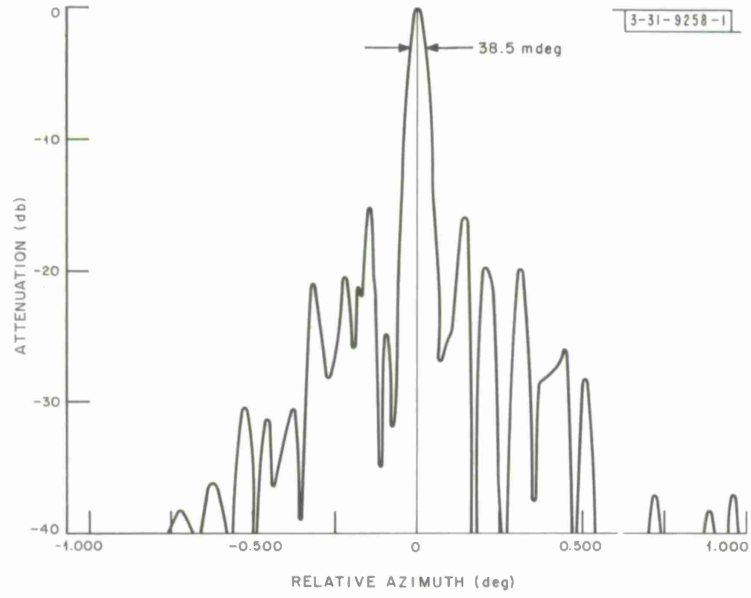


(b) 15.745 GHz.

C31-993

Fig. III-11. Haystack antenna pattern.

(or 70 millidegrees),* and a reasonable goal for pointing accuracy is ±25 seconds of arc (or ±7 mdeg). This accuracy is about one-tenth beamwidth and is sufficient to keep the gain reduction caused by pointing error at a value less than 3 percent. In other words, the accuracy should be sufficient to permit pointing at precisely known celestial coordinates for long integration periods when the objects themselves are not immediately detectable.

In one test of Haystack pointing capability, the procedure outlined below was followed. The antenna pointing system was given the command to track the source Cassiopeia A. The bias control wheels for azimuth and elevation were adjusted to put the center of the beam on the center of brightness of the source. Then the command was given for the antenna to scan slowly back and forth across the center of the source. The scan was halted on the side of the source, and the tracking was continued in this fashion while radiometer records were taken. Separate records were made, first with the source off-side in azimuth, then in elevation. Figures III-12 (a-b) show graphically the sort of data obtained. The fluctuations apparent in these records represent the more or less random wander of the servo system in azimuth and in elevation, respectively, while the computer is directing the antenna at sidereal rates.

These tracking runs were of sufficient duration for antenna motion to make an appreciable change in the pattern of the radome space frame in front of the dish. The data do not appear to reflect any appreciable "squint" in the antenna beam due to radome effects. The mean level of the signal is a sensitive indicator of the mean position of the beam relative to the source.

With this evidence that there are no appreciable small-scale variations in the beam position due to the radome, the problem of pointing calibration essentially involves repeated measurements on radio sources at many points in the sky.

The three brightest radio sources, Cassiopeia A, Cygnus A, and Taurus A, were used for these calibrations. Cassiopeia A is circumpolar, covering the azimuth interval 315° through 0° to 45°, and Taurus A covers the interval 70° to 290°. Cygnus A passes within 2° of the zenith and covers the whole range of elevation angles. All these sources have angular sizes of the order of 3 or 4 minutes of arc. Accurate positions of the centers of these sources have been measured with the Cal Tech interferometer,† consisting of two 90-foot steerable paraboloids. However, the Cal Tech measurements were made at a frequency of 960 MHz, and there is no assurance that the center of brightness, as found by Haystack, might not differ by as much as a minute of arc. If these bright sources are to be used for pointing calibration, it is necessary to verify or correct the source positions as well as determine the instrumental pointing corrections. It is possible to accomplish both these tasks, if two conditions are satisfied: (1) the azimuth coordinate must be precisely calibrated to an undetermined constant bias; and (2) the azimuth axis of the instrument must be precisely vertical, or any deviation must be known precisely, so that it can be taken into account. For the initial calibration of Haystack, we used azimuth calibration data based on optically measured shaft positions. The accuracy of this calibration is estimated to be about ±2 mdeg. The azimuth axis was aligned when the antenna was assembled, and the axis is believed to be within 3 mdeg of vertical.

---

*Millidegrees (mdeg) is used here rather than milliradians or minutes and seconds of arc because the digital angle pickoffs of the antenna utilize decimal fractions of a degree. (1 mdeg = 3.6 sec arc.)

†R. B. Read, Astrophys. J. 138, 1 (1963); E. B. Fomalont, T. A. Matthews, D. Morris, and J. D. Wyndham, Astron. J. 69, 772 (1964).

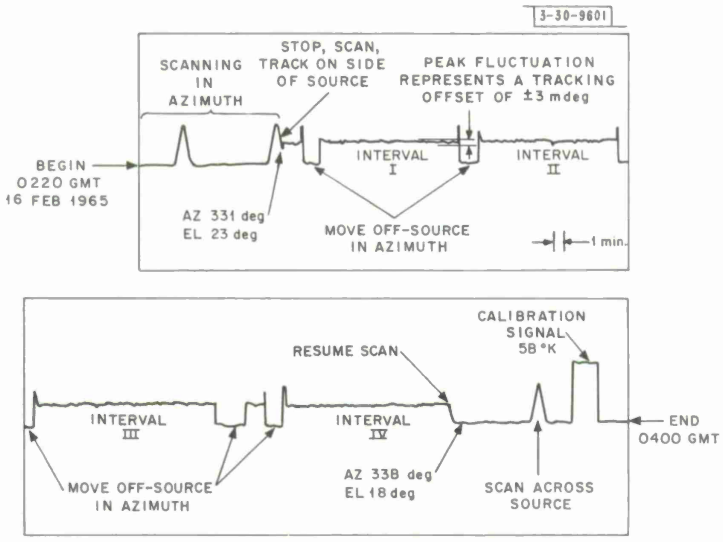


(a) Azimuth.

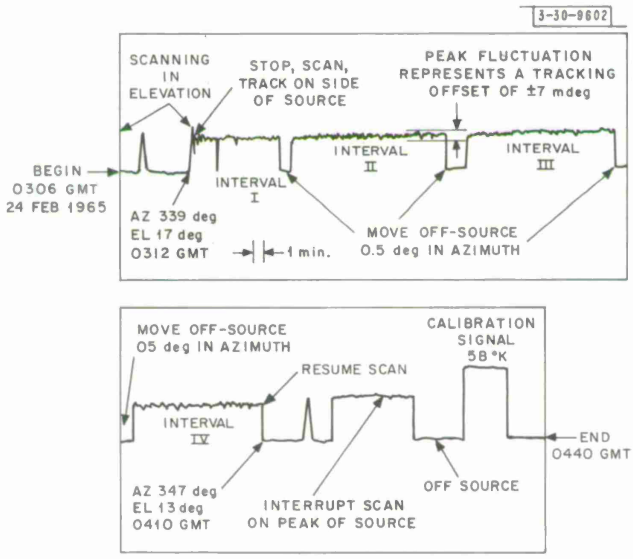


(b) Elevation.

Fig. III-12. Scan and tracking run with elevation offset radio source (Cassiopeia A).

The procedure for instrumental calibration and correction of apparent source position is to plot azimuth error against elevation angle or azimuth angle. The pattern formed by these points can be interpreted in terms of a combination of source position error and instrumental errors. For a given source, the separation of these effects is not completely unique, but the requirement for consistency in the instrumental error from source to source makes this procedure feasible. The upper half of Fig. III-13 shows the uncorrected azimuth errors for Cassiopeia A plotted against elevation angle. The pattern of these errors is a tilted ellipse. Azimuth errors characteristic of various source position errors can be obtained easily from the pointing program on the Univac 490. When the best estimate of the apparent source position is taken into account, one obtains the plot shown in the lower half of the figure. Here the data points show a constant bias of about 30 mdeg, roughly independent of azimuth. Following these corrections for Cassiopeia A and similar ones for Taurus A and Cygnus A, the elevation errors were examined. Figure III-14 shows the pattern of these points. (Refraction corrections have been made by the pointing program and thus do not appear in these data.) Data in this figure include cases in which the source was rising and setting. The spread in elevation-error data is within ±5 mdeg. The slope of the elevation-error data is such that the correction increases as the elevation increases. Hence the antenna beam does not sag lower at lower elevations, but moves slightly upward instead. This is probably due to a slight movement of the subreflector under gravitational forces. This effect appears to be elastic and reproducible, and consequently it can be compensated for in the pointing program.

The azimuth-error data as a function of azimuth still show evidence of some remaining position errors and possibly axis-alignment errors. However, the spread of azimuth errors is such that 95 percent of the points lie within ±7 mdeg. The pattern of the azimuth-error data points indicates that the calibration can be improved, perhaps by a factor of two, when the remaining systematic errors can be taken into account.

The source positions used for the pointing calibration are shown in Table III-2. For comparison, this table also includes the positions determined by Cal Tech at 960 MHz. All these positions are with reference to the epoch of 1950.0.

### 6. Polarization Measurements

The existence of a polarized radio source, Taurus A, whose properties have been measured previously, makes it possible to measure some aspects of the polarization performance of a large antenna. On the basis of measurements by Mayer, McCullough, and Sloanaker* at NRL at wavelengths of 3.15 cm and 3.47 cm, one would expect that Taurus A at 8 GHz would show a linearly polarized component on the order of 7 percent. The plane of this polarization would be expected to be oriented at a position angle of 140° ± 2° measured from north toward east on the celestial sphere.

The polarization measurements made on Taurus A at Haystack were performed as follows:

(a) The plane of polarization received by the radiometer was rotated in steps of 45° by turning the waveguide and the attached dipole at the focus of the Clavin feed.

---

*C. H. Mayer, T. P. McCullough, and R. M. Sloanaker, Astrophys. J. 139, 248 (1964).

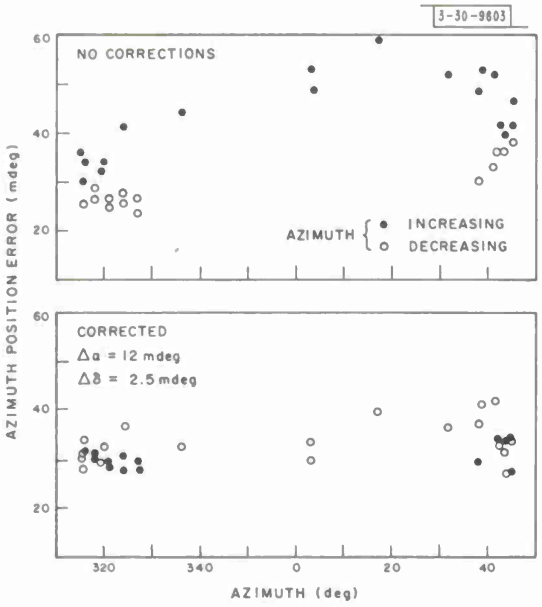


Fig. III-13. Haystack pointing calibration (Cassiopeia A).

Fig. III-14. Haystack pointing calibration.

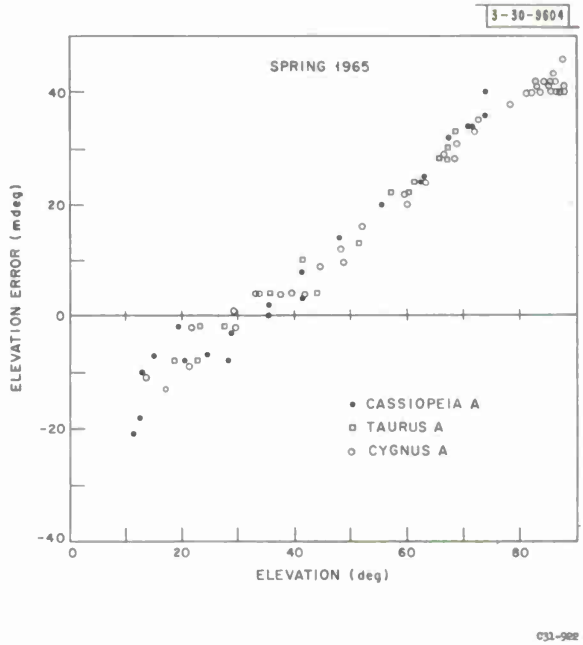

TABLE III-2

POSITIONS OF THE BRIGHT RADIO SOURCES
(Referred to Epoch of 1950.0)

| | Right Ascension | | | Declination | | |
|---|---|---|---|---|---|---|
| | h | m | s | d | m | s |
| Cassiopeia A | | | | | | |
| Haystack calibration | 23 | 21 | 12.0 | +58 | 32 | 40 |
| Cal Tech (960 MHz) | 23 | 21 | 6.8 (±0.8)* | +58 | 32 | 47 (±6)* |
| Taurus A | | | | | | |
| Haystack calibration | 5 | 31 | 30.9 | +21 | 58 | 49 |
| Cal Tech (960 MHz) | 5 | 31 | 30.5 (±0.3) | +21 | 59 | 02 (±5) |
| Cygnus A | | | | | | |
| Haystack calibration | 19 | 57 | 44.7 | +40 | 35 | 47 |
| Cal Tech (960 MHz) | 19 | 57 | 44.5 (±0.4) | +40 | 35 | 46 (±6) |

*1 sec of right ascension is equal in angular magnitude to 15 arc sec of declination.

(b) Measurements were made with the plane of polarization in the vertical plane and at angles of 45°, 90°, and 135°.

(c) Before and after measurements on the source, background measurements were made with the antenna offset by 0.5° in azimuth from the source position.

(d) Polarization angle and percent polarization were determined by a least-square fitting to the source data with the average background subtracted.

(e) The position angle relative to the vertical plane was corrected, on the basis of local-hour angle, to obtain the position angle of the polarization on the celestial sphere.

Measurements of the polarization properties of Taurus A were made at five different local-hour angles to determine whether the radome or the antenna position influenced these measurements of polarization. For two of the measurements, there was some moisture on the radome, and these measurements showed departures from the other three measurements that were made in clear weather. The results of these measurements are shown in Table III-3. Tabulations include the local-hour angle, the polarization angle relative to a vertical plane, the position angle on the celestial sphere, the percent polarization, and the average antenna temperature of Taurus A. The position angles show a spread of 2.6°. Measurements made while the radome was damp gave lower values of the average antenna temperature, as might be expected.

TABLE III-3
POLARIZATION MEASUREMENTS ON TAURUS A

| Local-Hour Angle | Position Angle (relative) | Position Angle (absolute) | Polarization (percent) | $T_A$ (average in °K) |
|---|---|---|---|---|
| $00^h\ 27^m$ | 40.4° | 144.2° | 6.2 | 37.5 |
| 00 30 | 39.4 | 144.6 | 7.6 | 37.4 |
| −00 36 | 74.6 | 146.6 | 7.7 | 36.9 |
| −01 52 | 98.6 | 146.8 | 8.7* | 33.0 |
| −01 53 | 96.9 | 144.9 | 9.0* | 32.8 |

* Moisture on the radome.

## D. SPECIALIZED COMPUTER PROGRAMS

The digital computer (Univac 490) that is used to point the Haystack antenna has sufficient capacity to permit some on-line data analysis in addition to the pointing computations. The output of the radiometers is fed directly into the computer as described in Sec. III-B. Hence it is possible, using programs prepared for the purpose, to process the radiometric data in real time to obtain calibrated antenna temperatures.

At the beginning of an observing period, the calibration constants for the particular radiometer in use are stored in the computer memory by typing these data on a teletype keyboard in answer to a sequence of programmed questions that are typed out under computer control at the beginning of the radiometric data processing program. Prior to observations of radio sources, the observer makes a calibration of the radiometer outputs by first integrating for one minute (normally) with the calibrated noise source on and then integrating for a similar period with the noise source off to obtain a base level. With this information in its memory, the computer can begin to calculate the antenna temperatures directly in degrees Kelvin. The integration period for observations is then selected, and upon command to begin observations, these computations are made in real time and printed on the high-speed printer that is attached to the computer. The observer has available the usual analog chart record of radiometer output during an observation, but the quantitative records for reporting experiments are taken from the output of the high-speed printer.

Table III-4 shows a sample sheet of the printer output. This record gives the Universal time at the middle of an integration interval, the coordinates of the antenna beam (right ascension, declination, and elevation), the antenna temperatures above the base level for both radiometer channels, the standard deviation of these temperatures, and a printer plot of the antenna temperatures. The same data are recorded on magnetic tape if subsequent data processing is to be performed.

In order to make the observation of discrete radio sources automatic, an additional computer program called the Discrete Source Scanning (DSS) routine has been written to perform the

TABLE III-4

SAMPLE OF PRINTER OUTPUT FROM RADIOMETRIC OBSERVATION

POINTING AND B# TESTS USING 3C273B 07/26/65

| TIME | RIGHTA | DECLIN | ELEV | T(1) | T(2) | DEL(1) | DEL(2) | -2 0 2 4 6 |
|---|---|---|---|---|---|---|---|---|
| 00 33 48.1 | 186.707 | 02.251 | 27.510 | 0002.11 | 0001.92 | 00.087 | 00.044 | I OX |
| 00 33 52.1 | 186.714 | 02.251 | 27.503 | 0002.20 | 0002.37 | 00.088 | 00.144 | I 1 |
| 00 33 56.1 | 186.718 | 02.251 | 27.495 | 0001.80 | 0002.22 | 00.155 | 00.175 | I X O |
| 00 34 00.1 | 186.725 | 02.251 | 27.488 | 0002.08 | 0002.10 | 00.138 | 00.093 | I 1 |
| 00 34 04.1 | 186.730 | 02.252 | 27.481 | 0002.17 | 0002.18 | 00.255 | 00.145 | I 1 |
| 00 34 08.1 | 186.736 | 02.252 | 27.474 | 0001.87 | 0002.23 | 00.082 | 00.082 | I X O |
| 00 34 12.1 | 186.742 | 02.251 | 27.466 | 0002.07 | 0002.21 | 00.148 | 00.095 | I XO |
| 00 34 16.1 | 186.747 | 02.251 | 27.458 | 0001.95 | 0002.29 | 00.113 | 00.177 | I X O |
| 00 34 20.1 | 186.752 | 02.251 | 27.450 | 0001.87 | 0002.10 | 00.084 | 00.074 | I XO |
| 00 34 24.1 | 186.757 | 02.252 | 27.443 | 0001.89 | 0002.34 | 00.107 | 00.148 | I X O |
| 00 34 28.1 | 186.762 | 02.251 | 27.434 | 0001.70 | 0001.96 | 00.078 | 00.116 | I XO |
| 00 34 32.1 | 186.770 | 02.251 | 27.429 | 0001.69 | 0002.05 | 00.153 | 00.060 | I X O |
| 00 34 36.1 | 186.775 | 02.251 | 27.421 | 0002.03 | 0002.44 | 00.206 | 00.107 | I X O |
| 00 34 40.1 | 186.780 | 02.252 | 27.414 | 0001.98 | 0002.13 | 00.095 | 00.118 | I XO |
| 00 34 44.1 | 186.786 | 02.251 | 27.406 | 0002.23 | 0002.26 | 00.141 | 00.153 | I 1 |
| 00 34 48.1 | 186.790 | 02.251 | 27.397 | 0002.17 | 0002.34 | 00.050 | 00.095 | I XO |
| 00 34 52.1 | 186.797 | 02.251 | 27.391 | 0002.20 | 0002.24 | 00.082 | 00.153 | I 1 |
| 00 34 56.1 | 186.802 | 02.251 | 27.383 | 0002.40 | 0002.53 | 00.140 | 00.124 | I 1 |
| 00 35 00.1 | 186.808 | 02.252 | 27.377 | 0002.88 | 0003.00 | 00.068 | 00.092 | I XO |
| 00 35 04.1 | 186.813 | 02.252 | 27.369 | 0003.49 | 0003.46 | 00.161 | 00.045 | I 1 |
| 00 35 08.1 | 186.819 | 02.251 | 27.361 | 0004.27 | 0004.06 | 00.215 | 00.244 | I OX |
| 00 35 12.1 | 186.823 | 02.251 | 27.353 | 0004.22 | 0004.61 | 00.150 | 00.106 | I X O |
| 00 35 16.1 | 186.829 | 02.250 | 27.345 | 0004.82 | 0004.66 | 00.191 | 00.091 | I OX |
| 00 35 20.1 | 186.834 | 02.252 | 27.338 | 0004.41 | 0004.63 | 00.115 | 00.063 | I XO |
| 00 35 24.1 | 186.841 | 02.251 | 27.331 | 0004.10 | 0004.23 | 00.137 | 00.113 | I XO |
| 00 35 28.1 | 186.847 | 02.251 | 27.324 | 0003.68 | 0003.63 | 00.165 | 00.250 | I 1 |
| 00 35 32.1 | 186.851 | 02.251 | 27.316 | 0003.11 | 0003.10 | 00.214 | 00.098 | I 1 |
| 00 35 36.1 | 186.857 | 02.251 | 27.308 | 0002.44 | 0002.70 | 00.120 | 00.130 | I XO |
| 00 35 40.1 | 186.864 | 02.252 | 27.303 | 0002.08 | 0002.18 | 00.168 | 00.043 | I 1 |
| 00 35 44.1 | 186.868 | 02.250 | 27.293 | 0002.34 | 0002.39 | 00.107 | 00.060 | I 1 |
| 00 35 48.1 | 186.875 | 02.252 | 27.287 | 0002.13 | 0002.36 | 00.056 | 00.082 | I XO |
| 00 35 52.1 | 186.880 | 02.252 | 27.279 | 0002.44 | 0002.43 | 00.166 | 00.208 | I 1 |
| 00 35 56.1 | 186.886 | 02.251 | 27.272 | 0001.92 | 0002.18 | 00.234 | 00.168 | I XO |
| 00 36 00.1 | 186.888 | 02.252 | 27.263 | 0001.98 | 0002.50 | 00.219 | 00.120 | I X O |
| 00 36 04.1 | 186.896 | 02.252 | 27.257 | 0002.29 | 0002.37 | 00.085 | 00.088 | I 1 |
| 00 36 08.1 | 186.903 | 02.251 | 27.250 | 0002.16 | 0002.31 | 00.102 | 00.069 | I XO |
| 00 36 12.1 | 186.910 | 02.252 | 27.244 | 0002.26 | 0002.14 | 00.094 | 00.082 | I OX |
| 00 36 16.1 | 186.914 | 02.251 | 27.235 | 0002.24 | 0002.25 | 00.064 | 00.092 | I 1 |
| 00 36 20.1 | 186.919 | 02.251 | 27.227 | 0002.15 | 0002.25 | 00.110 | 00.170 | I XO |
| 00 36 24.1 | 186.924 | 02.251 | 27.219 | 0002.09 | 0002.28 | 00.096 | 00.188 | I XO |
| 00 36 28.1 | 186.930 | 02.252 | 27.213 | 0001.90 | 0002.28 | 00.073 | 00.060 | I X O |
| 00 36 32.1 | 186.937 | 02.251 | 27.205 | 0001.83 | 0002.40 | 00.225 | 00.217 | I X O |
| 00 36 36.1 | 186.941 | 02.251 | 27.197 | 0001.99 | 0002.39 | 00.095 | 00.061 | I X O |
| 00 36 40.1 | 186.947 | 02.251 | 27.189 | 0002.17 | 0002.35 | 00.084 | 00.098 | I XO |
| 00 36 44.1 | 186.952 | 02.250 | 27.181 | 0002.21 | 0002.29 | 00.172 | 00.068 | I 1 |
| 00 36 48.1 | 186.958 | 02.252 | 27.175 | 0002.06 | 0002.40 | 00.249 | 00.081 | I X O |
| 00 36 52.1 | 186.964 | 02.253 | 27.169 | 0001.84 | 0001.96 | 00.172 | 00.127 | I 1 |
| 00 36 56.1 | 186.969 | 02.251 | 27.160 | 0002.27 | 0002.43 | 00.084 | 00.089 | I XO |
| 00 37 00.1 | 186.975 | 02.251 | 27.152 | 0002.09 | 0002.32 | 00.121 | 00.055 | I XO |
| 00 37 04.1 | 186.963 | 02.251 | 27.133 | 0001.98 | 0002.25 | 00.187 | 00.160 | I X O |
| 00 37 08.1 | 186.884 | 02.249 | 27.068 | 0002.30 | 0002.60 | 00.143 | 00.097 | I X O |
| 00 37 12.1 | 186.766 | 02.302 | 27.016 | 0002.73 | 0002.78 | 00.122 | 00.247 | I 1 |
| 00 37 16.1 | 186.456 | 02.593 | 27.011 | 0002.11 | 0002.59 | 00.020 | 00.101 | I X O |
| 00 37 20.1 | 186.458 | 02.589 | 26.999 | 0002.08 | 0002.36 | 00.144 | 00.186 | I XO |

necessary observations sequentially and to reduce the data in real time. This program determines (1) the position offsets to the center of the source, (2) the widths to half maximum in right ascension and declination, and (3) the peak antenna temperature of the source. The program operates as shown in Fig. III-15. Note that the control of the antenna for the second scan (in declination) is determined by the computed maximum of the antenna temperature from the first scan (in right ascension). If the offsets determined by this program are not small, it is desirable to repeat the program with the first measured offsets inserted for the estimated offsets of the center of the source.

This program has been checked against manual measurements of the same quantities and has been shown to be accurate.

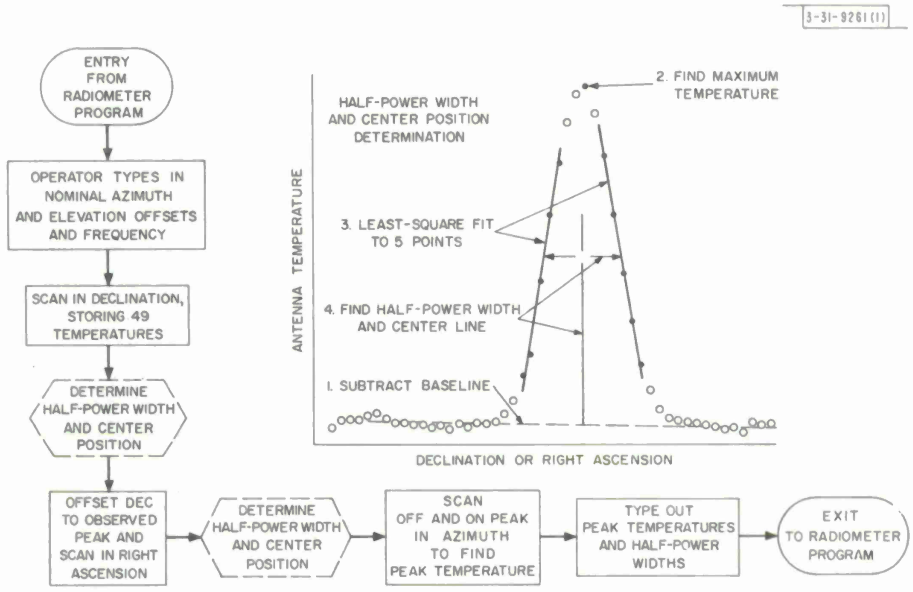


Fig. III-15. Haystack DSS routine.

# IV. RADAR ASTRONOMY

## A. PLANETARY STUDIES

### 1. Introduction

If one neglects the influence of the different radio albedos of the planets, and of their different rotation rates, on the ability one has of detecting them by radar, a table (Table IV-1) can be drawn up showing how the relative echo strengths depend upon their sizes and distances. These relationships are illustrated in Fig. IV-1. Here the months indicated against the bars for Mars and Mercury show the difference between the most favorable and least favorable close approaches (which always occur in the same months). In an actual radar situation, the high rotation rate of Mars renders it less detectable than Mercury by an amount which depends upon whether the radar operates as a CW or pulsed radar.

So far, only Mars, Venus, and Mercury have been detected reliably by radar, and their relative detectabilities measured at decimeter wavelengths are illustrated in Fig. IV-2. The dotted line indicating pulsed observation of Mars has been calculated on the assumption that a duty cycle of 1 in 16 can be achieved in the transmitter. For the Millstone radar, the echoes from Venus are about equal to the intensity of the noise level in the receiver at close approach. By integrating over several days, some 30-db improvement in signal-to-noise ratio can be achieved. Thus it is possible to observe Venus for seven months centered on inferior conjunction (which occurs every 19 months). Mars and Mercury, on the other hand, may be detected only at close approach.

It is expected that the Haystack radar will be able to observe Mercury and Venus for longer than Millstone, but Mars may be no more easily detectable, since initially a CW radar will be used. In order to place our work in perspective, in the next section we review the planetary observations that have been made by a number of groups, commencing in 1961. In Sec. IV-A-3, we summarize the Millstone Hill observations in 1964. Section IV-A-4 covers the observations made at Millstone during the first six months of 1965.

### 2. History

Price, et al.,[1] were the first to claim radar detection of the planet Venus. These measurements, conducted in 1958, seemed to indicate that Venus was an anomalously bright scatterer having a cross section equal to its projected area. (The moon has a radar cross section of about 7 percent of its projected area.) Also, they yielded a value of 149,467,000 km for the Astronomical Unit. During a second series of measurements in 1959, using improved equipment, this group failed to detect an echo,[2] thereby casting doubt on their original results. Meanwhile, at Jodrell Bank, Evans and Taylor[3] searched for an echo at the range predicted by Price, et al.,[1] and obtained weak statistical evidence for one. However, the intensity corresponded to a cross section of only 2 percent of the projected area. In retrospect, it is clear that both these measurements were erroneous, though reasons have never been advanced as to why apparently strong returns were obtained in the 1958 observations of Price, et al.[1]

TABLE IV-1
DETECTABILITY OF PLANETS

| Planet | Distance from Earth ($\times 10^6$ km) | | Range Factor $(R_v/R)^4$ (db) | | Cross Section Relative to Venus (db) | Echo Strength Relative to Venus at Close Approach (db) | | Travel Time for Pulse (minutes) | |
|---|---|---|---|---|---|---|---|---|---|
| | Maximum | Minimum | Maximum | Minimum | | Maximum | Minimum | Maximum | Minimum |
| Mercury | 217.6 | 76.8 | −30 | −12 | −8 | −20 | −38 | 24.6 | 8.6 |
| Venus | 259.2 | 38.4 | −33 | 0 | 0 | 0 | −33 | 28.9 | 4.3 |
| Mars | 398.4 | 54.4 | −40 | −6 | −5 | −11 | −45 | 44.5 | 6.1 |
| Jupiter | 963.2 | 585.6 | −56 | −48 | +21 | −27 | −35 | 107 | 65 |
| Saturn | 1649 | 1189 | −65 | −60 | +20 | −40 | −45 | 184 | 141 |
| Uranus | 3142 | 2570 | −76 | −72 | +13 | −59 | −63 | 350 | 286 |
| Neptune | 4664 | 4285 | −84 | −82 | +11 | −71 | −73 | 520 | 478 |
| Pluto | 7488 | 4240 | −92 | −82 | 0 | −82? | −92? | 835 | 472 |

$R_v$ = minimum distance from Earth to Venus.

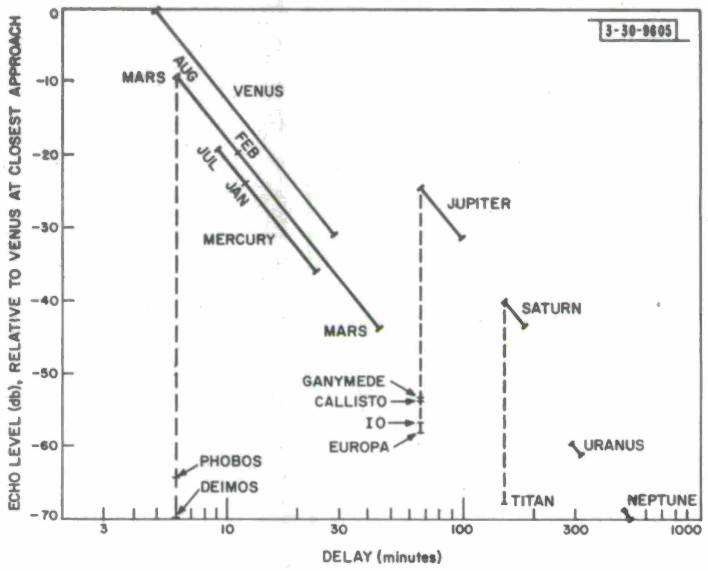


Fig. IV-1. Relative radar detectability of planets, neglecting albedos and rotation rates.

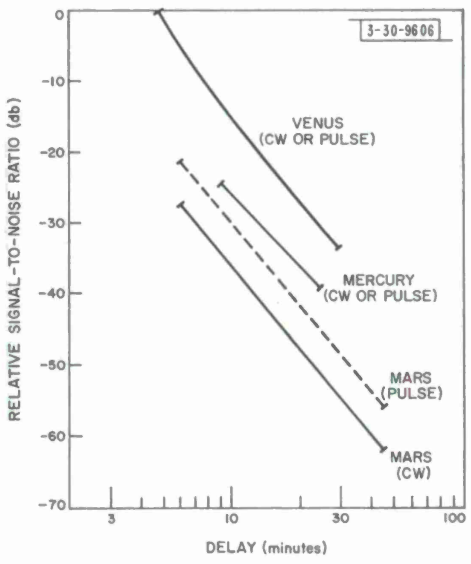


Fig. IV-2. Relative detectabilities based upon radar measurements.

The first reliable radar observations of Venus were made in 1961 by groups in the U.S. (Victor and Stevens[4]; Staff, Millstone Radar Observatory[5]; Maron, et al.[6]), in the United Kingdom (Thomson, et al.[7]), and in the U.S.S.R. (Kotel'nikov[8]). Final reports of this work have been published by Victor, et al.[9]; Muhleman, et al.[10]; Pettengill, et al.[11]; Smith[12]; Kotel'nikov, et al.[13] These observations indicated that Venus has an albedo at decimeter wavelengths of about 12 percent, a very slow rotation period (possibly retrograde), and that the value for the Astronomical Unit is close to 149,598,000 km.[14] The Russian workers[13] were unable to decide from their observations whether the rotation period was fast (~10 days) or slow (>100 days), but following further observations in 1962, they concluded that the motion is retrograde with a probable period of 200 to 300 days.[15] A similiar conclusion was reached independently by Goldstein and Carpenter[16] from observations at the Jet Propulsion Laboratory in 1962. A period of 250 ± 40 days retrograde was reported by Carpenter[17] and 248 ± 36 days retrograde by Goldstein.[18] The position of the pole as given by Goldstein[18] lies within a cone with solid angle ±15° centered on 119° RA and −78° δ.

From these 1962 observations, Carpenter[17] and Kotel'nikov, et al.,[15] were able to obtain some information concerning the scattering behavior of Venus and show that it is similar in character to that for the moon. Most of the energy is reflected from a highlight near the apparent center of the disk. James and Ingalls[19] and Klemperer, et al.,[20] reported meter wave observations of Venus during the 1962 inferior conjunction. At this wavelength, the slow rotation period gives rise to long period (i.e., several seconds) fading of the signals. The radar cross section implies that reflection still occurs at the planetary surface (and not in an ionosphere).

Few results have been published thus far of the measurements made during the 1964 inferior conjunction. The Jodrell Bank workers (Ponsonby, et al.[21]) have reported that the rotation period is retrograde, but were unable to improve on the value for the period published by Goldstein and Carpenter. The group at the Jet Propulsion Laboratory has made range measurements for which the accuracy claimed is comparable to the values reported here (Tausworthe[22]).

Russian workers (Kotel'nikov, et al.[23]) were the first to observe radar reflections from Mercury. They reported that the radar cross section was 6 percent of the projected area and that the value for the Astronomical Unit obtained was consistent with that derived from observations of Venus. The group at the Jet Propulsion Laboratory (Carpenter and Goldstein[24]) later reported observations of Mercury with similar results.

The Russian work in this field has been reviewed by Kotel'nikov,[25] the Jet Propulsion Laboratory measurements by Goldstein,[26,27] and a general review has been published by Thomson.[28]

### 3. Millstone Hill Observations in 1964

During 1964, the Millstone Hill L-band radar was employed in observations of Venus and Mercury. The radar parameters during that year are listed in Table IV-2. Observations of Venus were conducted from March to October at approximately weekly intervals. A variety of pulse lengths was employed (Table IV-3) and the echoes integrated both coherently and incoherently. By employing phase coded pulses and coherent integration for samples taken at 20-μsec intervals, the range could be determined to an accuracy of ±1.5 km throughout June and July. At the beginning and end of the observation period, the accuracy was reduced to ±75 km by the reduced echo strength.

TABLE IV-2

EQUIPMENT PARAMETERS OF MILLSTONE HILL WHEN OPERATED AS A PLANETARY RADAR

| | |
|---|---|
| Frequency | $f_o$ = 1295.0 MHz |
| Antenna | 84-foot parabola with Cassegrainian feed arrangement |
| Beamwidth between half-power points | 0.6° |
| Antenna gain (over a lossless isotropic radiator) | 46.5 db |
| Effective antenna aperture | 190 $m^2$ |
| Transmitter peak power | 3 to 4 Mw (measured continuously) |
| Transmitter average power | 100 to 120 kw (measured continuously) |
| System temperature $T_s$ | ~100°K (measured continuously) |
| Overall feed line and other losses | 2 db |
| Polarization | |
| Transmitted | Right circular |
| Received | Left circular |

TABLE IV-3

PULSE LENGTHS AND SAMPLE INTERVALS EMPLOYED AT MILLSTONE HILL IN OBSERVATIONS OF VENUS IN 1964

| Effective Pulse Length (msec) | PRF (Hz) | Incoherent Sample Interval (μsec) | Coherent Sample Interval (μsec) |
|---|---|---|---|
| 4 | 8.3 | 200 | 500 |
| 2 | 16.7 | 200 | 200 |
| 0.5 | 60 | – | 120 |
| 0.36* | 8.3 | – | 120 |
| 0.04* | 60 | – | 20 |

*Using phase-coded pulse compression.

Echoes from Mercury were obtained on five days around the inferior conjunction which occurred on 30 April 1964. The radar cross section appeared to be about 10 percent of the projected area of the disk. The radar cross section for Venus had an average value of 15 percent which is close to most other values at meter and decimeter wavelengths. The angular scattering law for Venus was determined by averaging results for the echo power vs delay obtained on many different days. It was concluded that Venus has a surface that is considerably smoother than the moon's. The average slope of surface elements in the range of about 5 to 50 meters across appears to be 8°. There are, however, regions that are distinctly rough and caused a lowering of the radar cross section when they rotated under the subradar point. By contrast, Mercury appeared somewhat rougher than the moon.

A detailed account of this work has been prepared for the September 1965 issue of the Astronomical Journal.[29]

### 4. Observations at Millstone Hill in 1965

Mars was the only planet favorably located for detection during the first six months of 1965. Accordingly, observations were made near opposition which occurred in March. The equipment was operated with 4-msec pulses at a prf of 8 per sec, but in place of the normal 250-Hz matched filter one 500-Hz wide was employed. This represented an attempt to increase the detection capability by making allowance for the large amount of Doppler broadening introduced by the rapid rotation of the planet. Incoherent addition of pulses was carried out for a period of over ten hours during the nights of 2/3, 3/4, 9/10, and 10/11 March 1965. The plot of power over the time base thus achieved was then convolved with the expected echo shape to simulate the effect of a 4-msec postdetector matched filter. The results are shown in Fig. IV-3. A statistically significant echo corresponding to a 0.75°K increase in system temperature is evident at a range approximately 1 msec earlier than predicted. If it is assumed that the echo power is distributed in frequency over the full 500-Hz band accepted by the receiver, we compute a cross section of 14 percent.

Observations of Mars at 12.5-cm wavelength have been reported by Goldstein and Gillmore[30] and by Kotel'nikov, et al.,[31] at about 40-cm wavelength. Both groups of workers report that the cross section is highly variable, and depends upon what part of the Martian surface lies at the subradar point. According to Goldstein and Gillmore, a peak cross section of 15 percent is observed at 280° longitude, but the average value is only 3 percent. The Russian results for cross section vs longitude are less reliable because of the poor signal-to-noise ratio achieved. An average value of 7 percent was reported. Variations of cross section with time seemed present in the results reported here, but the signal-to-noise ratio was inadequate to permit reliable estimates.

It is anticipated that the next series of planetary radar observations to be conducted at Millstone will begin in October 1965, when Venus once more comes within range. Considerable importance attaches to the accurate range measurements to be made in this series, because no previous precise measurements are available for this part of the orbit. Venus is not visible to Arecibo at this time because of its southerly declination.

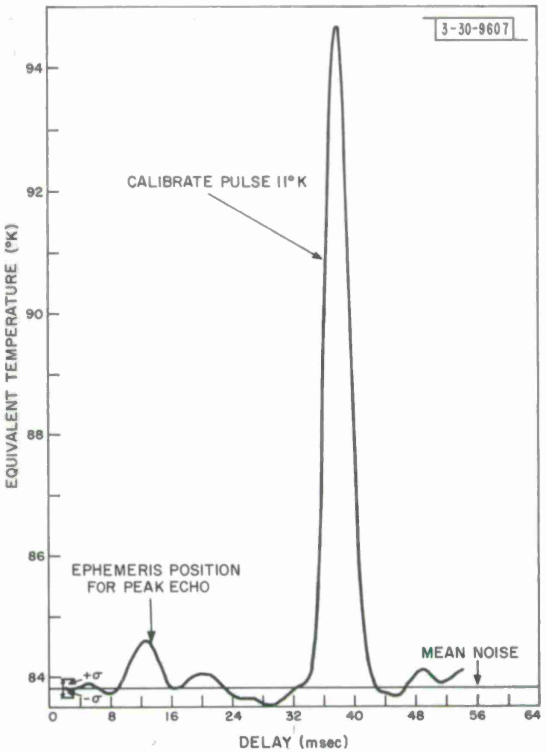


Fig. IV-3. Observation of Mars.

## B. POLARIMETRIC OBSERVATIONS OF THE MOON

### 1. Introduction

Previously the moon and several of the near planets have been the subject of different types of radar exploration. Measurements of the total backscattered power have been used to infer the reflectivity and hence the dielectric constant of the body. For frequencies in the range 400 to 3000 MHz, the dielectric constant of the lunar surface has been about 2.6 to 2.8.[32,33] Studies of backscattered power as a function of range beyond the subterrestrial point on the moon have led to models of the lunar surface which can be described as gently undulating with mean slopes on the order of 10° to 12° on the scale of about one meter.[33] Several of the young craters or the rayed craters on the moon have been shown to be anomalously strong scatterers, and it has been inferred that they are rougher and must have a higher intrinsic reflectivity than their surroundings.[34]

Depolarization studies have been made to the extent that the two orthogonal circularly polarized waves have been observed when a circularly polarized wave was transmitted.[32] These measurements have shown that a very appreciable amount of power (~6 to 7 percent of the total) is being returned in that circular component which should contain no power, if the reflector were an ideal plane mirror. This has been interpreted to mean that the surface must contain a small scale structure which backscatters partly in a manner akin to that of a collection of randomly oriented dipoles. Randomly oriented linear dipoles should, however, depolarize to the extent that the two circularly polarized backscattered waves should have equal power when illuminated with a circularly polarized wave. If the same model were illuminated by a linearly polarized wave, it can be shown that three-quarters of the backscattered energy should be polarized in the same plane as the incident wave.

In view of the polarization results described above, we might conclude that the lunar surface when illuminated with linearly polarized waves will reflect almost all the energy with the same polarization as the incident wave. The general picture of the lunar surface that has emerged from radar observations alone has therefore been one of a sandy desert-like surface (for quartz sand $\epsilon \cong 2.6$) of fairly gentle undulations, with a few rocks strewn over it to act as discrete scatterers at very oblique incidence.

Radiometric studies of the thermal emission from the lunar surface have also suggested models for the lunar surface. Measurements have been made of the emission temperature of the lunar surface throughout complete lunations, and the thermal cycle of the moon has been obtained at several different wavelengths. These measurements basically are sensitive to the ratio of the penetration depths of the thermal wave and the electromagnetic wave of observation. The results of these measurements show that the upper layers of the surface must have a very high thermal inertia possibly corresponding to an extremely tenuous medium.[35]

Another observation consists of the measurement of temperature distribution across the lunar disk. The amount of limb darkening can be translated into an equivalent dielectric constant of the surface. The results of such observations have generally indicated a dielectric constant of $\epsilon = 1.1$ to $1.7$,[36] again corresponding to an extremely tenuous medium.

The most direct method of obtaining data on the lunar surface material from radiometric observations appears to be the measurement of emission polarization as a function of angle of incidence on the surface.[37] These observations have been carried out by a number of observatories and they nearly all seem to agree that the surface must be a material with a dielectric constant $\epsilon$ in the range 1.6 to 1.8.[38-41]

Attempts to reconcile the radiometric and radar data by carefully considering the effect of roughness on the thermal emission properties have brought about a somewhat closer agreement, but a very significant discrepancy still persists.

Inspection of the Ranger photographs seems to show that the surface of the moon is quite smooth, even down to a scale of a meter or so. The surface irregularities, even on a small scale, can be described as gentle undulations. In particular, there seems to be a complete absence of the visible protruding structures which correspond to rocks strewn over the surface, such as one might have expected from radar data alone.

### 2. A New Type of Observation

In view of the discussion of different data presented above, the thought arose that the backscattering at oblique incidence on the lunar surface might arise from some sort of irregular structure actually buried underneath a tenuous surface layer on the moon. If this layer were of sufficient thickness (i.e., in excess of the wavelength of observation) it could be argued that the strength of the backscattering should be systematically different for the two linearly polarized components in and across the local plane of incidence of the wave. Specifically, the return having its E-field in the plane of incidence should be stronger than the orthogonally polarized return. Such a systematic effect would arise from the difference in the transmission coefficients of the two linearly polarized waves which penetrate the top layer. Obviously these differences can be studied only if it is possible to resolve fairly small areas on the moon.

An experiment to distinguish between two such linearly polarized waves was realized as follows: A circularly polarized wave illuminating the whole moon was transmitted. The radiation was pulsed so that various rings of constant range from the radar could be distinguished by range gating on the time base of the receiver. The additional coordinate necessary to resolve specific areas on the moon was provided by spectral analysis in each range ring. Because of the apparent libration of the moon, the approaching limb will scatter at a somewhat higher Doppler frequency than the center of the moon and the receding limb at a somewhat lower frequency. Lines of constant Doppler displacement correspond to straight lines across the apparent disk of the moon, parallel to the instantaneous apparent libration axis. This is the range-Doppler process described by Pettengill and Henry.[42]

The two orthogonal linearly polarized components returned from the moon were studied separately but simultaneously. One of these was aligned (E-field) with the instantaneous libration axis of the moon (component a) and the other was perpendicular to this axis (component b) as in Fig. IV-4. If one were to assume the correctness of the supposition concerning penetration of a tenuous surface layer, a systematic difference in the backscattering of the two linearly polarized components should be observed as follows: For any given range ring, component a should be stronger than component b near the libration axis, i.e., near zero frequency, and component a should be weaker than component b near the extreme frequencies of the range ring. The two linearly polarized components should be equally strong at 0.707 times the maximum frequency for any range ring.

### 3. Experiments at Millstone Hill

The Millstone Hill radar was used in the experiment described above with a pulse length of 200 μsec and an interpulse period of 30 msec. The Doppler frequency, the rate of change of Doppler, and the direction of the instantaneous libration axis were predicted from the lunar ephemeris for every five minutes, and corresponding adjustments were made to the receiving equipment before every five-minute run. The direction of the polarization on reception was controlled by combining two orthogonally polarized received signals by means of a network consisting of two 3-db hybrid couplers and two variable length sections of transmission line. The two linearly polarized signals received were amplified by separate receiver systems and detected in pairs of phase detectors so that both the in-phase and quadrature components of the signals were available for both channels. The four outputs of the phase detectors were sampled simultaneously and assigned in sequence a sign and one of 64 levels. A region of the time base 14.4 msec long was sampled every 160 μsec, beginning 2.56 msec before the predicted leading edge of the echo (in order to permit a noise base line to be established). The digital data thus obtained were stored on magnetic tape.

Several of the range boxes have been analyzed by using the CG 24 computer to provide the frequency spectra. The frequency analysis was performed over the range −18 to +18 Hz with respect to the expected center frequency of the echo, with a resolution of 2 Hz. The noise base line was subtracted by frequency analyzing the noise immediately preceding the echo in the same way as the signal. This was necessary to remove DC components introduced at the phase detectors.

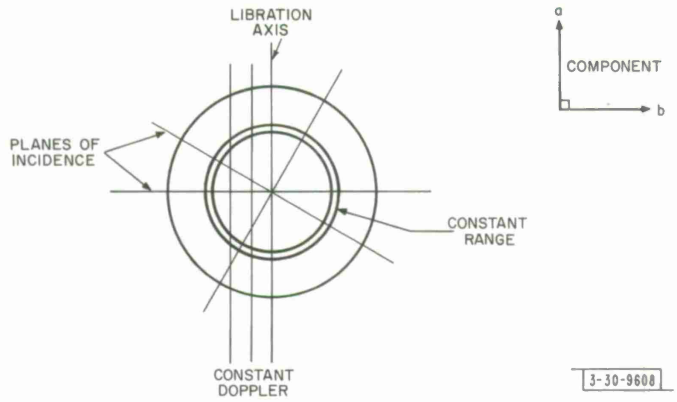


Fig. IV-4. Lunar disk with range-Doppler coordinates and with two received linearly polarized components a and b.

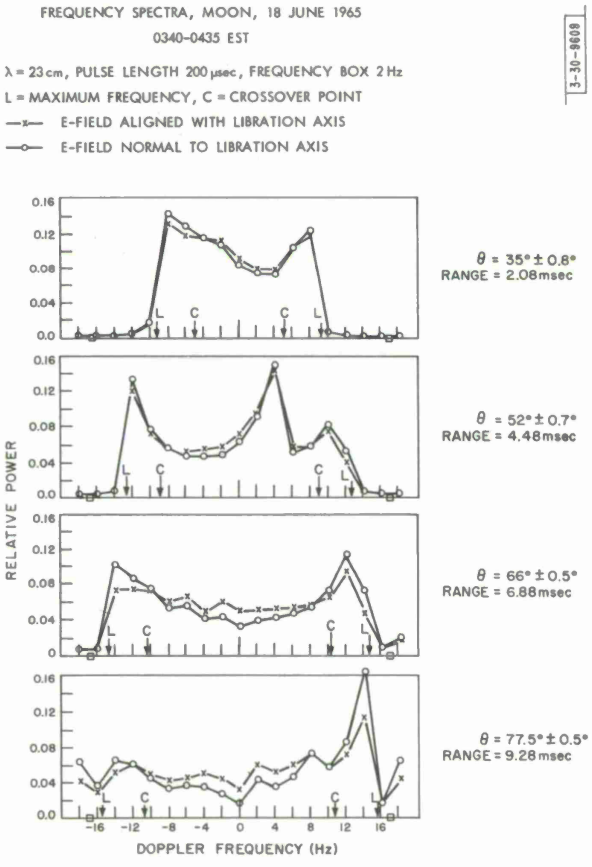


Fig. IV-5. Normalized frequency spectra for four range rings.

The power spectra corresponding to the two polarizations were normalized so that the areas under the curves were made the same. (This is justified since a given range ring should reflect the same total power. Further, it provides a means of removing the effects of different receiver gains.)

Twenty-five minutes of data were analyzed and the various spectra were summed. This could be done in this particular case because the libration axis moved only by about 4° during the run and the predicted Doppler width did not change by more than 5 percent. The statistical uncertainty in the resulting curves is equal to approximately 1/55 of the mean values of the power at any frequency offset.

The spectra for four of the different range rings are shown in Fig. IV-5. As can be seen, the effect predicted from the assumption of penetration through a top layer is clearly visible, because the component with E-field along the plane of incidence is scattered more strongly than the orthogonal one. The extreme frequencies are marked by L and the predicted crossover points by C. Note also that the difference in the intensity of the two components is increasing with increasing angle of incidence. There is a very sharp peak at a range of 4.48 msec, at a frequency offset of +4 Hz. At this peak, the ratio of the two components is unexpectedly close to unity – compare the ratio of +4 Hz for the same range ring. At the time of observation, the predicted range-Doppler coordinates of Tycho were 4.30 msec and +2 Hz; therefore, it seems plausible to ascribe the anomalous peak to the Tycho region, which is known to be an outstanding scattering area (Pettengill and Henry[42]).

The Faraday rotation of the linear received components was estimated to be less than 10° and was therefore neglected. In future experiments, it will be measured directly and compensated for continuously.

### 4. Discussion

In order to test the hypothesis of a penetration mechanism through a tenuous top layer on the lunar surface somewhat further, the ratio of the power in the two orthogonal linearly polarized components was derived as a function of the angle of incidence on the mean lunar surface. This information was most readily derived from the region near zero frequency. The same information could, in principle, be derived from the maximum frequency regions also, but in these latter regions the angles between the planes of polarization and the plane of incidence change much more rapidly with changes in frequency offset than they do near zero frequency; for this reason, the ratios were computed only on the basis of information derived from the power spectra near zero-frequency offset.

The scattering mechanism inside the top layer was assumed to scatter back principally in the same linear polarization as that of the incident wave. This appears to be justified in view of previous circular-to-circular depolarization studies (Evans and Pettengill[32]) as discussed in Sec. IV-A-1. On this assumption, one would expect the ratio of the backscattering coefficients of the two linear polarizations to be equal to the square of the ratio of the corresponding transmission coefficients. In Fig. IV-6, the square root of the ratios derived from the ratio of the backscattering coefficients is plotted against the mean angle of incidence. The ratios of the

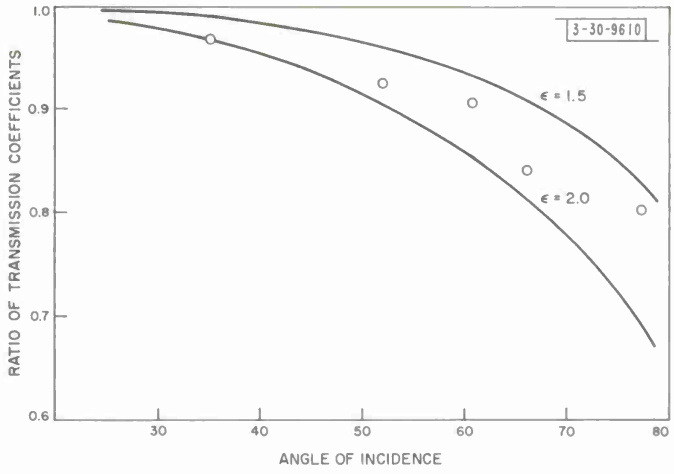


Fig. IV-6. Ratio of transmission coefficients derived from data as compared with theoretical predictions.

corresponding transmission coefficients for dielectric constants of 1.5 and 2.0 are shown in the same diagram. As might be seen, it is very tempting to ascribe to the top layer a dielectric constant of about 1.7 to 1.8. It is interesting and it might be quite significant that this value corresponds very closely to the ones derived from radiometric observations of the polarization of the thermal emission from the lunar surface.[38-41] The fact that no systematic difference in the backscattering coefficients of the two polarizations is seen in the Tycho region may be interpreted to mean that this region does not have a tenuous surface layer or that it is quite thin, probably less than a few centimeters. Elsewhere the top layer must be at least some tens of centimeters, since the depth of the surface layer must be greater than about a wavelength for the pronounced polarization effects observed to occur.

Let us next discuss our interpretation in the light of other data. First, we have to reconcile our model with radar observations of cross section which, when interpreted on the basis of a single-layer model, appear to give a dielectric constant of 2.6 to 2.8. On the assumption of a double-layer model, the upper layer being of random thickness and having a dielectric constant of 1.8, it is possible to obtain the right amount of reflection with a base layer with $\epsilon = 4.5$ to 5.0. If the top layer is only of the order of 1 to 2 meters deep, this model will, in addition, explain the increase in cross section observed by Davis and Rohlfs[43] at wavelengths between 10 and 20 meters, since at such long wavelengths a thin layer would be unimportant. The radiometric determinations of the dielectric constant based on the polarization of the thermal emission might also be brought into line with our naive two-layer model. Calculations show that near grazing angles of incidence, the polarization of the emission will be determined almost entirely by the top layer. It therefore appears that a two-layer model of the lunar surface of the type suggested provides a rather self-consistent explanation of several different types of observations made of the moon by radio waves. The simple two-layer model suggested here could possibly be refined by introducing a gradual change in the dielectric constant with depth, but it does not appear that the experimental data warrant such a refinement as yet.

The double-layer model of the lunar surface described appears to fit Gold's "dust" hypothesis,[44] and it also might fit Kuiper's ideas about a rock froth layer of low density.[45] The density of the surface layer cannot be derived unambiguously from the data presented here. If the surface material in compacted form has a dielectric constant of 4.5 to 5 as we suggest for the bottom layer, the porosity of the top layer can be estimated on the basis of either Odelevskii and Levin's expression[36] or on the basis of Twersky's[46] formula, both of which can be derived from the Lorentz-Lorenz expression. The porosity turns out to be about 70 percent. If the dielectric constant of the material in bulk is much greater, the porosity must be correspondingly higher.

## 5. Conclusions

It appears that the results presented above provide fairly direct evidence for the presence of a tenuous surface layer on the moon nearly everywhere in excess of some 20 cm in depth and having a dielectric constant of about 1.7 to 1.8. There is also good evidence that the young crater Tycho does not have such a surface layer in the same measure as the rest of the moon.

The technique described could well be exploited much more extensively to explore several different features on the moon for possible classification in terms of the extent to which they possess such a layer. Much better bounds on layer depth could be obtained if other radar systems working at different wavelengths could be used in the same type of experiment. It should also be noted that similar observations could be made on some of the near planets in order to gain some further insight into their surface characteristics or possibly their atmospheres.

The firm demonstration of a frequency dependence of lunar cross section would provide additional evidence concerning the hypothesis of the tenuous surface layer. Uncertainties in calibrations of the different radars with which cross sections have been obtained in the past, as exemplified in Fig. IV-7, do not permit definition of such a dependence. Availability of the

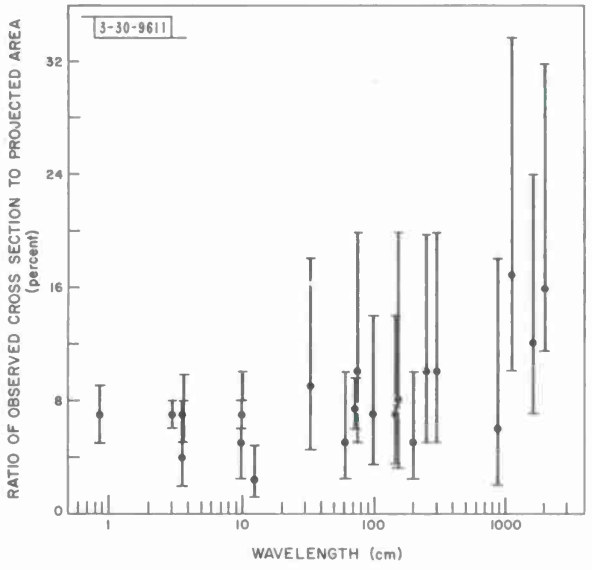


Fig. IV-7. Various experimental determinations of lunar cross section.

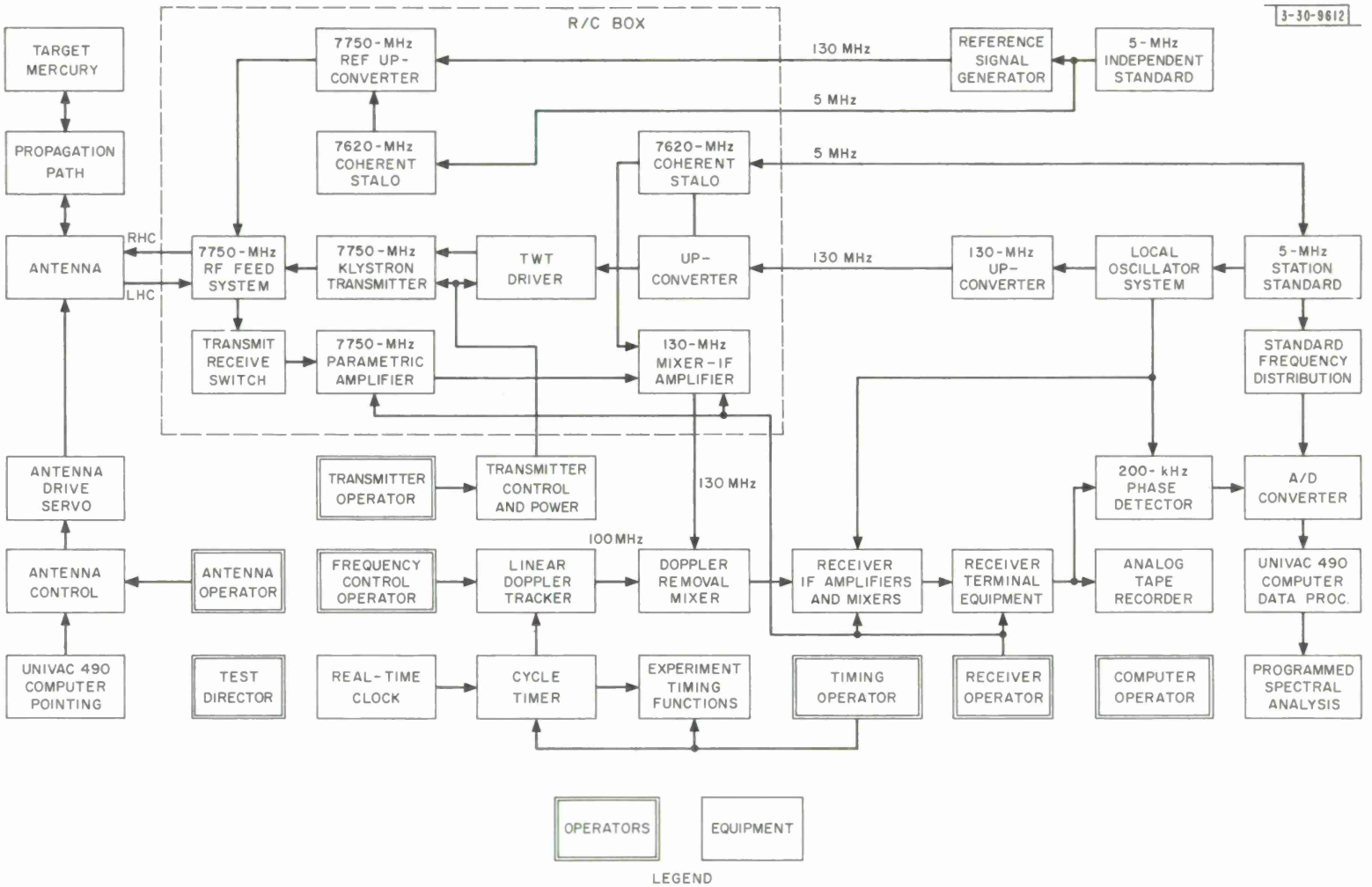


Fig. IV-8. Haystack radar configuration for CW Mercury observations.

orbiting Lincoln Calibration Sphere, already being used to standardize the Millstone radar, should make possible accurate cross-section determinations (±0.3 db) with a number of radars. It is hoped that such measurements can be arranged.

## C. FIRST PLANETARY OBSERVATIONS WITH HAYSTACK

### 1. Introduction

The first opportunity to make planetary radar observations using the newly completed Haystack system came in April 1965, when Mercury was observed at inferior conjunction. As reported in Sec. IV-A-1, Mercury has previously been detected at wavelengths of 70 cm (at Arecibo, Puerto Rico), 40 cm (at the deep-space tracking station in the Crimea), 23 cm (Millstone Hill), and 12.5 cm (by the Jet Propulsion Laboratory at Goldstone, California). All observers report a radar cross section on the order of 5 percent of the projected area of the disk, except the Millstone group who reported a value near 10 percent.

The Haystack measurements reported here are the first radar observations of Mercury at X-band. We now outline the way in which the equipment was employed for this experiment, and the experimental results.

### 2. The Radar System

The parameters of the Haystack radar as employed in the observations of Mercury in April 1965 are set forth in Table IV-4. Figure IV-8 provides a block diagram of the equipment. The full output power of the Haystack transmitter (100 kw) had not been realized at the time of these observations and accordingly measurements were made using lower power (25 kw). In order to obtain the largest possible signal-to-noise ratio, the transmitter was made to radiate unmodulated for the length of time required for the signals to travel to Mercury and return (approximately 10 minutes). Thereafter the transmitter was shut down and an equal length

TABLE IV-4

HAYSTACK – APRIL 1965

SYSTEM PARAMETERS FOR THE MERCURY CW RADAR

| | |
|---|---|
| Frequency | 7750 MHz (3.87 cm). Locked to frequency standard |
| Transmitted power | 25-kw CW klystron |
| Antenna | 120-foot-diameter parabola, space frame radome. Cassegrainian feed, circular polarization. |
| Antenna gain | 66.1 db over isotropic |
| Beamwidth | 0.070° half power |
| Antenna pointing | Computer controlled from ephemeris data |
| Receiver | Nitrogen-cooled parametric amplifier |
| System temperature | 145°K |

period of reception ensued. A further receive period followed in order to establish the noise level in the receiver in the absence of any signal.

Throughout the observations the antenna was directed to follow the position of Mercury in the sky by the Univac 490 computer. During transmission, the pointing program directed the antenna ahead of Mercury to compensate for the time of flight, even though the angular extent of the antenna beam (0.07°) was just large enough to include both the optimum transmit and receive positions. The computer, in addition, performed real-time processing of the received signals.

Great care was taken in the design of the transmitter exciter system to ensure that a monochromatic signal is transmitted. The transmitter signal frequency was derived from the 5 MHz station standard oscillator. The spectral width of the radiated signal was of the order of 0.1 Hz.

The RF amplifier employed in the receiver was a liquid-nitrogen-cooled parametric amplifier which gave a system temperature of 145°K. The receiver was a multiple superheterodyne system whose local-oscillator frequencies are synthesized from the same frequency standard that is used to drive the transmitter. The Doppler shift of the received signal (caused by the motion of Mercury relative to a terrestrial observer) was compensated in the receiver by adjusting the frequency of one of the local-oscillator signals, using a coherent frequency synthesizer which was programmed to change its frequency linearly with time. Each linear fit to the varying Doppler shift was chosen as being best for the following 10-minute interval. The maximum error introduced by this approximation was about ±2 Hz. An ephemeris computing program was employed in advance of the observations to generate predictions for the range, Doppler shift, etc., which is basically the same as that often employed for Millstone radar observations. It is believed that the predicted Doppler shift was about 10 Hz higher than the true value during these observations. This suggests that Mercury was in advance of its predicted position.

The final IF output signal of the receiver was fed to two phase detectors driven in phase quadrature, yielding the sine and cosine components of the radar signal. The overall bandwidth of the receiver was set to be 250 Hz by low-pass filters inserted at this point. Analog tape recordings of the IF signal with a bandwidth of 1 kHz were made simultaneously. The outputs of the phase detectors were sampled by means of an A/D converter at a 500-Hz sampling frequency for each component and transferred into the U490 computer. A Fourier spectral analysis of the signals was performed by the computer, which in effect synthesized a bank of nine filters. Each had a bandwidth of 25 Hz and the separation between filters was also 25 Hz. The outputs were squared and averaged over the round trip delay time of approximately 10 minutes.

An actual experimental run consisted of a CW transmission period somewhat longer than the planetary round-trip time, followed first by a period of signal reception equal to the round-trip time and second by a calibration period of reception equal in all respects to the signal reception period. These calibration periods were used to establish the bandpass response of the receiver, and since the noise level was considerably higher than the intensity of the signal, a simple subtraction of each calibration run from the previous signal reception period served to remove first-order effects of any irregularities in the response of the system. Since the receiver gain and/or noise level unavoidably changed slightly between signal and noise reception, the exact base line

of the signal spectrum was not established. The Mercury signal level for a single run in the 25-Hz filter bandwidth was only about 2°K out of a typical system noise level of 145°K. The system sensitivity was calibrated in terms of independently measured system temperature. Unfortunately, an accurately calibrated reference signal source was not available during the experiment.

### 3. Experimental Results

Thirty-eight experimental runs were attempted during the period from 15 to 23 April 1965. Of these, 32 were judged to be useful runs in that no obvious equipment malfunctions occurred. Real-time data processing was accomplished for 31 of these runs. Later, the analog magnetic tape records of 25 runs were processed. For the real-time runs, it was possible to synthesize only nine 25-Hz filters and hence cover 200 Hz of the echo spectrum. The tape records were processed by using fifteen filters which covered 350 Hz.

In a typical run shown in Fig. IV-9, the system operated with an equivalent temperature of 154°K. The noise standard deviation was computed to be 2°K for this run with the 25-Hz predetection noise bandwidth and effective postdetection addition of the calibration results to those of the signal period. Since the strongest echo contribution (in the centrally located filter) was only about 2.0°K, it may be seen that a single run does not provide a conclusive result. However, the signal-to-noise ratio achieved by averaging all the available runs is enough to make identification of an echo from Mercury quite certain.

The absolute scales of the outputs of the individual filter channels were determined from the known system temperature and the output levels observed for the calibration period of

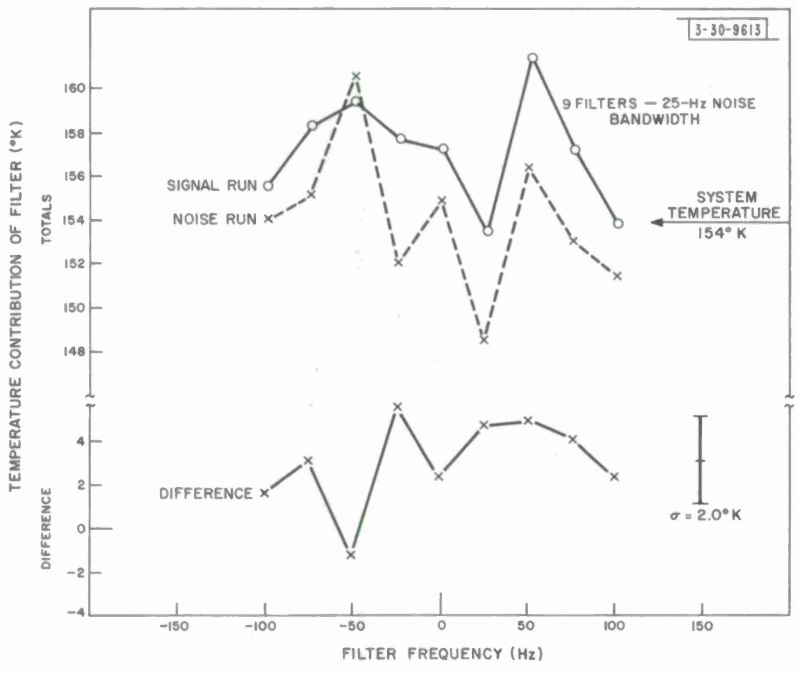


Fig. IV-9. Haystack Mercury CW radar, 17 April 1965, run 107-4.

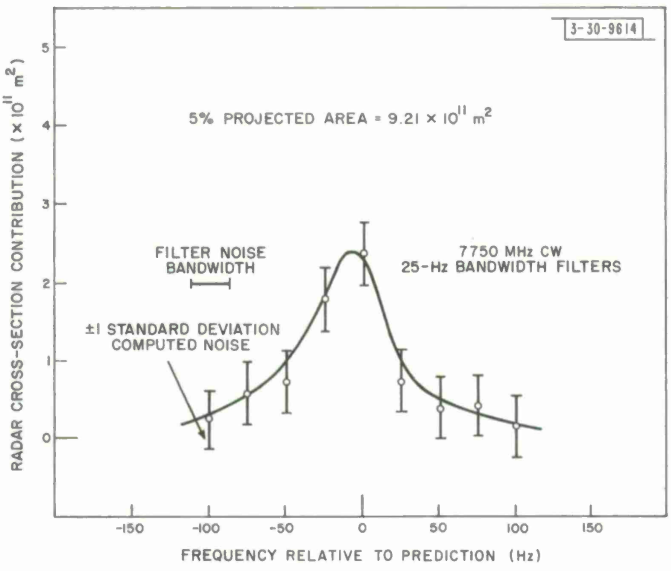


Fig. IV-10. Mercury, April 1965, signal power spectrum. Real-time data. Average, 31 weighted runs.

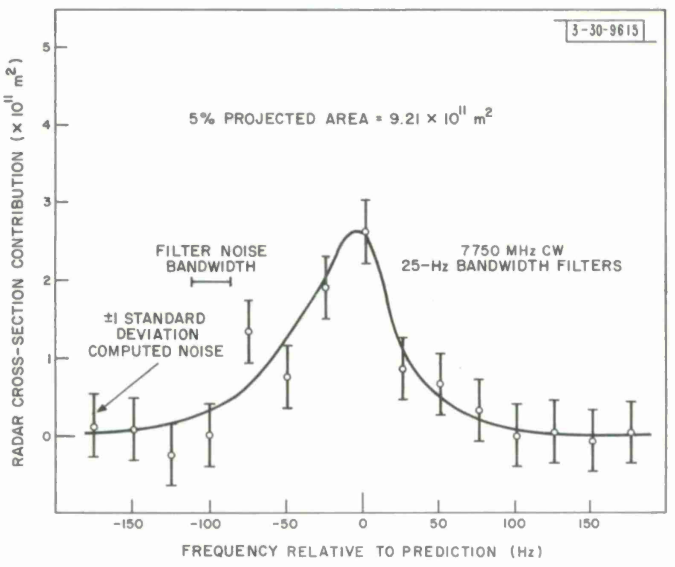


Fig. IV-11. Mercury, April 1965, signal power spectrum. Analog playback data. Average, 25 weighted runs.

integration. These values for the echo power (in terms of an equivalent increase in system temperature) were converted into equivalent radar cross-section contributions, using the known and measured system parameters. The results of the individual 31 live runs were added with a weighting proportional to the expected signal-to-noise ratio; that is, with weights taking into account transmitted power, system temperature, target range, and integration time. The weighted mean result is shown in Fig. IV-10. A similar plot for 25 analog recorded runs is shown in Fig. IV-11. The frequency scale in these figures has an origin which depends upon the planetary ephemeris program.

The base lines of the echo power shown in the figures have been established primarily by assuming negligible echo power in the wings of the spectrum. It is largely for this reason, rather than uncertainty in the values of the system parameters, that a ±3-db error estimate on the radar cross section is given.

If the echo power in all the filters is added and the radar cross section computed, a result of $9 \times 10^{11}$ $m^2$ (5 percent of Mercury's projected area) is obtained. The computed noise standard deviations of the averaged spectra are shown on each diagram. The signal-to-noise ratio is inadequate to permit extensive conclusions about details in the spectrum. The half-power width of the spectrum appears to be about 50 to 75 Hz, but it must be remembered that the measured spectrum is the result of convolution of the 25-Hz filters with the actual spectrum, and in addition is corrupted by noise. A systematic change in the ephemeris error during the course of the experiment could also cause the spectrum to appear wider than it should.

The shape of the spectrum (Figs. IV-10 and IV-11) suggests the presence of both quasi-specular and diffuse scattering components. Thus, the spectrum has a relatively narrow spectral peak (which, in reality, could be narrower than is indicated) which we associate with quasi-specular reflection. There seems definite evidence of wings to the spectrum, but the signal-to-noise ratio does not allow any real measure of the limb-to-limb Doppler shift or of the planetary rotation rate.

It would be most desirable to have experimental results in which the signal-to-noise ratio is sufficiently high to provide useful results in a single run rather than in the aggregate of many. It would then be possible to recognize many experimental faults that might otherwise be overlooked. Effects of systematic change in ephemeris errors could be eliminated, such as a change in Doppler prediction or in range delay for pulse experiments. Further Mercury experiments are planned for December 1965, when the 100-kw transmitter will be available and the signal strength correspondingly improved.

## D. A "FOURTH TEST" OF GENERAL RELATIVITY

### 1. Introduction

In 1964, I. Shapiro[47,48] proposed a fourth test of the theory of general relativity which Albert Einstein postulated in 1916. It occurred to Shapiro, while he was engaged in studies related to planetary radar astronomy, that the predicted gravitational effect of the sun on radar waves passing close by could be sought for experimentally by means of a modern high-power radar system designed specifically for the task.

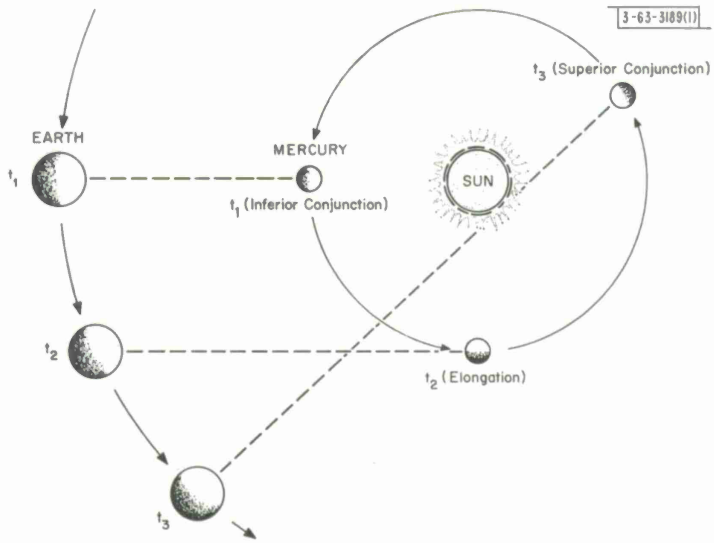


Fig. IV-12. Effects of general relativity on interplanetary time-delay measurements.

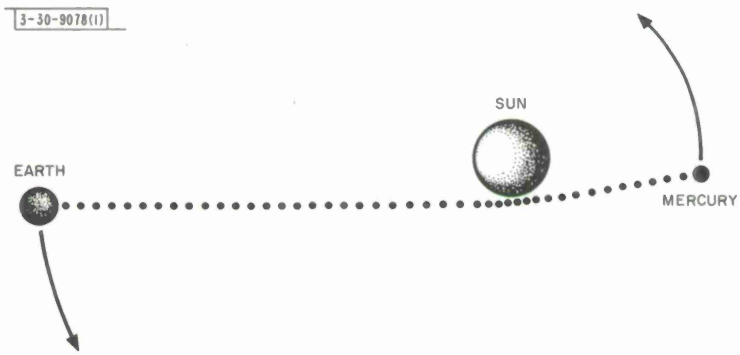


Fig. IV-13. Relativistic effect on electromagnetic wave propagation.

Previous tests of the theory of general relativity, which is basic to modern physics, have been few. To a large degree, this is due to the difficulty in measuring the small differences between the behavior predicted by Newtonian theory and that predicted by general relativity. Three tests previously proposed by Einstein involve: (a) the interaction of matter on electromagnetic waves, e.g., the bending of light passing near the sun, (b) the interaction of matter on matter, e.g., the advance of the perihelion of Mercury's orbit (43 seconds of arc per century in excess of the Newtonian prediction), and (c) the relativistic red shift – normally sought in emissions from the sun, where the spectral line emission takes place in a high gravitational field. In probably the most accurate experiment to date, Pound and Snider[49] in 1964 used the Mössbauer effect to measure the frequency shift in gamma rays moving in the earth's gravitational field. Although the results of the Pound and Snider experiment appear consistent with the theory of general relativity, as do astronomical studies of the bending of light waves and the observed changes in the orbit of Mercury, high-accuracy determations are so difficult that a different type of test affording improved accuracy would be a substantial contribution.

### 2. Nature of Test

Basically, Shapiro proposes that a state-of-the-art planetary radar be used to measure accurately the time of flight of signals to and from one of the inner planets at intervals throughout the orbit, including times near superior conjunction. At such times, the propagation path passes near the sun (Fig. IV-12), with the result that, according to general relativity, the intense gravitational field will cause a slowing of the velocity of propagation on both the outbound and return trip of the radar energy* (Fig. IV-13).

Shapiro's computed predictions of the gravitational effect around the orbits of Mercury and Venus are plotted in Figs. IV-14 and IV-15, respectively. Near superior conjunction, a relativistic increase in the time of flight of nearly 200 μsec is predicted, as compared with a predicted effect of less than 20 μsec between elongation and inferior conjunction.

It remains, then, to attempt to check one of these predicted curves experimentally by making the series of range measurements. The fact that the effect is appreciable over a fair fraction of the orbit makes it unnecessary to rely solely on observations very near superior conjunction, when echoes are weakest and solar noise is most troublesome. A long series of such measurements will in fact be required to refine the elements of the orbit sufficiently to allow a relativistic effect to be detected. These data, if taken over a sufficient time, can serve also in determining still more accurately the relativistic advance in the perihelion of the orbit.

### 3. Feasibility

It is evident that of the facilities available to Lincoln Laboratory, only the Haystack Research Facility (Appendix B) may be capable of sufficient radar performance to observe the inner planets at superior conjunction.

From the point of view of sensitivity alone, the radar of the Arecibo Ionospheric Observatory with its 1000-foot-diameter reflector, would be able to make the necessary measurements.

---

* A bending effect on the order of 1 arc second is also predicted, which today's radars, of course, cannot observe.

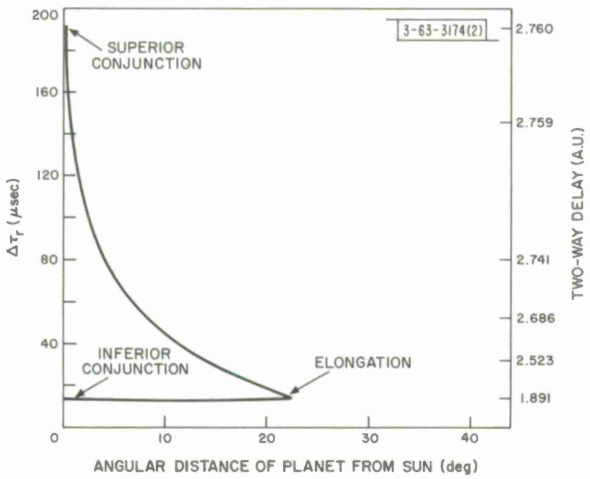


Fig. IV-14. Relativistic effect on Earth-Mercury time delays.

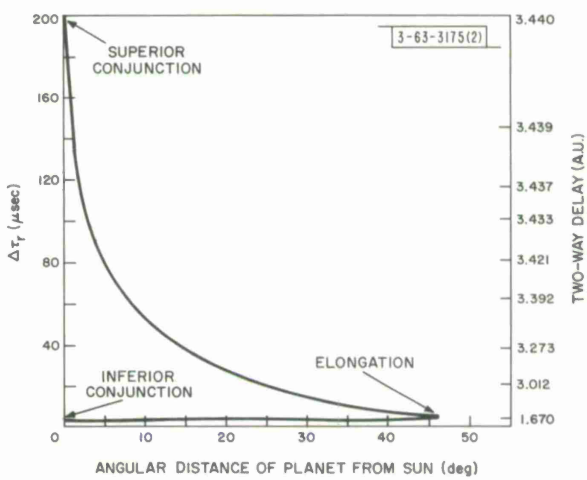


Fig. IV-15. Relativistic effect on Earth-Venus time delays.

Unfortunately, at the 430-MHz operating frequency of Arecibo, it has been calculated, using the results of Erickson[50] that the effect of the solar plasma, when the radar waves pass within four solar radii of the sun, would produce a delay several times that predicted from general relativity, even during the quiet sun period.

The present 85-ft Venus radar at JPL's Goldstone station is insufficiently sensitive to make the measurements. Further, at its operating frequency of 2388 MHz, the plasma effect will be appreciable. Indeed, by the time the projected 210-ft antenna is ready at the Mars site of Goldstone, increasingly disturbed solar conditions may make a meaningful experiment of this sort impossible for some years.

Fortunately, at the 7750-MHz frequency of Haystack, the effect of solar plasma will be very small, e.g., on the order of 1 μsec during the quiet sun period and some 7 μsec when the sun is most active. It remains to show that sufficient radar sensitivity can be achieved at Haystack to permit measurements of the required accuracy.

In preliminary computations made shortly after the experiment was proposed, it was indicated that mere CW detection of either Mercury or Venus near superior conjunction would be marginal with the radar initially planned for Haystack. Measurements of range to the required accuracy seemed out of the question. However, it also appeared that, if an overall increase of 10 db in radar performance could be achieved, the measurements would become possible.

Developments already under way in high-power X-band klystrons and in X-band receiving masers indicate that a radar having a 7-db improvement in transmitter power and a 3-db reduction in receiver noise temperature with respect to the presently planned system seems achievable.

Postulating such a radar, and assuming the validity of the 5-percent cross-section determination for Mercury reported in Sec. IV-C, one may summarize the conditions for a worthwhile experiment at Haystack as set forth in Table IV-5.

### 4. Instrumentation and Plans

The high-accuracy range measurements required in the "fourth test" will be undertaken by a projected high-performance radar in combination with a sophisticated signal processing system – probably a rake-radiometer technique.* A simplified block diagram is given in Fig. IV-16. The transmitter produces a constant-envelope signal the phase of which is reversed under the control of an appropriate code generator. During reception, the echo signal is processed through a matched filter, the output from which is coherently detected, digitized, and processed in a high-speed computer to produce a range-range rate "map" of the planetary echo. System Doppler and range corrections necessary to compensate for changes due to earth's rotation and relative orbital motion of the planets are derived from precomputed and recorded ephemerides.

The rake-radiometer processing, which has been proposed by R. Price but not as yet published externally, is accomplished by ascertaining the time alignment which gives the maximum correlation between the received $r$-$\dot{r}$ map and a reference map stored in the computer.

* Techniques used at Millstone and elsewhere have made range determination to ±10 μsec possible for some time. However, the rake-radiometer method should be perhaps 2 db more sensitive than earlier methods, since it uses all the target energy.

TABLE IV-5

POSSIBLE EXPERIMENTAL PARAMETERS AND POWER BUDGET FOR RANGE MEASUREMENTS TO MERCURY AT SUPERIOR CONJUNCTION (Haystack at 7750 MHz)

| | |
|---|---|
| Antenna gain (including radome) | 64.2 db vs isotropic |
| Antenna aperture (including radome) | 25.0 db vs 1 $m^2$ |
| Transmitted average power | 57.0 dbw |
| kT* | −210.0 dbw |
| System losses | − 1.2 db |
| System threshold on nondispersive target (signal = noise in 1-Hz filter) | 357.4 db |
| System threshold vs Mercury (in 20-Hz filter) after 10,000-sec integration | 364.4 db |
| Path loss to Mercury (favorable superior conjunction) | 355 db |
| S/N for a CW detection | ≈10 db |
| Probable degradation due to range quantization | ≈ 3 db |
| Useful S/N for range determination | ≈ 7 db |

*Equivalent T ≈ 75°K, estimated (in °K) as follows:

| | |
|---|---|
| Receiving line loss | 10 |
| Receiver temperature | 15 |
| Radome | 15 |
| Background (including sun) | 35 |
| | 75 |

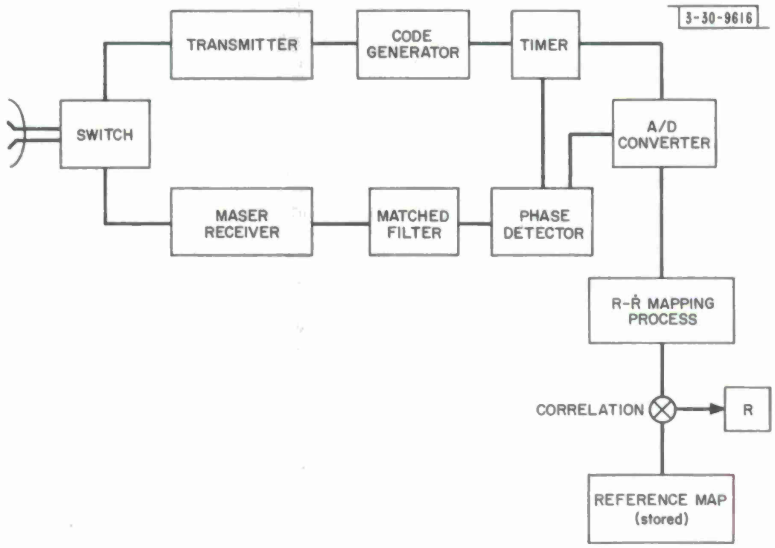


Fig. IV-16. Haystack radar for Shapiro test.

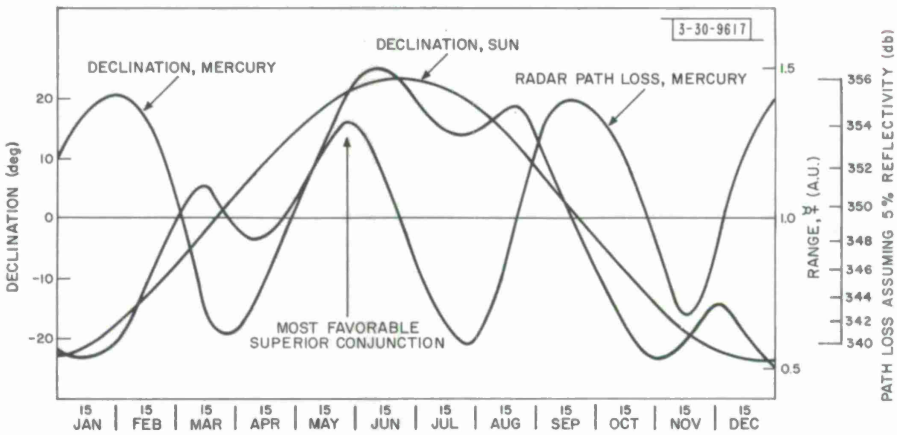


Fig. IV-17. Declination and path loss for Mercury, 1966.

This reference map is prepared from the target's estimated scattering function, based upon earlier measurements made near inferior conjunction when the echo is strong.

A completely new RF box (Appendix B) is under construction which will contain an X-band 500-kw transmitter and a traveling-wave maser contributing on the order of 10° to 15° of excess noise temperature. These components plus careful microwave engineering are expected to yield the 10 db of additional radar sensitivity shown earlier to be required for the "fourth test." The new assembly will be called the PR or planetary radar box.

The transmitter will incorporate two 250-kw klystrons with associated phasing and drive equipment. These tubes, currently under development, will have beam control electrodes and will be switched off by a suitable modulator during receive time.

Particular attention is being paid to the maintainance of high spectral purity in transmitter and local-oscillator chains (line width of 0.1 Hz is being sought), and to the accurate measurement of delay time. A hydrogen maser has been provided to serve as the prime frequency source in experiments such as this one.

A high-speed computer has been installed for handling much of the data processing, but formidable interfacing and programming tasks remain before measurements can be undertaken by the methods proposed.

At least until X-band Venus measurements are made to determine the exact cross section,* Mercury will remain the center of planning for the Shapiro test. Its synodic period of 116 days yields some three superior conjunctions each year. Not all these are favorable for the "fourth test," since differences in declination prevent the planet from passing close to the sun. Figure IV-17 is a composite plot showing declination of the sun, declination of Mercury, and radar path loss† to that planet as a function of time during CY 66. It will probably not be possible to make measurements applicable to the Shapiro test during the favorable conjunction of May 1966, but it will be valuable to begin measurements as soon thereafter as possible.

---

*Karp, et al.,[51] deduced a 1-percent figure from X-band measurements with Project West Ford equipment.

†Here defined to be the loss in decibels of the path from the terminals of an isotropic transmitting antenna to the terminals of a unit aperture receiving antenna pointed at the target.

## REFERENCES


1. R. Price, et al., Science 129, 751 (1959).
2. G.H. Pettengill and R. Price, Planet. Space Sci. 5, 70 (1961).
3. J.V. Evans and G.N. Taylor, Nature 184, 1358 (1959).
4. W.K. Victor and R. Stevens, Science 134, 46 (1961).
5. Staff, Millstone Radar Observatory, Nature 190, 592 (1961).
6. I. Maron, G. Luchak, and W. Blitstein, Science 134, 1419 (1961).
7. J.H. Thomson, G.N. Taylor, J.E.B. Ponsonby, and R.S. Roger, Nature 190, 519 (1961).
8. V.A. Kotel'nikov, Brit. Inst. Radio Engrs. 22, 293 (1961).
9. W.K. Victor, R. Stevens, and S.W. Golomb, Technical Report 32-132, Jet Propulsion Laboratory, Pasadena, California (1961).
10. D.O. Muhleman, D. Holdridge, and N. Block, Astron. J. 67, 191 (1962).
11. G.H. Pettengill, et al., Astron. J. 67, 181 (1962).
12. W.B. Smith, Astron. J. 68, 15 (1963).
13. V.A. Kotel'nikov, et al., Doklady Akad. Nauk SSSR 145, 1035 (1962).
14. I.I. Shapiro, presented to the International I.A.U. Meeting, Paris, 1963.
15. V.A. Kotel'nikov, et al., Doklady AN SSSR 151, 532 (1963).
16. R.M. Goldstein and R.L. Carpenter, Science 139, 910 (1963).
17. R.L. Carpenter, Astron. J. 69, 2 (1964).
18. R.M. Goldstein, Astron. J. 69, 12 (1964).
19. J.C. James and R.P. Ingalls, Astron. J. 69, 19 (1964).
20. W.K. Klemperer, G.R. Ochs, and K.L. Bowles, Astron. J. 69, 22 (1964).
21. J.E.B. Ponsonby, J.H. Thomson, and K.S. Imrie, Nature 204, 63 (1964).
22. R.C. Tausworthe, IEEE Trans. Space Electron. Telem. SET-11, 78 (1965).
23. V.A. Kotel'nikov, et al., Doklady Akad. Nauk SSSR 147, 1320 (1962).
24. R.L. Carpenter and R.M. Goldstein, Science 142, 3590 (1963).
25. V.A. Kotel'nikov, Vestnik AN SSSR 2, 39 (1964).
26. R.M. Goldstein, IEEE Trans. Mil. Electron MIL-8, 199 (1964).
27. _____, Rev. Geophys. 2, 579 (1964).
28. J.H. Thomson, Quart. J. Roy. Astron. Soc. 4, 347 (1963).
29. J.V. Evans, R.A. Brockelman, J.C. Henry, G.M. Hyde, L.G. Kraft, W.A. Reid, and W.W. Smith, Astron. J. 70, 486 (1965).
30. R.M. Goldstein and W.F. Gillmore, Science 141, 1171 (1963).
31. V.A. Kotel'nikov, et al., Doklady AN SSSR 151, 811 (1963).
32. J.V. Evans and G.H. Pettengill, J. Geophys. Res. 68, 423 (1963).
33. R.D. Rea, N. Hetherington, and R. Mifflin, J. Geophys. Res. 69, 5217 (1964).
34. G.H. Pettengill and T.W. Thompson, private communication.
35. V.S. Troitskii, Astron. Zh. 41, 724 (1964).
36. V.C. Krotikov and V.S. Troitskii, Astron. Zh. 39, 1089 (1962).
37. V.S. Troitskii, Astron. Zh, 51, 511 (1954).

38. N.S. Soboleva, Astron. Zh, 39, 1124 (1962).

39. C.E. Heiles and F.D. Drake, Icarus 2, 281 (1963).

40. J.W.M. Baars, P.G. Mezger, N. Savin, and H. Wendker, private communication.

41. F.F. Gardner, private communication of results from the CSIRO Parkes antenna.

42. G.H. Pettengill and J.C. Henry, "Radio Measurements of the Lunar Surface," in The Moon, Ed. by Z. Kopal and Z.K. Mikhailov (Academic Press, London, 1962), p. 519.

43. J.R. Davis and D.C. Rohlfs, J. Geophys. Res. 69, 3257 (1964).

44. T. Gold, "Processes on the Lunar Surface," in The Moon, Ed. by Z. Kopal and Z.K. Milhailov (Academic Press, London, 1962), pp. 433-439.

45. G.P. Kuiper, NASA Technical Report 32-700, National Aeronautics and Space Administration (1965), pp. 9-73.

46. V. Twersky, J. Math. Phys. 3, 724 (1962).

47. I.I. Shapiro, "Effects of General Relativity on Interplanetary Time-Delay Measurements," Technical Report 368, Lincoln Laboratory, M.I.T. (18 December 1964), DDC 614232.

48. _____, Phys. Rev. Letters 13, No. 26, 789 (28 December 1964), DDC 613894.

49. R.V. Pound and J.L. Snider, Phys. Rev. Letters 13, No. 18, 539 (2 November 1964).

50. W.C. Erickson, Astrophys. J. 139, 1290 (1964).

51. D. Karp, W.E. Morrow, Jr., and W.B. Smith, Icarus 3, Nos. 5, 6, 473 (1964).

# V. ATMOSPHERIC RESEARCH

## A. IONOSPHERIC STUDIES

### 1. Introduction

In recent years, the study of the upper part of the earth's ionosphere has received considerable impetus from the development of satellite and rocket methods of exploration. In the measurement of electron density, outstanding results have been obtained with the satellite Ariel and the topside sounder Alouette. In addition, the rocket measurements made from Wallops Island, Virginia, have been particularly successful.

Despite the extent of this work, the complex chemical and dynamic behavior of the F-region remains incompletely understood. An understanding of the behavior of the ionospheric F-layer could perhaps be derived from observations in which the following quantities are measured simultaneously as functions of height: (a) electron density; (b) electron temperature; (c) ion temperature; (d) ion composition; (e) neutral density; (f) neutral temperature; (g) neutral composition; and (h) the incident solar radiation. At the present time, many of these quantities are being measured individually by means of satellites, but it is often difficult to extract from these data the separate dependence of, for example, the electron temperature on height, local time, latitude (and longitude), and variations in the solar flux. Thus, rockets appear to provide the best means of making these measurements, but so far none have been equipped to measure simultaneously more than three of the quantities involved. Further, in order to observe temporal variations, repeated rocket launchings are required which involve considerable effort and expenditure.

One relatively inexpensive ground-based method can provide measurements of the quantities (a) through (d) but, since it is a radio method, it is insensitive to the quantities (e) through (h). This method is the radar incoherent backscatter technique discussed by Gordon[1] and employed to study the ionosphere, first by Bowles[2,3] and later by Pineo, et al.[4,5] At the present time, the technique is being employed to study the ionosphere at the Jicamarca Radar Observatory (Lima, Peru), the Arecibo Ionospheric Observatory (Arecibo, Puerto Rico), Millstone Hill Field Station (Westford, Massachusetts), Prince Albert Radar Laboratory (Prince Albert, Saskatchewan, Canada), and the Royal Radar Establishment (Malvern, England). Another facility is under construction at Nançay in France.

The Millstone Hill backscatter facility in its present form came into operation in January 1963, and this report presents an account of some of the work conducted since then. In Sec. V-A-2, we review briefly the theory of the method. A short description of the incoherent backscatter radar facility at Millstone Hill is provided in Sec. V-A-3, the observational methods are discussed in Sec. V-A-4, and reduction procedures are presented in Sec. V-A-5. Some of the results are reviewed in Sec. V-A-6.

## 2. Theory

Electron-Density Distribution:– Gordon[1] pointed out that if a very powerful radar beam were directed at the ionosphere, a weak but detectable echo from the free electrons there might be obtained. The intensity of the echo can be computed by assuming that the electrons scatter independently with a scattering cross section $\sigma_c$ given by the square of the classical radius $r_e = (e^2/mc^2)$. Some confusion has arisen because this cross section is defined as that which scatters energy into unit solid angle, whereas, in radar calculations, it is customary to normalize the cross section to correspond to power reflected into $4\pi$ solid angle. Hence the radar cross section $\sigma_e$ is expected to be $4\pi\sigma_c (\sim 10^{-28}\ m^2)$. For a volume containing N electrons, the phase of the N-reflected waves will be independent and the powers should add to give an average scattered power proportional to $N\sigma_e$. Because at any given height the electrons completely fill the radar beam, the echo power should vary with range R only as $1/R^2$, not $1/R^4$ as for conventional ("point") targets. For observations conducted in the zenith, it may be shown that the echo power $P_r$ is given in

$$P_r = \frac{P_t \eta_r^2 c\tau N\sigma\lambda^2}{64\pi^2 h^2} \int_\Theta G^2(\Theta) \sin\Theta \, d\Theta \quad , \tag{1}$$

where $P_t$ is the transmitter power, $\eta_r$ is the efficiency of the waveguide or feeder system, c is the velocity of light, $\tau$ is the pulse length, $\lambda$ is the radio wavelength, and h is the height to the pulse center. $G(\Theta)$ is the antenna gain over a lossless isotropic radiator, assuming that the antenna pattern is cylindrically symmetrical about its axis, and $\Theta$ is the angle subtended in any direction from this axis. The electron cross section $\sigma$ is usually different from $\sigma_e = (4\pi\sigma_c)$ for reasons which will be given. For a typical parabolic antenna, Eq. (1) can be reduced to

$$P_r = 0.74 \frac{P_t \eta_r^2 c\tau N\sigma A_o}{16\pi h^2} \tag{2}$$

where $A_o$ is the effective antenna aperture. From Eq. (2) we see that, for the detection of a given density N at a given height h, the radar designer can adjust only the product $P_t \tau A_o$. If, however, it is necessary to obtain a given height resolution $\Delta h = c\tau/2$, we have no choice but to employ both a high transmitter power $P_t$ and large effective aperture $A_o$ to obtain useful results. One of the largest systems so far constructed (at Arecibo, Puerto Rico) employs the same transmitter power $P_t$ as the Millstone Hill radar, but has a value of $A_o$ which is twenty times that at Millstone. If the electron density were independent of height, the Arecibo radar could be expected to detect echoes four times higher than Millstone, but in practice this ratio will be more nearly two times.

Signal Spectra:– Bowles[2] was first to discover that the Doppler width of the reflected signals was considerably less than expected for a model of the scattering in which it is assumed that each electron contributes a signal with a Doppler shift proportional to the component of its velocity in a direction to the radar. Bowles correctly attributed this behavior to the role played by the ions in the plasma. Subsequent theoretical papers by Fejer[6] and others have shown that

when the radar wavelength $\lambda$ is greater than $4\pi\lambda_D$, where $\lambda_D$ is the Debye length ($= \sqrt{kT/4\pi Ne^2}$), the simple model above must be replaced by one in which the collective behavior of the electrons and ions is considered. The motions of the ions govern fluctuations in the electron density (with a scale of $\lambda_D$), and these fluctuations constitute small changes in the refractive index. When the radar wavelength is significantly larger than the size of these fluctuations, they must be thought of as the scattering centers and not the individual electrons. The situation becomes more complex when observations are conducted in directions normal or nearly normal to the magnetic-field lines, for then the gyrorotation of the ions causes the ion motions to be ordered. This case has been considered by Fejer[7] and others, and experimental verification of the narrowing of the spectrum has been reported by Pineo, et al.,[8] based upon measurements obtained by him and his colleagues from Millstone, utilizing the Trinidad UHF radar. As magnetic effects play no part in observations at the Millstone Hill observatory, they will not be discussed further here.

In the theory developed by Fejer[6] it is assumed that both electrons and ions have Boltzmann energy distributions and that collisions are infrequent and may be neglected. Then, if it is further assumed that only singly charged ions of mass $m_i$ are present, the shape of the echo spectrum takes the form shown in Fig. V-1. It is clear from this figure that the echo power frequency spectrum is a function of both the electron temperature $T_e$ and ion temperature $T_i$; hence, by determining the shape of the spectrum, the ratio $T_e/T_i$ can be determined. If, in addition, $m_i$ is known, then $T_i$ can be obtained from the total width of the spectra. The first observations of the spectrum shapes from which these quantities were extracted were reported by Evans[9] and Pineo and Hynek.[10]

Electron Cross Section:— The cross section of the electrons $\sigma$ is proportional to the area under the curve in Fig. V-1 and, as such, depends upon the ratio $T_e/T_i$. This dependence has been considered by Bunneman[11] and others. Bunneman gives for $\sigma$ the expression

$$\sigma = \sigma_e \left\{ 1 - \frac{1}{1 + \left(\frac{4\pi\lambda_D}{\lambda}\right)^2} + \frac{1}{\left[1 + \left(\frac{4\pi\lambda_D}{\lambda}\right)^2\right]\left[1 + \left(\frac{4\pi\lambda_D}{\lambda}\right)^2 + \frac{T_e}{T_i}\right]} \right\} . \qquad (3)$$

Thus, for very short wavelengths, $4\pi\lambda_D \gg \lambda$, $\sigma \to \sigma_e$. In the ionosphere, at heights presently being studied by this technique, the Debye length $\lambda_D$ is of the order of a few millimeters, and for these radars $\lambda > 4\pi\lambda_D$. When $\lambda \gg 4\pi\lambda_D$, Eq. (3) becomes

$$\sigma = \sigma_e \{1/[1 + (T_e/T_i)]\} \qquad (4)$$

and thus the highest cross section that can be expected (under conditions of thermal equilibrium) is $\sigma = 0.5\sigma_e$ ($= 0.499 \times 10^{-28}$ m$^2$).

If $T_e/T_i$ is a function of altitude h, the electron-density profile N(h) can be determined from Eq. (2) only if the height dependence of $\sigma$ is known. This complication was not immediately recognized and some published backscatter profiles of electron density are now thought to be in error. This difficulty has caused Bowles,[12] operating at 50 MHz, and Greenhow, et al.,[13] operating at 398 MHz, to adopt a method of deriving an electron-density profile from measurements of the Faraday rotation of the radio waves in place of the echo power. The technique is difficult to implement at frequencies above 100 MHz, where the amount of rotation is small.

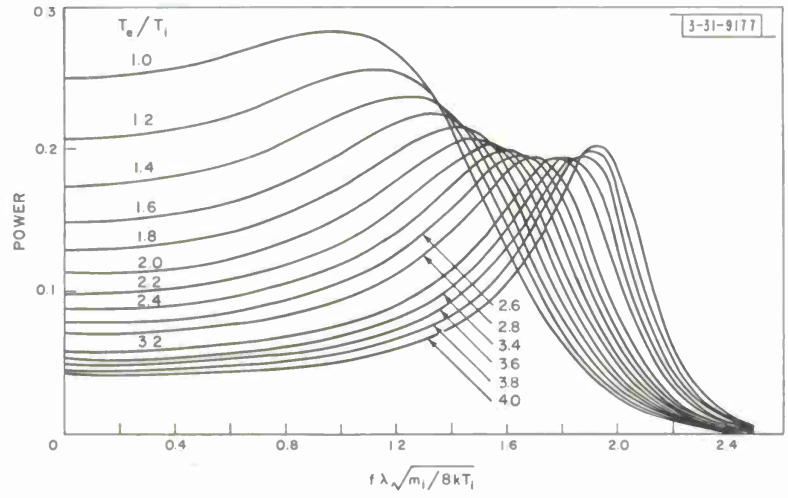


Fig. V-1. Theoretical spectra of ionospheric backscatter signals computed for various values of electron-to-ion temperature ratio $T_e/T_i$. Spectra are symmetrical about center frequency. It has been assumed that mass $m_i$ of ions is that of $O^+$. Abscissa is Doppler shift f normalized by multiplying by radio wavelength $\lambda$ and a term inversely proportional to velocity of sound for ions.

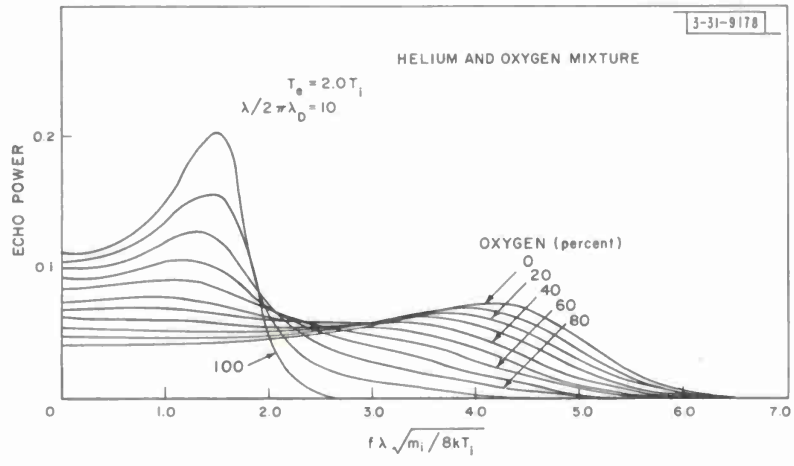


Fig. V-2. Effect on spectrum in which $T_e/T_i = 2.0$ as progressively larger amounts of $He^+$ ions are introduced into $O^+/He^+$ mixture. Abscissa same as Fig. V-1, and $m_i$ represents mass of heavier constituent ($O^+$).

In the measurements to be described, the echo power $P_r$ has been obtained as a function of height, and N(h) obtained from Eq. (2) by determining the variation of $\sigma$ with height. This is accomplished by simultaneous measurements of the signal spectra corresponding to different heights from which $T_e/T_i$ can be obtained. The height dependencies of $T_e/T_i$ and $T_i$ are, of course, of interest in their own right.

Mixtures of Ions:– As the ion mass $m_i$ enters the equations in the form $(m_i)^{1/2}$, it seems that $O^+$ and $N^+$ (or $O_2^+$ and $NO^+$) could be considered for all practical purposes as identical, in that it would not be possible experimentally to distinguish one from the other. Below about 200 km, it is expected that significant concentrations of several of these ions exist, and Petit[14] has considered the experimental accuracy required to determine the ratio of the heavier to the light ions. Observations conducted at the Millstone Hill observatory during 1963 are restricted to a height range of approximately 200 to 750 km. The lower limit is set by ground clutter echoes, and the upper limit by the strength of the signals. Over much of this height range, $O^+$ is expected to predominate. However, above about 750 km by day and perhaps 500 km at night, $H^+$ and $H_e^+$ ions become important constituents. Their presence can modify the scattering considerably by changing the shape of the signal spectra. Figure V-2 shows the influence of increasing the amount of $He^+$ in an $O^+/He^+$ mixture on the shape of the spectra for the case $T_e/T_i = 2.0$. It is clear that the presence of large amounts of $He^+$ (e.g., 50 percent) can be recognized readily. However, if only small amounts of $He^+$ are present, the spectra might be interpreted as indicating an erroneously high value of $T_i$ and low value of $T_e/T_i$. Moorcroft[15] has considered how the quantities $T_e$, $T_i$ and the ratio between the percentages of $He^+$, $H^+$, and $O^+$ ions might be extracted from spectrum observations. In principle, it is possible to perform such an analysis provided that: (a) the measurements can be made to a very high degree of precision; and (b) it is possible to remove some ambiguities in the interpretation by observations conducted at higher and lower altitudes. In practice, where pulsed radar observations are made one must consider also the distortion of the theoretical spectra by the finite width of the transmitter pulses, and in any radar system there will be some further smoothing due to the finite width of the filters employed in the spectrum analyzer. Considerable effort has been made to compute these effects for the Millstone ionospheric radar instrumentation (Sec. V-A-5).

### 3. Equipment

The parameters of the UHF ionospheric radar are listed in Table V-1. The antenna is a 70-meter parabola directed vertically. The feed system is a circular horn coupled to a turnstile junction. In practice, circularly polarized waves of one sense are transmitted and the opposite sense is received. The transmitter and receiver frequencies are controlled by synthesizing all the needed oscillator frequencies from a single frequency standard. The first amplifier in the receiver is a Zenith Radio Corporation electron-beam parametric amplifier which is synchronously pumped at 880 MHz.

The electron-density profiles are obtained from measurements in which the echo power as a function of height is determined. This is accomplished by placing in the receiver a filter whose bandwidth (25 kHz) is sufficient to accommodate all the frequency components of the reflected signal. This filter is connected to a square-law detector, the output of which is sampled

TABLE V-1
PARAMETERS OF UHF IONOSPHERIC RADAR

| | |
|---|---|
| Antenna | 70-meter fixed parabola |
| Polarization | Circular |
| Effective aperture $A_o$ | 1600 $m^2$ |
| Frequency f | 440 MHz |
| Transmitter power $P_t$ | 2.5 Mw |
| Transmitter pulse lengths $\tau$ | 0.1-, 0.5-, and 1.0-msec pulses used |
| Pulse repetition frequency | 50 Hz |
| Receiver bandwidth b | 25 kHz |
| System temperature $T_s$ | ~200°K (monitored continuously) |
| Post-detector integration | ~20 db |

TABLE V-2
TYPICAL EQUIPMENT OPERATION SEQUENCE

| Pulse Length (msec) | Computer Integration (minutes) | Spectrum Delay (msec) |
|---|---|---|
| 0.1 | 10 | – |
| 0.5 | 15 | 1.5, 2.0, 2.5 |
| 1.0 | 15 | 3.0, 4.0, 5.0 |
| 0 | 5 | (and 6.0) |

by a digital voltmeter at intervals of 200 μsec and assigned one of 256 possible levels. The digital numbers representing these voltages are continuously summed in the CG 24 computer to form a plot of the integrated echo power vs delay over the time base. This integration process is continued usually for periods of 10 to 20 minutes, thereby reducing the fluctuation in power by at least 20 db (to ±3°K). A resolution of 100 μsec (15 km) is achieved by making the interpulse period an odd number of 100-μsec intervals and interlacing two time bases sampled at 200-μsec intervals.

The signal spectra are explored by a bank of 24 filters. The outputs of the filters are rectified with linear detectors, and these voltages are then summed by carefully constructed analog integrators. The filters are driven by a wide-band (50-kHz) amplifier which is normally switched off, and gated on for a part of the time base equal to the length of the transmitter pulse (0.5 or 1.0 msec). The delay t between this gated portion and the time at which the transmitter pulse is radiated determines the height at which the signal spectrum is being explored. In order to calibrate the gains of the filter channels and detectors, and to remove any influence of the earlier stages of the receiver on the shape of the spectra, a second gated portion of the time base is applied to the filter bank. This second portion is equal in width to the first, but at a delay corresponding to a height from which no detectable signal is expected. The outputs of the detectors are switched to store the voltages corresponding to this second gate in another set of 24 integrators. Thus the first set stores signal plus noise and the second set only noise; by taking a ratio between the two sets, equipment effects can be eliminated. Both halves of the spectrum should be identical. (Even if asymmetry were to exist, it would be destroyed by the receiver.) Thus, only one-half is normally measured and either the upper or lower side band can readily be selected for spectrum analysis. The integrators have a self-time constant of several hours. At the end of a 5-minute integration period, the receiver pulses to the filter bank are removed and the 48 stored voltages are automatically sampled in turn and measured by means of a 14-bit digital voltmeter. These voltages, together with the time, are recorded on a punched paper tape.

### 4. Observing Procedures

Observations have been made at weekly intervals through 1963 and every two weeks in 1964. Each period of observation usually commenced near 0900 EST and ended at about 1700 EST on the following day. In this way, the daytime behavior was observed twice during any one run. Typically, in any one hour the equipment was operated as shown in Table V-2.

The sums of echo power formed in the computer were recorded on magnetic tape for later analysis. Spectrum measurements at any one delay (Table V-2) normally occupy 5 minutes. Thus, to explore the full range of heights takes almost an hour. During the daytime in summer, useful measurements were obtained with a delay of 6 msec, but in winter at nighttime there was insufficient signal strength to make measurements beyond about 3 msec. The voltage outputs of the integrators were recorded in binary fashion on a punched paper tape for later analysis. It is also possible to record the receiver IF signals for spectrum analysis at a later time; this can be useful when it is required to determine the behavior more rapidly than once per hour. By determining the antenna gain, the transmitter power, and the system noise temperature, it is possible to compute the electron density at any height provided that the ratio $T_e/T_i$ is known

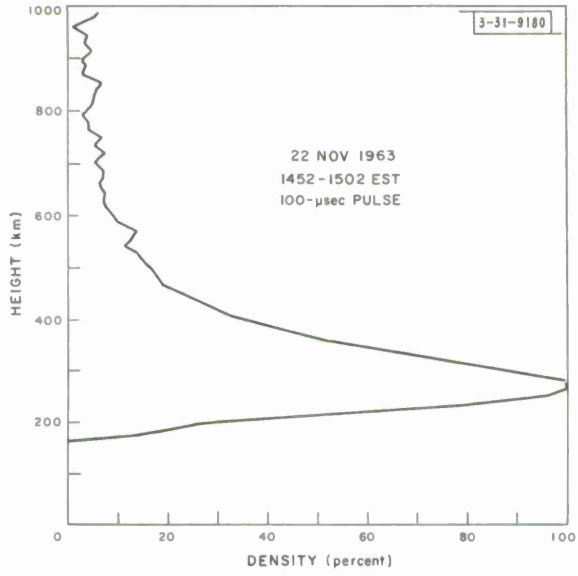


Fig. V-3. Plot produced by computer of electron density N'(h) vs height. Computer draws straight lines between measured points which are at 15-km height intervals. Fluctuations observed above 500-km height are errors due to noise and not true variations in electron density. Below 200 km, receiver was suppressed against ground clutter echoes.

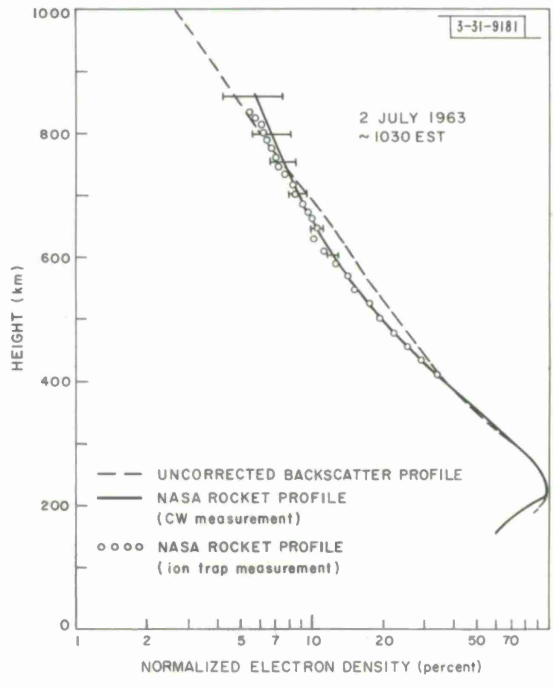


Fig. V-4. Example of combined electron-density profile obtained from plots (e.g., Fig. V-3) for 0.1-, 0.5-, and 1.0-msec pulses. These particular measurements were made at the same time as the rocket was launched from Wallops Island, Virginia. Difference between rocket and backscatter profile is largely due to the fact that $\sigma$ has been assumed constant to obtain this profile.

at that height. However, the accuracy of determining the gain and transmitter power is probably not better than ±2 db. Hence, for the most part, the absolute value of the echo power is not used to determine the electron density; instead, the profiles are assigned an absolute scale from ionosonde measurements in which $f_oF2$ is determined. The ionosonde is located within 1 km of the backscatter radar.

### 5. Data Analysis

Profile Measurements:– Plots of echo power vs delay are recorded on magnetic tape and later analyzed by the computer. First, the mean noise level is established from the values of about 20 points near the center of the time base, and this mean is then subtracted from all the points. Echo power is scaled up in proportion to the square of the height to obtain an electron-density profile N'(h) which is printed out later. The computer normalizes the electron-density profile to the peak value and plots it as a function of height (Fig. V-3). Smooth curves are drawn through these plots by hand, and a single density profile is extracted from the plots of the 0.1-, 0.5-, and 1.0-msec pulse observations in the same hour. Figure V-4 presents an example of such a combined profile. At this point, the profile N'(h) may differ from the true profile N(h) if $\sigma$ is a function of height but, as Fig. V-4 shows, the error is not extremely large. Thus, by assigning the value for $f_oF2$ observed on the ionosonde to the point of peak electron density, an absolute scale is established which enables the approximate value of the plasma frequency $f_p$ at all other heights to be estimated. This is necessary in order to interpret the spectrum measurements accurately.

Later, when the values for $T_e/T_i$ have been obtained as a function of height (Fig. V-5), a first-order correction can be applied by using Eq. (4) to obtain the true density profile N(h). Figure V-6 shows the corrected version of the profile shown in Fig. V-4, after adjustment to allow for the temperature inequality shown in Fig. V-5.

Spectrum Measurements:– The punched paper tape on which the 48 integrator voltages have been recorded is later analyzed by the computer. All the values are squared and a ratio is then taken of each of the values of the 24 signal-plus-noise to the 24 noise powers to obtain the signal-to-noise power at each frequency. By subtracting one from these ratios, the signal spectrum is obtained.

In order to analyze the spectrum measurements, it is simply necessary to compare each measured spectrum with a set of theoretical spectra to find which agrees best. Because the electron-to-ion temperature ratio $T_e/T_i$ controls the ratio x between the power in the wing to that at the center frequency, this quantity (x) is scaled from the records. A second quantity f, the frequency difference between the center and a point of half peak power, is also scaled and for a given ion mass $m_i$ may be regarded as a measure of the ion temperature $T_i$. The effect of the transmitter pulse and the frequency resolution of the receiver spectrum analyzer must be allowed for, and in order to do this it has been necessary to compute a large number of theoretical spectra (Fig. V-1). These spectra were then convolved, first with the spectral distribution of the power in the transmitter pulse, and second with the power-vs-frequency response of one of the filters in the receiver. The effect of the convolution on theoretical spectra corresponding to given values of $T_i$ and $T_e/T_i$ is to lower x and increase f.

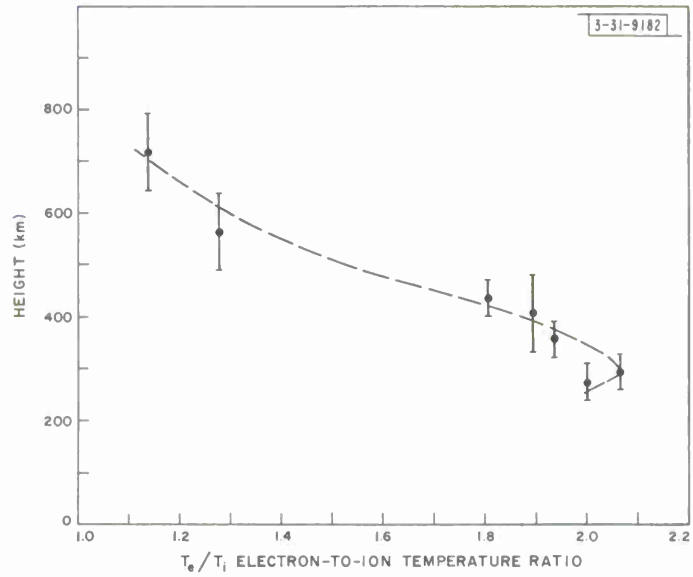


Fig. V-5. Variation of electron-to-ion temperature ratio $T_e/T_i$ obtained from spectra measured during period 0834 to 1005 hours EST on 2 July 1963.

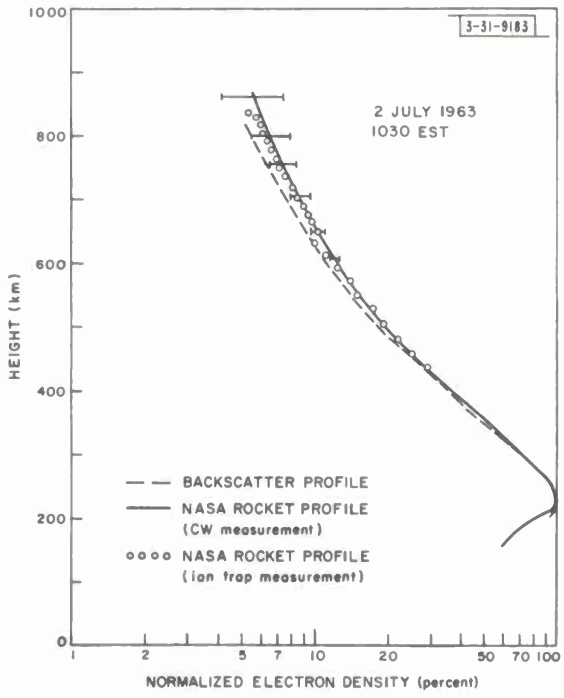


Fig. V-6. Backscatter electron-density profile (Fig. V-4) after correcting for variation of electron cross section $\sigma$, with height according to Eq. (4) and results for $T_e/T_i$ presented in Fig. V-5. Rocket measurements were made at 0922 hours, but ground clutter echoes obscured F-region peak in backscatter measurement until 1030 hours.

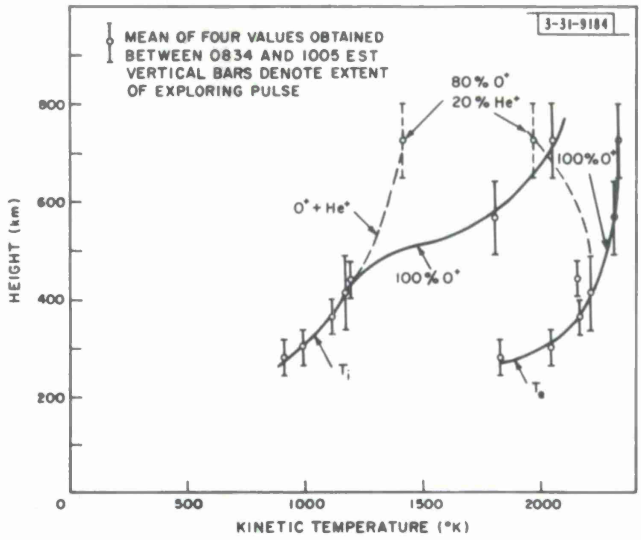


Fig. V-7. Variation of electron ($T_e$) and ion ($T_i$) temperatures observed on 2 July 1963. Solid lines denote values deduced on assumption that only $O^+$ ions are present at all heights. Dotted lines indicate how temperature might vary if percentage of $He^+$ ions becomes significant above 500 km and increases to value of 20 percent of total at 720 km.

The values of $T_e/T_i$ corresponding to the measurements shown in Fig. V-5 are shown in Fig. V-6 and the separate dependence of $T_e$ and $T_i$ on this occasion is shown in Fig. V-7.

It is possible that above 500 km appreciable amounts of $He^+$ were present at the time these measurements were made. At no time during the course of the backscatter measurements have spectra been obtained which definitely indicate the presence of $He^+$ ions, though the spectra obtained for the uppermost heights (750 km by day, 500 km by night) are uncertain due to the low signal-to-noise ratio, and perhaps as much as 30 percent of $He^+$ might be undetected (Fig. V-2). Figure V-8 shows that the measurements made on 2 July at 720-km equivalent height are consistent with theoretical spectra computed for a plasma containing no $He^+$ (100 percent $O^+$) or one containing as much as 20 percent $He^+$. Unfortunately, the presence of even small amounts of $He^+$ requires a significant change in the interpretation of the results. In the specific example shown in Fig. V-8, it is not possible to distinguish experimentally between the two extreme cases: (1) wholly $O^+$, $T_e/T_i = 1.14$, $T_e = 2320\,°K$, $T_i = 2040\,°K$; and (2) 80 percent $O^+$, 20 percent He, $T_e/T_i = 1.4$, $T_e = 1960\,°K$, $T_i = 1410\,°K$. These diverging interpretations are indicated in Fig. V-7.

In principle, it should be possible to determine the ratio $O^+/He^+$ by careful measurement of the slope of the spectrum near the point of half-peak intensity (Fig. V-2). In the measurements described here, this slope has been set largely by the distortion introduced by the transmitter pulse and receiver filter characteristics thereby making this rather difficult.

In summary, it may be said that the interpretation of the spectra corresponding to heights of more than 500 km is uncertain at the present time owing to the likely presence of $He^+$ ions. In all the results obtained to date, this effect has been neglected and the measurements interpreted on the assumption that only $O^+$ ions are present.

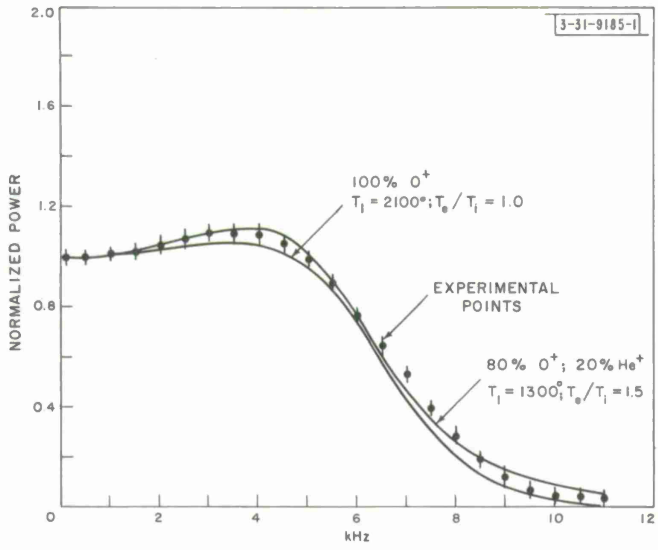


Fig. V-8. Mean of all experimental profiles obtained at greatest height (720 km) during period 0834 to 1005 hours on 2 July 1963 is here compared with closest fitting precomputed curves for an $O^+$ gas and mixture containing 80 percent $O^+$, 20 percent $He^+$. A better fit could be obtained by adjusting theoretical curves so that for $O^+$, $T_i = 2040°$ and $T_e/T_i = 1.14$, and for $O^+/He^+$, $T_i = 1400°$ and $T_e/T_i = 1.40$. When this is done, solutions are experimentally indistinguishable.

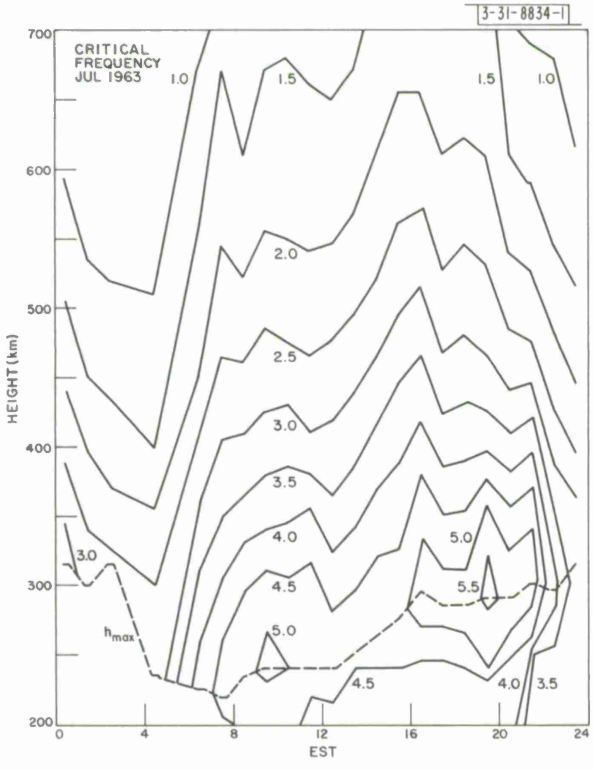


Fig. V-9. Variation of plasma frequency as a function of height and time obtained by averaging all results for July 1963.

More detailed descriptions of the backscatter radar facility and its operation have been published by Evans and Loewenthal[16] and Evans.[17]

## 6. Results

Observations made during 1963 have been analyzed and reported in Evans.[17] Examples of the average diurnal variation of the electron density (expressed as a plasma frequency) $T_i$ and $T_e$ over the height range that could be explored for the month of July are shown in Figs. V-9 through V-11. As can be seen in Fig. V-9, the summertime electron-density behavior is distinctly anomalous, since a maximum is reached in the evening. This behavior, the subject of a separate paper,[18] has been explained in terms of a downward motion of electrons from the magnetosphere caused by the large fall in electron temperature that occurs at sunset (Fig. V-11). A similar phenomenon was observed during a total solar eclipse that occurred in July 1963, which lends support to this explanation. Evans reported the eclipse results,[19] and discussed them further in Ref. 20. A like phenomenon is also observed in winter months (November – January) in the early hours of the morning. This is believed to be caused by the cooling of the magnetosphere following sunset in the southern (summer) hemisphere. These winter observations and their interpretation are discussed in Evans.[21] In a sixth paper by Evans,[22] observations of anomalously high nighttime temperatures in the month of September are reported and discussed. These high temperatures are associated with magnetic disturbances and are believed to be the result of particle precipitation from the Van Allen radiation belt. Finally, the electron temperatures derived in this work have been compared by Evans[23] with values reported

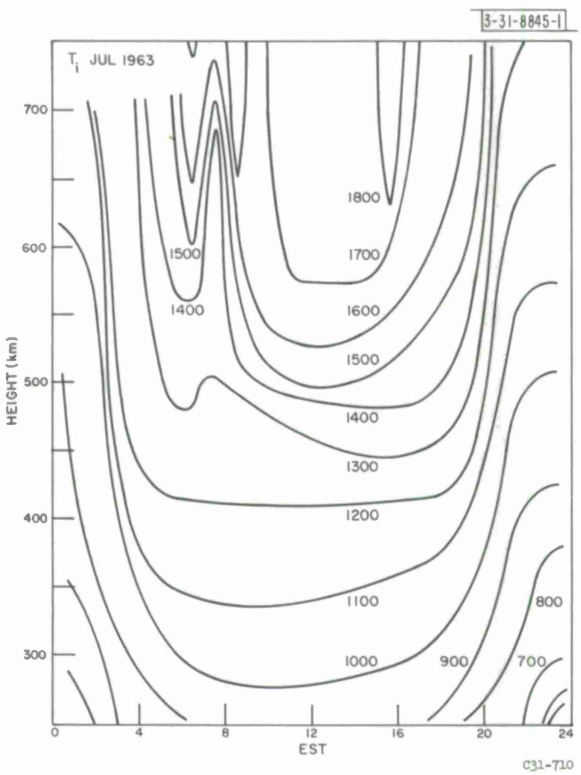


Fig. V-10. Variation of ion temperature as a function of height and time obtained by averaging all results for July 1963.

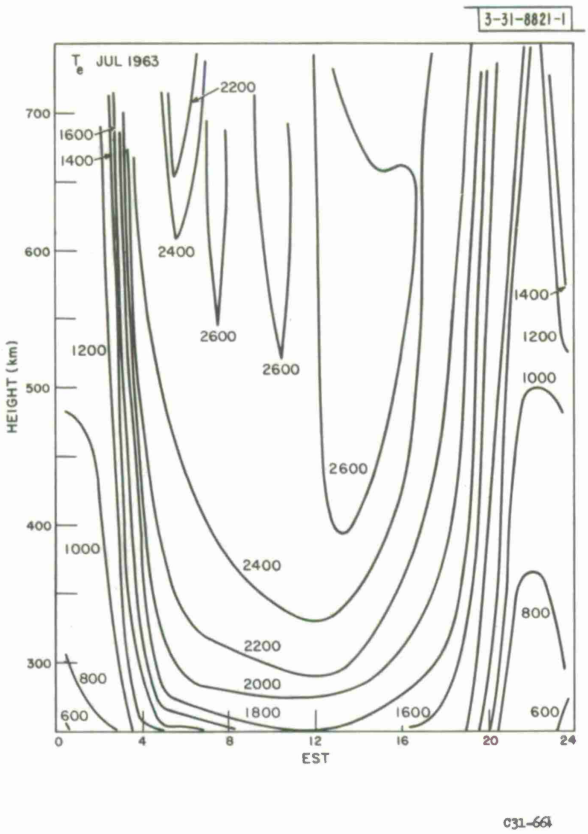


Fig. V-11. Variation of electron temperature as a function of height and time obtained by averaging all results for July 1963.

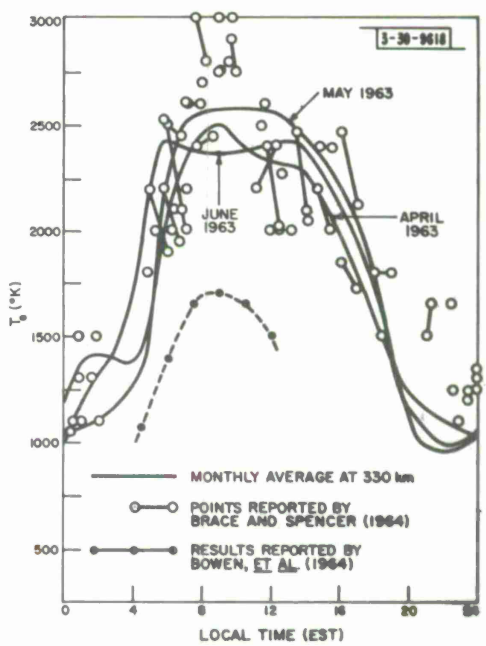


Fig. V-12. Comparison of radar and satellite determinations of electron temperature. Points reported by Brace and Spencer[24] were for altitudes in 260- to 400-km range, hence a curve corresponding to 330 km has been drawn to represent radar results.

from rocket flights and satellite measurements. Figure V-12 illustrates the good agreement found between the determinations of electron temperature by the Explorer 17 satellite reported by Brace and Spencer[24] and the radar measurements. The work outlined above has been reported during the last six months at two overseas meetings. These were "The Third NATO Conference on Electron Density Profiles in the Ionosphere and Exosphere" which was held at Finse in Norway, and the COSPAR meeting held at Mar del Plata in Argentina.

### 7. Work in Past Six Months

Apart from the work involved in reporting the results of the 1963 measurements as outlined above, the ionospheric backscatter program has been continued into 1965, albeit at a somewhat reduced observing rate. The equipment is now operated once per month for a period of 48 hours continuously (spanning two complete days as against one and a half in the past). In addition, the observing procedure has been modified so that all the required information to construct height profiles of density and temperature are obtained in 30 minutes in place of about 1 hour 10 minutes as in the past. In practice, this is accomplished by recording in analog form the IF signals for later (i.e., nonreal time) spectral processing. Thus, although observations are made only once per month, about three times as many data points are obtained per run as previously. This increase will, it is hoped, permit the diurnal variations to be followed more clearly than hitherto.

Once-per-month observations are also taken using the Millstone L-band tracking radar described in Sec. II-B. The signals are considerably weaker with this radar so that useful measurements are possible only during daylight hours and at altitudes below 300 km. However, because the beam can be tilted, it is possible to place the ionospheric echo beyond any interfering ground clutter echoes, and hence examine altitudes in the range 100 to 200 km which cannot be observed with the UHF radar.

During the course of these last six months, the processing of the tape recordings has required the full-time services of one technician. That is, it takes one month to process the data obtained in a single 48-hour run. Despite this continuing activity, the equipment timing generator has been replaced by a new one permitting more efficient setup and control of the experiments. In addition, the spectrum analyzer has been modified so that the sample of noise taken on each sweep of the time base and used to calibrate the channel gains (Sec. V-A-3) is subtracted from the signal-plus-noise sample directly. This releases 24 integrators, making it possible to explore the full spectrum with 48 filters. For the analysis of the tape recordings, both halves of the spectrum are analyzed to increase the reliability of (and our confidence in) the results. By obtaining the full spectrum, we shall be able to reduce the time required to process tapes by a factor of two. Ultimately it is hoped, however, to devise a scheme which will provide all the required frequency spectra in real time. The present proposal for achieving this makes use of the high data rate that may be handled with the new SDS 9300 computer.

In the area of data analysis, our progress has been less satisfactory. Difficulties have been encountered with the CG 24 computer programs required to analyze the results. It is hoped that a new program for the SDS 9300 computer can be written to replace the existing program. Work with the assistance of Division 8 has resulted in new and improved computer programs which predict theoretically the spectrum shapes to be expected for different ionospheric conditions

and different radar parameters. Ultimately, it is hoped that this program can be made sufficiently fast to act as a prediction routine in a program that matches the experimental results and theory in a least-mean-squares sense. Progress in this area has been slow because of the pressure of other work at this Station.

The 1965 observations are being taken chiefly on the IQSY (International Years of the Quiet Sun) Quarterly World Days and Regular World Days. The three years' observations 1963 – 1965 should, we believe, provide an accurate description of the F-region behavior at midlatitudes at sunspot minimum. Observations beyond 1965 are required to determine the effects of increased sunspot activity, and these are expected to be large. In order to investigate fully the disturbed conditions that will arise, the equipment must be arranged in such a way that it can be operated at short notice. To this end, we hope to purchase additional items which will make the backscatter radar completely separate from the tracking radar, except for the common transmitter power supply and digital computer. A random operation schedule will preclude an orderly reduction of tape recordings (since here the equipment is common) and hence there is some urgency to devise the real-time spectrum analysis scheme outlined above.

## B. AURORAL OBSERVATIONS

A program of radar investigation of the ionization associated with the aurora borealis was begun at Millstone late in February 1965, using the L-band system and the 84-foot parabolic antenna. The objectives of the program are to determine the spatial distribution of auroral echoes at L-band and to measure their aspect sensitivity, effective radar cross section and Doppler spectrum. A search for auroral echoes was scheduled on one or two days each week from 1600 to 2000 hours EST, which is near the time of maximum diurnal rate of occurrence as determined from radar measurements made at lower frequencies.

By mid-July 1965, about 16 hours of data had been accumulated and a partial analysis had been made of some 4 hours of it. Based on these data and the analysis, the following general statements can be made:

(1) Auroral echoes were obtained on about 40 percent of the days on which a radar search was made.

(2) The duration of the echoes varied from a few minutes to almost four hours.

(3) The azimuth sector from which the echoes were obtained is approximately centered about the magnetic meridian and is variable in width, with widths as great as 60° being observed.

(4) Most of the echoes were obtained at elevation angles between 0° and 2.5°; however, on two days the maximum elevation angle was 5° and on one day (17 June) the maximum angle was 13°.

(5) Slant range to the echo source varied with elevation angle from about 400 km at 13° elevation to 1200 km at 0°.

(6) Normally, the region from which the echoes were obtained was at a height of about 100 km to 120 km. However, for a short period of time on 17 June, there were two separate regions with one at 80 km and the other at 118 km.

(7) The angle between the radar beam and the normal to the magnetic field lines at the echo source varied between −1.6° and +2.2°.

(8) The width of the Doppler spectrum was approximately 12 kHz.

(9) The displacement of the Doppler spectrum peak from zero varied from about +2 kHz looking east of magnetic north to −2 kHz looking west. This indicates an apparent east to west motion of the echo source at 230 meters per second.

(10) The effective radar cross section of the auroral echoes at L-band may have values up to many tens of square meters.

From the data obtained on 8 July, contours were prepared showing the distribution of auroral echo intensity as a function of slant range and azimuth. These contours for elevation angles of 0.5°, 1.0°, 1.5°, and 2.0° are shown in Figs. V-13 through V-16. The two "hot spots" with centers near 10° and 330° true are especially evident at the higher elevation angles.

L-band auroral observations will continue as presently scheduled on one or two nights each week. Computer programs are presently being written which will be used in the analysis of the Doppler and echo intensity data.

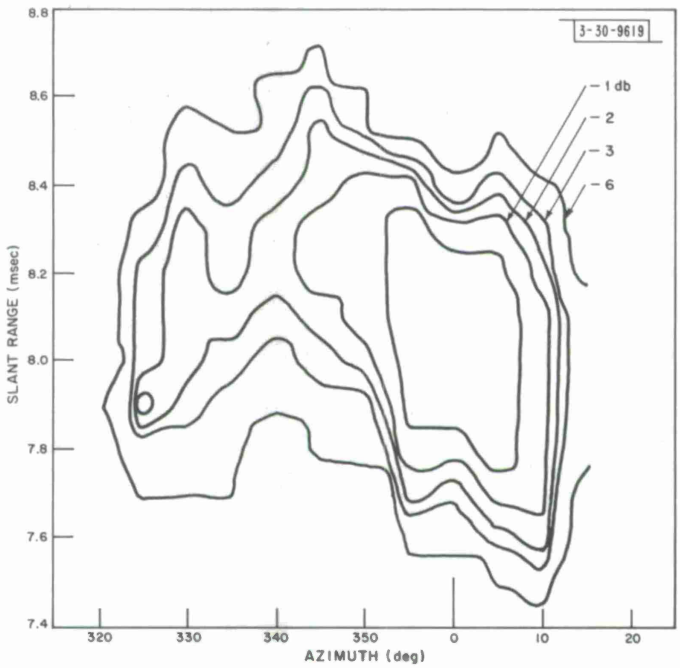


Fig. V-13. Distribution of L-band auroral echo intensity at 0.5° elevation, showing 1-, 2-, 3-, and 6-db contours.

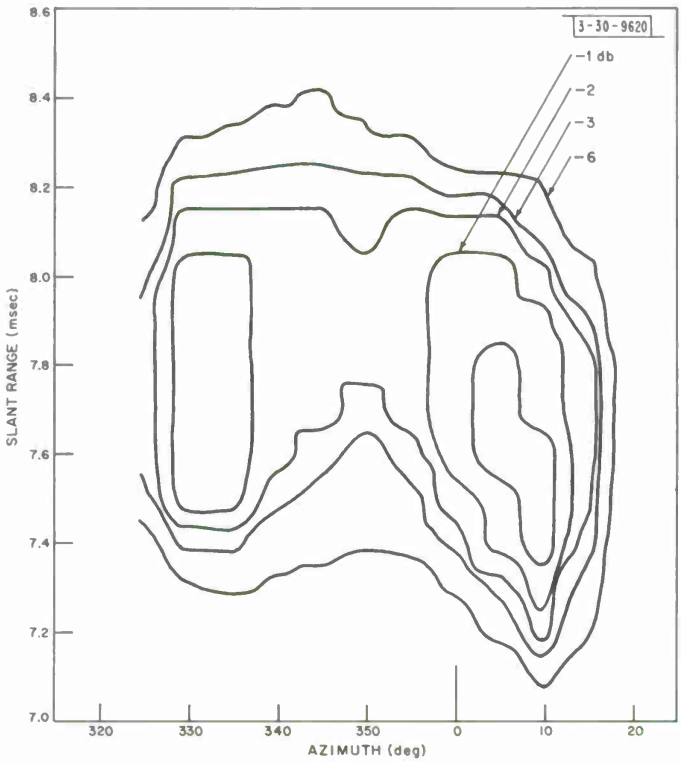


Fig. V-14. Distribution of L-band auroral echo intensity at 1.0° elevation, showing 1-, 2-, 3-, and 6-db contours.

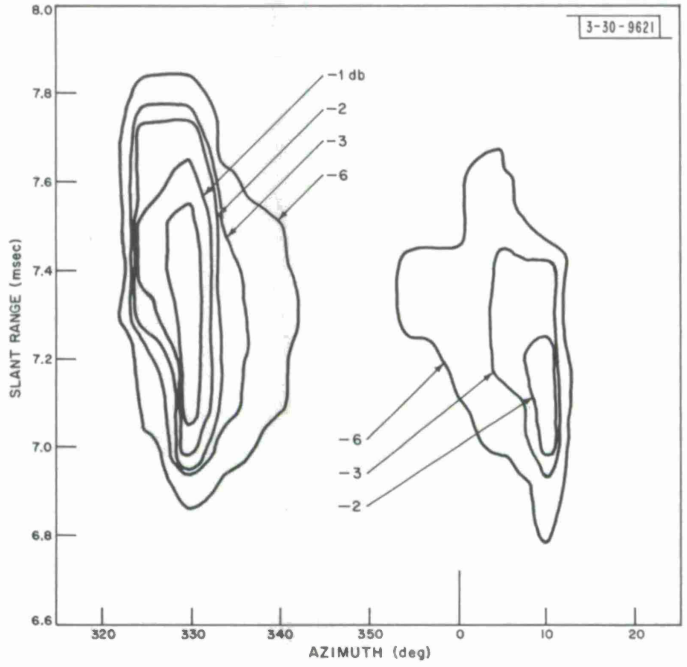


Fig. V-15. Distribution of L-band auroral echo intensity at 1.5° elevation, showing 1-, 2-, 3-, and 6-db contours.

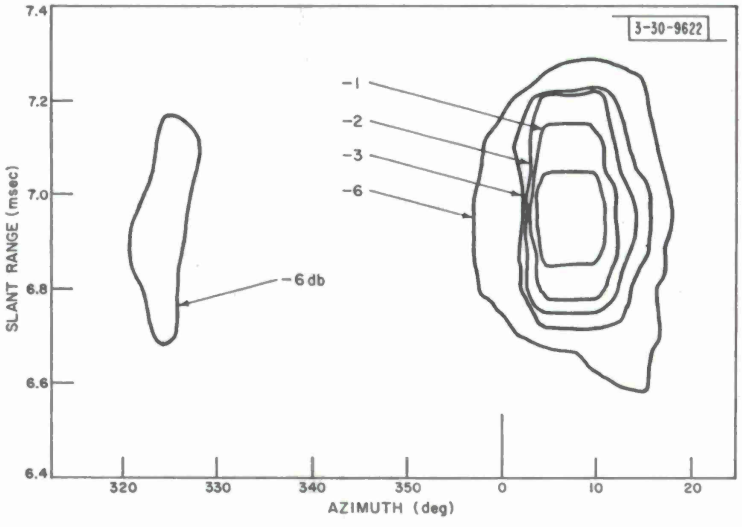


Fig. V-16. Distribution of L-band auroral echo intensity at 2.0° elevation, showing 1-, 2-, 3-, and 6-db contours.

## REFERENCES


1. W. E. Gordon, Proc. IRE 46, 1824 (1958).
2. K. L. Bowles, Phys. Rev. Letters 1, 454 (1958).
3. _____, J. Research Natl. Bur. Standards 65D, 1 (1961).
4. V. C. Pineo, L. G. Kraft and H. W. Briscoe, J. Geophys. Res. 65, 1620 (1960).
5. Ibid., p. 2629.
6. J. A. Fejer, Can. J. Phys. 38, 1114 (1960).
7. _____, Can. J. Phys. 39, 716 (1961).
8. V. C. Pineo, D. P. Hynek, and G. M. Millman, J. Geophys. Res. 68, 2695 (1963).
9. J. V. Evans, J. Geophys. Res. 67, 4914 (1962).
10. V. C. Pineo and D. P. Hynek, J. Geophys. Res. 67, 5119 (1962).
11. O. Bunneman, J. Geophys. Res. 67, 2050 (1962).
12. K. L. Bowles, Paper presented at 14th International URSI Meeting, Tokyo, September 1963.
13. J. S. Greenhow, H. K. Sutcliffe, and C. D. Watkins, J. Atmos. Terrest. Phys. 25, 197 (1963).
14. M. Petit, Compt. rend. 255, 2804 (1962).
15. D. R. Moorcroft, J. Geophys. Res. 69, 955 (1964).
16. J. V. Evans and M. Loewenthal, Planet. Space Sci. 12, 915 (1964).
17. J. V. Evans, Technical Report 374, Lincoln Laboratory, M. I. T. (22 January 1965), DDC 463164.
18. _____, J. Geophys. Res. 70, 1175 (1965), DDC 614310.
19. _____, ibid., p. 131, DDC 613886.
20. _____, ibid., p. 733, DDC 613889.
21. _____, ibid., 70, 4331 (1965), DDC 623606.
22. _____, ibid., 70, 2726 (1965), DDC 621233.
23. _____, ibid., 70, 4365 (1965), DDC 623603.
24. L. H. Brace and N. W. Spencer, J. Geophys. Res. 69, 4686 (1964).

# APPENDIX A
# ANALYSIS OF DIGITAL MONOPULSE SYSTEM (DIGIMON)

The operation and status of DIGIMON was discussed in Sec. II-C. A theoretical analysis is given here.

The theoretical limitation to which a radar can locate the direction of a target is determined by the antenna beamwidth and the signal-to-noise ratio. This limitation corresponds to about 15 seconds of arc for a Millstone radar measurement averaged over an 8-second interval.* This number is based on a 37-minute beamwidth, a per pulse signal-to-noise ratio of 25, and averaging over 120 pulses.

In virtually all radar systems to date the realized accuracies have been far below the potentialities. There have been mechanical limitations in knowing where the antenna is actually pointing, but these are being reduced at various installations.† The remaining problems are electrical, i.e., actually splitting the antenna beamwidth down to better than 1 part in 100. This is difficult, if not impossible, to achieve with analog monopulse techniques. For this reason a technique was developed in which the signals are handled digitally at as early a stage in the receiving system as possible.

A monopulse receiver consists of three receiver channels. One is the regular receiver connected to the antenna feed centered on the antenna boresight, often called the sum channel. The remaining two channels are the vertical and horizontal error channels. The horizontal error channel may be thought of as derived from two feed horns, one of which produces a beam to the left, the other to the right of the central beam. These two feeds are combined in phase opposition to yield zero signal for a target on boresight, but to yield a signal whose amplitude and phase depends upon the magnitude and the direction of the antenna pointing error. The signal for the vertical error receiver channel is similarly derived from another pair of feed horns; one above, the other below the central feed. Figure A-1 shows schematically the configuration of the various horns and the manner in which they are combined.

In the digital monopulse receiver the error channel signals are digitized directly at an intermediate frequency before narrow band matched filtering or detection. The digitized IF signals are then Fourier analyzed by forming summations of the form

$$\sum_{1}^{N} f(n\Delta t)\cos\omega n\Delta t \quad \text{and} \quad \sum_{1}^{N} f(n\Delta t)\sin\omega n\Delta t$$

where $\omega$ is $2\pi$ times the intermediate frequency and $\Delta t$ is the sample interval. If $n\Delta t$ is made equal to the radar pulse length (2 msec for Millstone), this processing corresponds to a filter optimally matched to the transmitted pulse.

---

*Manasse, R., "Summary of Maximum Theoretical Accuracy of Radar Measurements," MITRE SR-11-2, The MITRE Corporation (1 April 1960).

†Most interesting is the ±5 seconds of arc following error achieved with an 85 × 120-foot elliptical precision antenna at Jodrell Bank. Similar performance is being approached at Haystack.

Appendix A

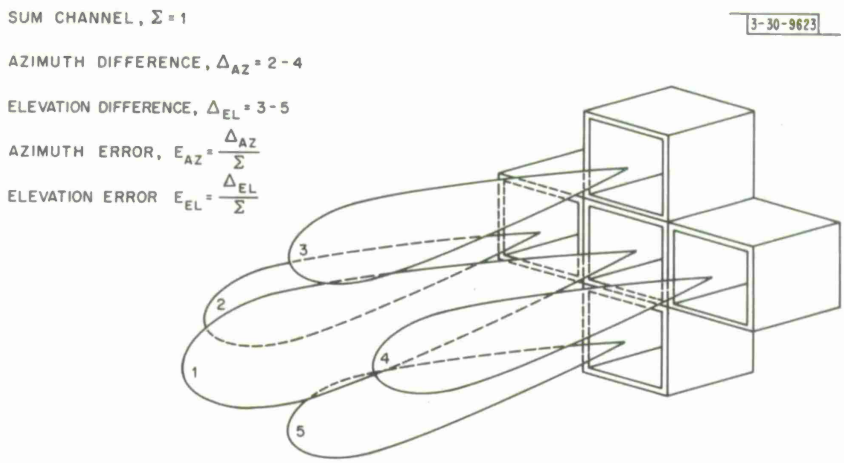


Fig. A-1. Concept of one type of monopulse feed horn.

The above arithmetic is in general quite formidable. To simplify it, the values of $\Delta t$ and $\omega$ may be chosen to make the values of the arguments $n\omega\Delta t$ be multiples of $\pi/2$. Then the sines and cosines assume the values of 1, 0, or $-1$, avoiding the need to perform multiplications or the calculation of trigonometric functions. A further saving is achieved by combining (adding) the several IF signals at different values of $\omega$, digitizing the combined signals, and separating the different signals in the digital filtering.

The above principles are embodied in a system in which the intermediate frequencies are $-1$, 0, $+1$ and 2 MHz, and the sample interval $\Delta t$ is 0.25 μsec. To admit the use of a negative frequency, the function f(t) is made a complex number realized by making the voltage out of one mixer the real part of f(t) and the voltage out of a mixer in phase quadrature the imaginary part of f(t). Separate A/D converters are used to digitize the real part and the imaginary part of f(t). The Fourier analysis may now be expressed by

$$F(\omega) = \sum_{n=1}^{N} f(n\Delta t)\, e^{-1\omega n\Delta t}$$

where $\omega = -2\pi \cdot 10^6$, 0, $2\pi \cdot 10^6$, or $4\pi \cdot 10^6$.*

We may write out explicitly the summations in terms of the real and imaginary parts for the above summation as follows

$$F_R(\omega) = \sum_{n=1}^{N} f_R(n\Delta t)\cos(\omega n\Delta t) + \sum_{n=1}^{N} f_I(n\Delta t)\sin(\omega n\Delta t)$$

$$F_I(\omega) = \sum_{n=1}^{N} -f_R(n\Delta t)\sin(\omega n\Delta t) + \sum_{n=1}^{N} f_I(n\Delta t)\cos(\omega n\Delta t)$$

* The frequency of 0 cycles per second provides a fourth channel either as a spare or for polarization studies.

For

$$\omega = -\frac{1}{\Delta t}\frac{\pi}{2},\ 0,\ \frac{1}{\Delta t}\frac{\pi}{2} \quad \text{and} \quad \frac{2}{\Delta t}\frac{\pi}{2}$$

where

$$F(\omega) = F_R(\omega) + iF_I(\omega) \quad \text{and} \quad f(n\Delta t) = f_R(n\Delta t) + if_I(n\Delta t)$$

we can write respectively

$$F\left(-\frac{1}{\Delta t}\frac{\pi}{2}\right) = u + iv$$

$$F(O) = p + iq$$

$$F\left(\frac{1}{\Delta t}\frac{\pi}{2}\right) = s + it$$

$$F\left(\frac{2}{\Delta t}\frac{\pi}{2}\right) = x + iy \quad .$$

Writing the respective summations as recurring sequences (modulo 4)

$$u = -f_I(\Delta t) - f_R(2\Delta t) + f_I(3\Delta t) + f_R(4\Delta t)$$

$$v = f_R(\Delta t) - f_I(2\Delta t) - f_R(3\Delta t) + f_I(4\Delta t)$$

$$p = f_R(\Delta t) + f_R(2\Delta t) + f_R(3\Delta t) + f_R(4\Delta t)$$

$$q = f_I(\Delta t) + f_I(2\Delta t) + f_I(3\Delta t) + f_I(4\Delta t)$$

$$s = f_I(\Delta t) - f_R(2\Delta t) - f_I(3\Delta t) + f_R(4\Delta t)$$

$$t = -f_R(\Delta t) - f_I(2\Delta t) + f_R(3\Delta t) + f_I(4\Delta t)$$

$$x = -f_R(\Delta t) + f_R(2\Delta t) - f_R(3\Delta t) + f_R(4\Delta t)$$

$$y = -f_I(\Delta t) + f_I(2\Delta t) - f_I(3\Delta t) + f_I(4\Delta t) \quad .$$

Thus, the Fourier analysis of the combined signals is reduced to a set of summation and switching operations to select as appropriate the in-phase (real), $f_R(t)$, or quadrature (imaginary), $f_I(t)$ mixer output.

It remains to interpret these complex numbers as antenna pointing errors. If x + iy represents the phasor of the voltage from the central feed horn and u + iv the phasor of the voltage from the azimuth error horn, the antenna pointing error may be represented as the component (Real part, Re) of the phasor u + iv along x + iy divided by the modulus of x + iy.

Thus the azimuth error is

$$\Delta Az = \mathrm{Re}\ \frac{u + iv}{x + iy}$$

$$= \frac{ux + vy}{x^2 + y^2} \quad .$$

Similarly, if true phases of the voltage at the elevation feed horn is s + it,

Appendix A

$$\Delta El = \mathrm{Re}\ \frac{s + it}{x + iy}$$

$$= \frac{sx + ty}{x^2 + y^2} \quad .$$

The eight numbers; u, v, p, q, s, t, x, and y are found in eight separate high-speed (4 MHz) adders. The calculations of the two quotients are done in a special-purpose slow-speed serial (bit-by-bit) computer.

The advantages of the digital monopulse may be summarized as follows:

(1) By multiplexing the error and reference IF signals on a common channel near the receiver front ends, the usual monopulse errors that arise from failure of separate IF channels to track are virtually eliminated. By the same token, maintenance adjustments should be reduced.

(2) Signals are converted into digital form early in the receiving system. Sources of error inherent in analog derivation of steering signals are thus also eliminated.

(3) Digitizing of the signal in a wide bandwidth followed by coherent digital filtering results in an overall system dynamic range much greater than could be achieved by using an A/D converter of the same bittage to quantize the narrow-band signal from a physical matched filter.

## APPENDIX B
## HAYSTACK RESEARCH FACILITY

Haystack is the most recent addition to the M. I. T. Lincoln Laboratory radio/radar experimental facilities that make up the Millstone Hill Field Station located at the confluence of Westford, Groton, and Tyngsboro, Massachusetts. All these facilities have been designed and are operated by Lincoln Laboratory for the U. S. Air Force.

Haystack is a multi-purpose experimental facility for research on many different aspects of space communication, radiometry, and radar. It is designed to operate as a ground terminal for satellite and space communication and radio propagation experiments, as a high-performance precision measurements radar, and as a high-resolution radio telescope. In addition, it serves as a vehicle for the evaluation and further development of the new techniques that are embodied in the design of the Haystack system itself, to provide practical guidance in the design of advanced microwave facilities.

The basic system includes a 120-foot diameter, computer-directed precision antenna; a 1-Mw high-voltage transmitter power supply; stable and accurate frequency standards and other equipment to generate precisely known signals; data-processing, calibration, and test facilities; and an extensive wiring network for power and signal distribution. Special-purpose radio and radar transmitting and/or receiving equipment is installed in interchangeable boxes that can be "plugged in" to the basic system, to utilize the general-purpose facilities for a wide variety of experiments at different frequencies and in different modes of operation. Figure B-1 is a composite cutaway showing the antenna with a box change in progress.

Two plug-in boxes have been provided for initial Haystack operations. Each box is 8 by 8 by 12 feet in size and can hold up to 2 tons of equipment. One contains radiometer receivers as described in Sec. III-B, to perform radio astronomy measurements; radiometers at other frequencies will be added. Another contains a high-power CW X-band (7750 MHz) transmitter, cryogenic low-noise receivers, and associated microwave circuits for communications experiments requiring simultaneous transmission and reception and for planetary radar experiments.

Figure B-2 is a block diagram designed to exemplify the flexible system arrangements afforded by the RF plug-in box philosophy.

Of special interest are the test docks. In the case of the high-power test dock a capability is provided for a full test of transmitter and receivers with the control room equipment while the antenna is otherwise occupied. The so-called "cornucopia" test dock provides a precisely measured standard gain Hogg horn, steerable in declination, which makes it possible not only to exercise the radiometers but also to use them in precise measurements of the flux from radio sources. The Haystack antenna can then be calibrated in terms of the standard horn using the same radio sources.

A Univac 490 computer is employed for direction of the antenna and is used in some operations to control range gates and Doppler compensation. A comprehensive software system for these applications has been provided which permits direction of the antenna and other system variables by English commands inserted by on-line teletypewriter. Astronomical tables for the celestial objects of greatest interest are stored on tape and accessed as required. Orbital elements for artificial satellites can also be used to direct the system. This control program

Appendix B

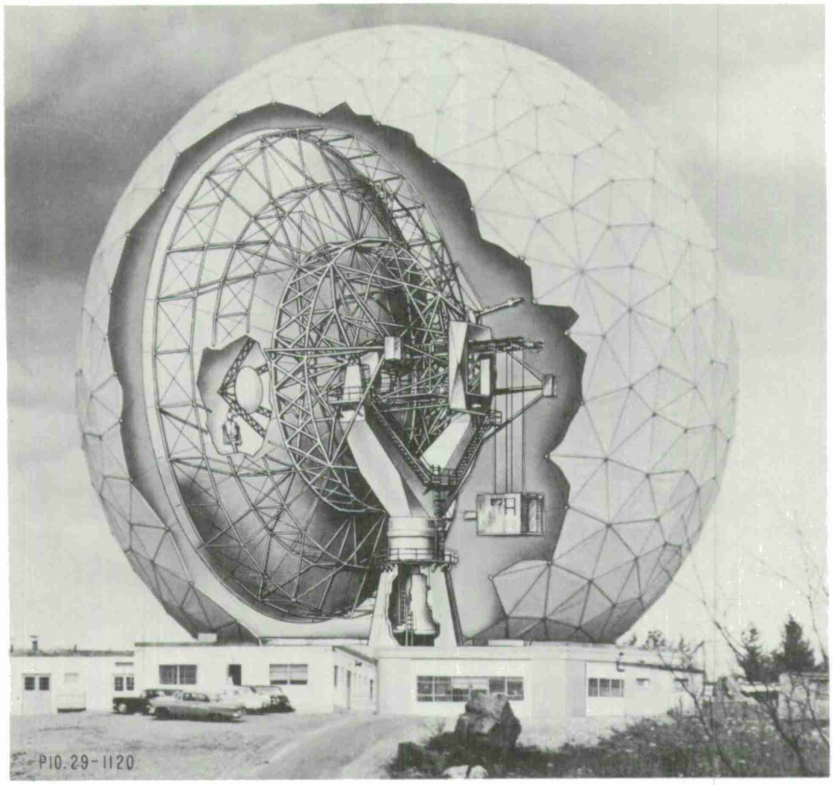


Fig. B-1. Haystack antenna.

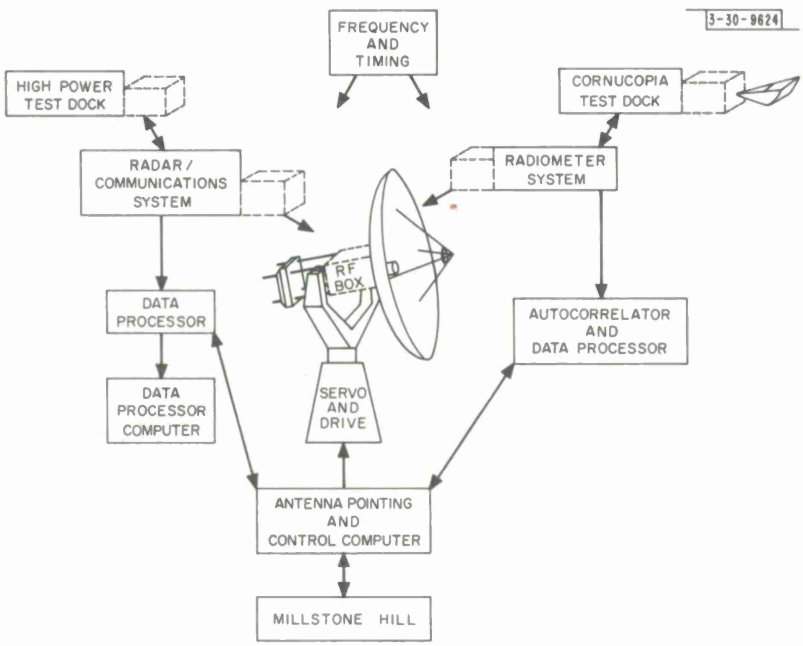


Fig. B-2. Haystack block diagram.

utilizes the bulk of available core storage in the U490. The U490 is, therefore, considered part of the Haystack radar/radiometric system.

Real-time data-processing needs and on-site general-purpose computing capability are handled primarily by a CDC 3200 computer, which is interfaced directly with the radar signal circuits.

Table B-1 sums up the facilities available at Haystack at this writing.

TABLE B-1
HAYSTACK CHARACTERISTICS
DECEMBER 1965

| | | |
|---|---|---|
| Antenna | | |
| | Size | 120-foot paraboloid "Cassegrain" |
| | Mount | Az-El |
| | Gain | 66 db (X-band) |
| | Frequency | 1 to 15 GHz |
| | Beamwidth | 0.070 deg at 7.75 GHz |
| | Radome | 150-foot space frame |
| | "Plug-in" module | RF Box (8 × 8 × 12 feet) |
| RF boxes | | |
| | Radiometer box | |
| | Feed | Clavin (variable polarization) |
| | Receiver | Tunnel diode (1-GHz bandwidth) |
| | Frequencies | 1.4, 1.6, 5, 8, 15.5 GHz |
| | Radar/communication box | |
| | Transmitter | 100 kw at 7.75 GHz (CW) |
| | Receivers | Paramps 100°K |
| Station equipment | | |
| | High-voltage power supply (1 Mw) | |
| | Antenna pointing computer U-490 | |
| | Data-processing computer CDC 3200 (not as yet fully integrated) | |
| | Rb standard and frequency translation equipment | |
| | 2-msec sequential Doppler processor (satellite tracking) | |
| | 100-channel autocorrelator, 10-MHz rate (radio astronomy) | |
| | Clocks (time and pulse timing) | |
| | Calibration, Hogg horn ($A = 65$ ft$^2$) | |
| | Mobile calibration terminal (Pack Monadnock Mountain) | |

## DOCUMENT CONTROL DATA – R&D

*(Security classification of title, body of abstract and indexing annotation must be entered when the overall report is classified)*

| | |
|---|---|
| 1. ORIGINATING ACTIVITY *(Corporate author)*<br>Lincoln Laboratory, M.I.T. | 2a. REPORT SECURITY CLASSIFICATION<br>Unclassified<br>2b. GROUP<br>None |

3. REPORT TITLE

Radio Physics and Astronomy

4. DESCRIPTIVE NOTES *(Type of report and inclusive dates)*

Semiannual Technical Summary – 1 April through 30 September 1965

5. AUTHOR(S) *(Last name, first name, initial)*

Meyer, James W. and Sebring, Paul B.

| 6. REPORT DATE | 7a. TOTAL NO. OF PAGES | 7b. NO. OF REFS |
|---|---|---|
| 15 October 1965 | 104 | 85 |

| | |
|---|---|
| 8a. CONTRACT OR GRANT NO.<br>AF 19(628)-5167<br>b. PROJECT NO.<br>649L<br>c.<br>d. | 9a. ORIGINATOR'S REPORT NUMBER(S)<br>Radio Physics & Astronomy 1965:1<br>9b. OTHER REPORT NO(S) *(Any other numbers that may be assigned this report)*<br>ESD-TDR-65-492 |

10. AVAILABILITY/LIMITATION NOTICES

Distribution of this document is unlimited.

| 11. SUPPLEMENTARY NOTES | 12. SPONSORING MILITARY ACTIVITY |
|---|---|
| None | Air Force Systems Command, USAF |

13. ABSTRACT

Much of the Laboratory's general research work in the fields of radio physics and astronomy is done with the facilities and by the staff of the Laboratory's Millstone Hill Field Station. This first issue of the Radio Physics and Astronomy report is intended not only to report our most recent research findings and experiment preparations in these fields, but also to provide sufficient background in our past work to give the reader an overall acquaintanceship with the extent and history of such work at Lincoln Laboratory.

Radar measurements on the moon and nearer planets with the Millstone radar are described, as are preparations for similar, more accurate measurements at Haystack Hill. Applications of techniques that were developed for radar astronomy to the improved detection and tracking of artificial satellites are also described. Studies of the electron and ion behavior in the ionosphere continue and the results are being co-ordinated with work elsewhere. Haystack Hill, the newest facility, is still in its early operating phase, with much of the effort of the station complement going into its increasingly complex instrumentation.

14. KEY WORDS

radio physics
radar astronomy
space surveillance techniques
atmospheric research
Millstone radar
Haystack Hill
ionospheric studies
auroral observations